Static aeroelasticity

CHAPTER TWO

Static Aeroelasticity – Unswept wing structural loads and performance

2.1 Background

All structures deform when external loads are applied although the deflections may be barely discernible. In most cases, the external and internal loads do not depend on the structural deformation. From an analysis perspective this means we can compute the internal loads and the external deflections independently.

These structural analysis problems are called statically determinate and include structural stability problems such as column buckling.

Figure 2.1.1 – Static aeroelasticity encompasses problems involving the intersection between steady-state aerodynamic and structural deformation interactions.

However, if the loads and structural deflection interact the structural analysis problem becomes very different, both physically and computationally, because the problem is statically indeterminate. Both loads and deflections must be determined simultaneously. This load/deflection interaction is represented graphically by the Venn diagram in Figure 2.1.1 in which the overlapping orange area represents the statically indeterminate problem area.

The purpose of this chapter is to illustrate the effect of aerodynamic load/structural deflection interactions on aircraft operation and performance. These problems are statically indeterminate and also involve considerations of structural stability. We will use simple models to reveal the causes of the aeroelastic phenomena and suggest cures for these problems. Chapter 2 contains homework problems to reinforce understanding these concepts.

2.1.2 Scope and purpose

As indicated in Figure 2.1.2, this chapter begins with a discussion of aeroelastic models and the introduction to special terminology required to define the features of these models. This includes a brief discussion of structural analysis matrix methods and concepts such as the shear center, aerodynamic coefficients and aerodynamic center of pressure.

A primary goal to Chapter 2 is the development of a *typical section aeroelastic model* to illustrate
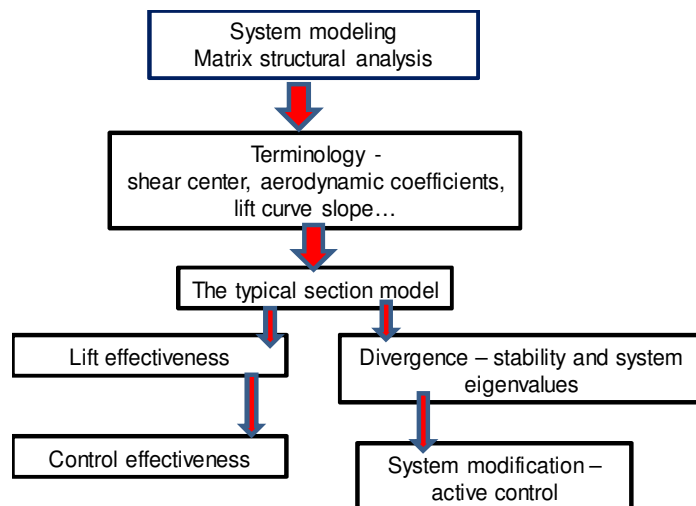
Figure 2.1.2 – Chapter 2 topical outline

interactions between the structural internal forces and the external aerodynamic forces. The typical section model development is followed by the development of a multi-degree of freedom model to illustrate the mathematical criteria for static stability of an aeroelastic system. This model is then used to introduce the concepts of lift effectiveness and structural stability, namely the aeroelastic divergence phenomenon. The divergence discussion includes the *eigenvalue problem* that characterizes the stability of multi-degree-of-freedom systems. In addition to illustrating aeroelastic effects on wing load distribution and internal stresses, control effectiveness and aileron reversal are described using the simple typical section model.

Finally, the modification of static aeroelastic response using ailerons as part of a feedback control system to adapt and adjust the lift and moments applied to flexible wings is also illustrated. This discussion will show how it is possible to modify the static stability and response of an aeroelastic system with feedback control. Although feedback control is seldom, if ever, used for static aeroelasticity this discussion shows the importance of controlling system interactions to aeroelastic response.

2.1.2 The structures enterprise and its relation to aeroelasticity

Every aircraft company has a large engineering division with a name such as "Structures Technology." The purpose of the structures organization is to create an airplane flight structure with structural integrity. This organization also has the responsibility for determining and fulfilling structural design objectives and *structural certification* of production aircraft. In addition, the organization conducts research and develops or identifies new materials, techniques and information that will lead to new aircraft or improvements in existing aircraft.

The structures group has primary responsibility for loads prediction, component strength analysis and structural component stability prediction. There is strong representation within this group of people with expertise in structural mechanics, metallurgy, aerodynamics and academic disciplines such as civil engineering, mechanical engineering, chemical engineering, and engineering mechanics, as well as the essential aeronautical engineering representation.

The structural design process begins with very general, sometimes "fuzzy," customer requirements that lead to clearly stated engineering design criteria with numbers attached. A summary of these general design criteria is shown in Figure 2.1.3.

Beginning at the top of the "wheel" we have design loads. These loads include airframe loads encountered during landing and take-off, launch and deployment as well as in-flight loads and other operational loadings. There are thousands of such "load sets." Once these load sets are identified, there are at least nine design criteria that must be taken into account. On the wheel in Figure 2.1.3 stiffness and flutter are one important set of criteria
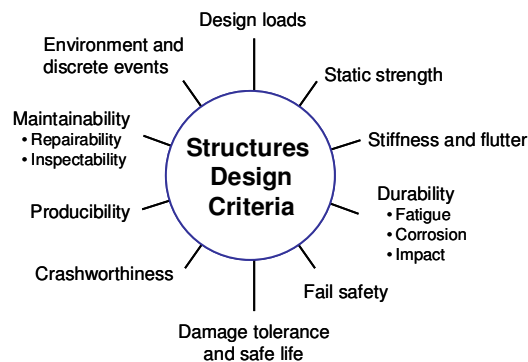
Figure 2.1.3 - Structural design requirements

that must be addressed.

The traditional airframe design and development process can be viewed as six interconnected blocks, shown in Figure 2.1.4. During Block 1 the external shape is chosen with system performance objectives in mind (*e.g.* range, lift and drag). Initial estimates of aircraft component weights use empirical data gathered from past experience. On the other hand, if the designs considered at this early stage have radical new forms, these estimates may be in error; but these errors will only be discovered later.
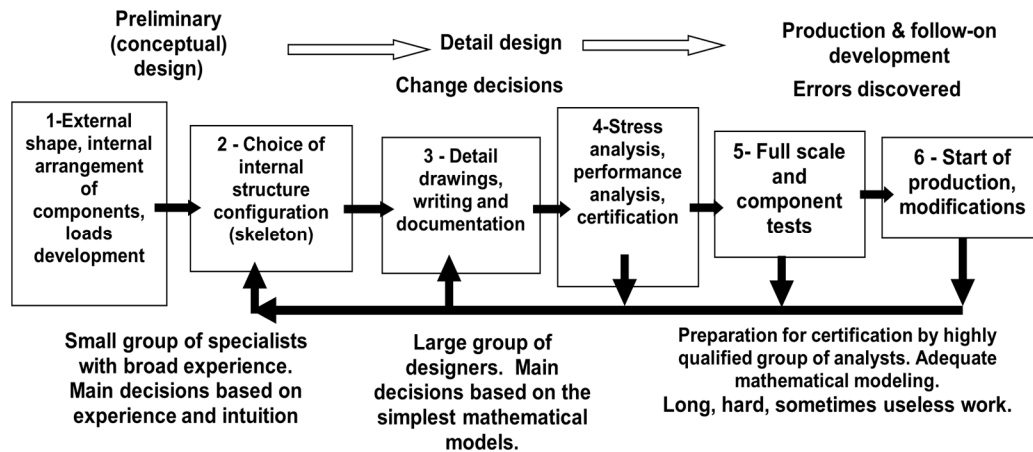
Figure 2.1.4 – The structural design and development process requires testing, analysis and feedback

Time is extremely important; the analysis scope and complexity during Block 1 is limited to very simple models despite the strong correlation between internal structural arrangement, materials selection, weight, manufacturability and cost. The ultimate success of the design effort depends heavily upon the training and real-world experience of the structural design team assigned to the Block 1 effort. Details that might escape the eye of a novice will be readily apparent to an experienced person. During Block 1, errors in judgment, caused primarily by lack of information, not lack of skill, are introduced, discovered in ensuing Blocks, and finally repaired.

Block 2 is concerned with selecting the internal structural layout. This delay in working out the details of the structure may seem strange since a great deal of effort is expended during Block 1 getting the external geometry (called the "outer mold lines") right. For a wing, the structural effort includes the choice of the number of spars and ribs and the location of critical components. The activities in Block 2 are characterized by low level structural analysis using simple beam models such as that shown in Figure 2.1.5 or other simple idealizations for element sizing and response estimation.[1] Seldom will the efforts in Block 2 revisit decisions made in Block 1, particularly those involving planform shapes.
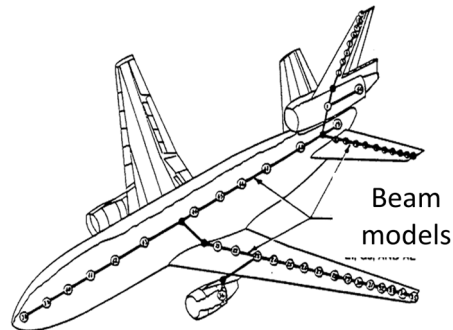
Figure 2.1.5 –Beam/stick models are used for preliminary flutter analysis (Reference 2.1)

Block 3 includes activities involving detailed drawings of frames, ribs, spars and attachments, as well as documentation. Here, extensive details emerge and if the manpower is available, higher fidelity models of critical components are created.

Block 4, the certification activity, requires extensive stress analysis. Stress analysis is labor intensive and involves large, analytical models developed from the drawings generated in Block 3. Usually these complex models involve discretized finite element models of the type shown in Figure 2.1.6. Next, Block

Figure 2.1.6 – Fighter aircraft finite element model showing interconnected aerodynamic and structural panels

5 includes full scale and component tests including fatigue and static loads tests. Block 6 is the beginning of production and delivery to the customer.

Note that Blocks 2 through 6 involve the opportunity and need to re-visit decisions made in earlier Blocks. Analytical modeling furnishes additional information that allows discovery and knowledge generation as the effort progresses. On the other hand, you cannot analyze what you have not defined, so surprises may visit the development team often.

2.1.3   The evolution of aircraft wing structures-form follows function

The structural mathematical models used in this book are simplistic and look very little like real aircraft structures such as the one shown in Figure 2.1.7. On the other hand, simplistic models led aeroelasticians and designers out of darkness into the light of understanding the inner workings of aeroelasticity and provided critical design guidance in the early years of aircraft development. To appreciate how analytical models are developed, we need some historical perspective on aircraft structural design evolution. A more complete perspective is contained in several books (References 2, 3, 4, 5 and 6) and references listed at the end of this chapter .
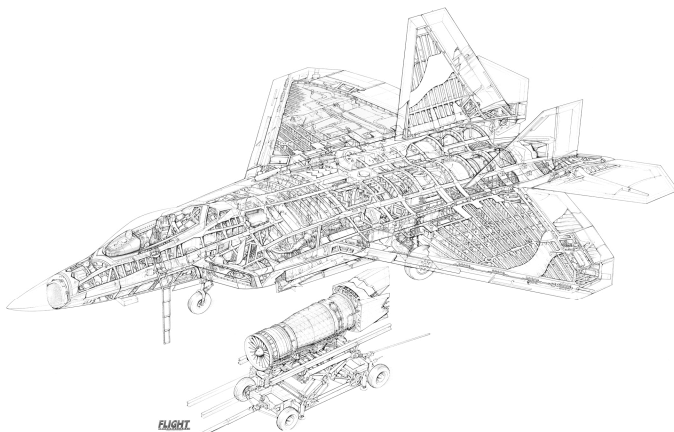
Figure 2.1.7-The F-22 structure is a complex geometric layout of basic structural elements created to transfer and resist external and internal loads.

The geometry of modern high speed/high performance wing structures such as the F-22 are anything but simple, consisting of complex geometric arrays with large numbers of different structural elements. On the other hand, compare the modern low speed, long endurance, high altitude Global Hawk with its

slender, high aspect wings to the ancient Hawker Hurricane shown below; notice how little (with the exception of materials and manufacturing) the basic structural concepts have changed in 60 or 70 years.
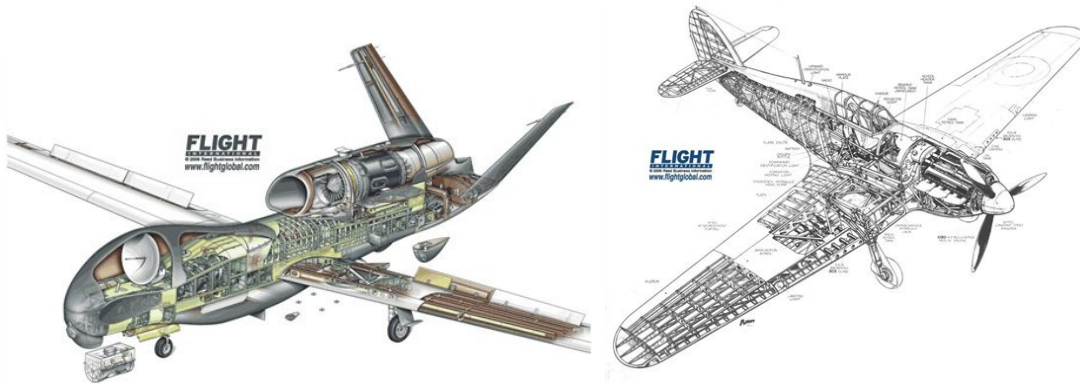
Figure 2.1.8-The Global Hawk unmanned air vehicle began in 1995. The wing material is advanced composite carbon fiber.   Sir Sydney Camm's Hawker Hurricane fighter first flew in 1935. The original aircraft had fabric covered wings. Metal stressed skin wings were introduced in 1939. Both vehicles use a standard stressed skin, multi-spar wing layout.

Wing structural design history is divided into two different eras; 1) the biplane/early monoplane era in which thin lifting surfaces were constructed of frame-like structures to which was attached a non-load-bearing cloth (or other material) material to give the surface its aerodynamic shape; and, 2) the reinforced, thick-wing, semi-monocoque wing era in which the entire surface, including the skin, carries structural loads and fuel and other components are housed in the wing.   No matter what era we look at, the structures themselves are constructed of many different types of components arranged in geometries that provide aerodynamic shape and provide structural integrity.
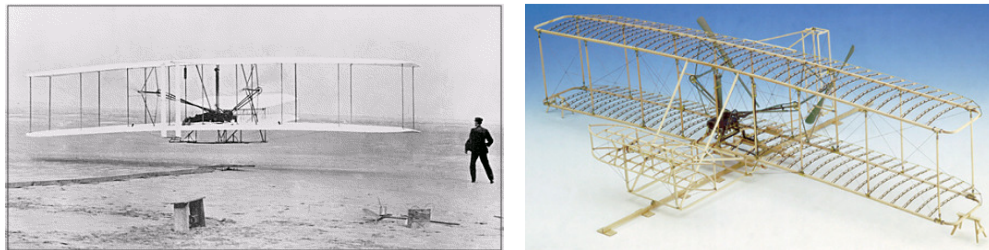
Figure 2.1.9-"Our invention relates to that class of flying-machines in which the weight is sustained by the reactions resulting when one or more aeroplanes are moved through the air edgewise at a small angle of incidence, either by the application of mechanical power or by the utilization of the force of gravity." Wright Brothers Patent Application, March 1903. The 1903 Flyer airframe weighed 405 lb. – the engine weighed about 200 lb. complete with radiator, water, fuel and accessories. Take-off weight was about 745 lb.

The first Wright Brothers airplane illustrates the type of biplane construction common to most aircraft during the first two decades of powered flight. While the Wrights added considerable technology to this aircraft, structural design was a settled subject, mostly due to previous efforts by Octave Chanute.

Octave Chanute was a distinguished railroad bridge engineer and self-made aeronautical hang-glider constructor who developed an interest in aviation at age sixty. He pioneered the biplane concept in the 1890's. His hang-glider flights in the Indiana sand dunes near Lake Michigan convinced him that biplanes were the most practical solution for combining strong practical structures and aerodynamics. Given his background, it is no coincidence that these biplanes resembled railroad bridge truss construction. The cloth skin attached to the structure generated aerodynamic loads but was incapable of supporting loads (and not intended to). Instead, the aerodynamic loads were transferred to wing ribs and spanwise structural members near the leading and trailing edges and then conveyed to the central part of the glider to support the pilot.

While Chanute and the Wright Brothers had solid scientific and engineering reasons for their biplane aerodynamic and structural designs, most early aviation experimenters neglected theory in favor of intuition and the artisan's experience. In a brief description of early design procedures in 1916, Arthur W. Judge wrote: *"In the earlier type of aeroplane body it was the usual practice to obtain the sizes of the different members by trial and error methods, or to make chance shots at the dimensions, and to trust to luck whether the resulting body has any margin of safety or not."*[*] Another article observed that *"Faulty construction is the most fertile source of accidents, and always will be until constructors put first-class engineering knowledge into their work."*[†] With few exceptions, analytical modeling of structures was not regarded as a primary study topic for most aeronautical engineers.

As a result, in the beginning, aircraft structures were little more than cloth covered trusses and frames. It was the French, with their interest in monoplanes and fast, light-weight airplanes who changed this, at least for fuselage construction. In 1911, Louis Bechereau expropriated an idea from Eugene Ruchonnet, a Swiss engineer who had worked as a shop foreman for the French Antoinette Airplane Company.

Ruchonnet focused his attention on the fuselage, which up to that time was constructed as a truss frame with cloth covering, much like the wing. Rather than simply attaching fabric to a truss structure, Ruchonnet's idea was to use the fuselage skin carry the structural load and eliminate the heavy truss. As a result, he built a laminated wood fuselage shell to create a streamlined shape. These wood layers were glued together with their grains running in different directions to strengthen the skin. Ruchonnet called the new technique "monocoque" or single-shell construction.

Bechereau used the monocoque fuselage idea, together with a frame/cloth skin monoplane design to build the Deperdussin streamlined, externally braced, mid-wing monoplane. This airplane won the Gordon Bennett Cup in 1913 with a speed of 125 mile per hour – only a decade after the Wright's first flight!

Later, as airplane size increased, the unreinforced, monocoque shell fuselage design concept was not suitable because the highly loaded compressive skin buckled under high loading. A variation of the monocoque concept, a reinforced or "semi-monocoque" structure was developed to create a light-

---

[*] A. W. Judge, *The Design of Aeroplanes*, Isaac Pitman and Sons, Ltd., 1917, p. 156. This 242 page textbook by Judge is one of the early textbooks on airplane design.
[†] *Aeronautical Journal*, July 1911, p. 125

Chapter 2

weight durable reinforced shells structure. This type structure is still used today, both for fuselage and wing construction.
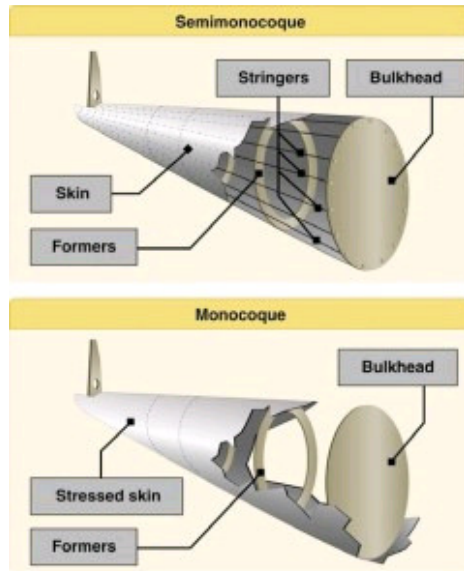
Figure 2.1.10-Ruchonnet's monocoque and semi-monocoque shell structures introduced yet another structural design concept into structural analysis and design. Deperdussin Racer "Le Monocoque" with monocoque shell structure fuselage, 1912. Compare this design to the Wright Brothers airplane only nine years earlier.

Thin-wing monoplane structures were not as strong or as stiff as biplane arrangements so they required external wire bracing (see Figure 2.1.11). To create greater strength, wings began to use a substantial load-carrying member, the wing spar, located near the front of the wing and extending from the fuselage to the wing tip. The wing spars were usually conventional beam designs lifted from civil engineering structures practice. Originally the spar was simply a heavy beam member, but developed into a hollow box design that also resisted wing torsional loads and rotation.

By the end of World War I, bi-plane wing design had matured to the extent that there were several variations of a common spar/rib configuration structure that supported a thin wing biplane or monoplane. This design used two spars with numerous ribs and spanwise *stringers* to help shape the wing.

Early monoplanes still used thin wings that required external wire bracing to keep the wings from folding in flight. In Germany, Hugo Junkers recognized that streamlining the airplane shape was the key to increasing speeds with limited engine power. Junkers began by studying thermodynamics and became independently wealthy after inventing an automatic water heater. Junkers was also Professor of Thermodynamics at
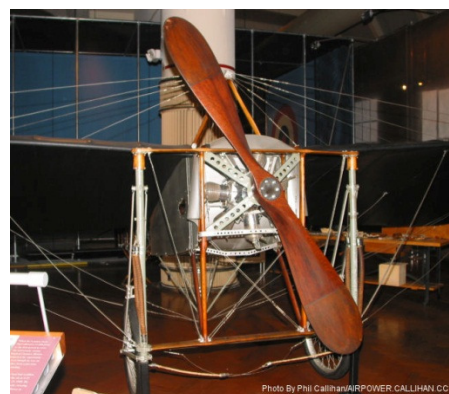
Figure 2.1.11-The externally wire-braced Bleriot XI flew between England and France in 1909.

Chapter 2

the Technical University of Aachen (Germany).
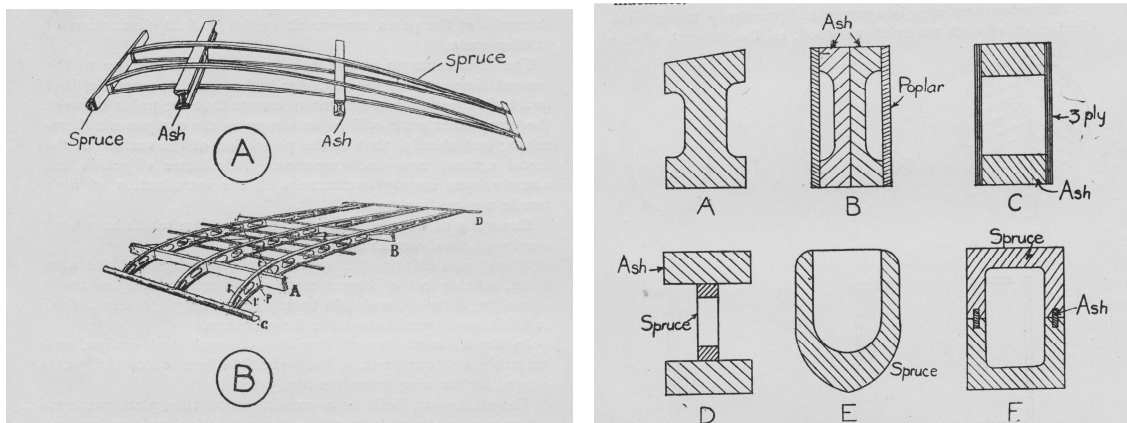
Figure 2.1.12-Arthur Judge discussed the latest (circa 1918) wing structural designs with two different types of ribs. Most wings were biplanes. Immediately after World War I aircraft structures had advanced to the point where there were at least six different types of wooden spars, including one with laminated shear webs. The spar in E is intended to be a hollow leading edge and was used by Farman and Nieuport designs.

Junkers found that thick airfoil sections performed better than thin sections in use at the time. He developed an internally braced cantilever monoplane design, made possible by thicker wings. Fixing the spar securely to the fuselage to create a cantilever beam arrangement allowed designers to eliminate the external bracing wires. Junkers' monoplane used combinations of steel beams interconnected by load-bearing skin to create a semi-monocoque wing structure. Junkers founded a successful company and later produced the Junkers Ju 52-3m tri-motor which for a time was the favored transport aircraft in Europe. A trademark of this design was its corrugated metal stressed-skin.

While cantilevered wings still used ribs and fabric to create the wing aerodynamic shape, designers began to use thin wooden veneers for skin. These wooden-skinned wings became known as stressed-skin wings because the veneers added strength while they shaped the wing surface itself. The structural material was nearly always wood, but Judge notes that *"…steel and other metals (are) replacing these nonhomogeneous materials (wood) and successful all-metal wings and indeed complete machines have been built." (Judge, p.68).*

In addition to Junkers, two others contributed to the development of revolutionary aircraft structures and airplanes with these structures before and after World War I. Like Junkers, these two were German. Claude Dornier and Adolf Rohrbach began their careers as structural engineers for the Graf Zeppelin Company. Both had extensive experience designing the internal metal framework for the large airships developed before World War I. Rohrbach's academic training was in shipbuilding. Both eventually went on to create their own aircraft companies.

Dornier worked for Count Zeppelin who, in 1914, asked him to develop flying boats. Dornier flying boats were famous and helped pioneer overseas routes for airlines. His structural designs were characterized by smooth wing skin that carried loads.
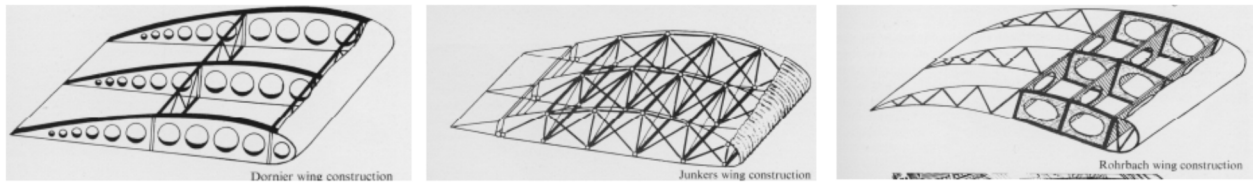
Figure 2.1.13-Three similar but different types of early stressed skin construction, left to right: Dornier, Junkers, Rohrbach. Dornier's design is the result of his experience building Zeppelin airship structures. Junkers' concept uses extensive trusswork. Rohrbach's concept is cellular. The basis for Rohrbach's wing design was a central box section girder of thick duralumin sheet stiffened by fore and aft bulkheads

Rohrbach worked for Dornier at the Zeppelin flying boat plant. After World War I he founded a company in Denmark to get around punitive features of the Versailles Treaty that forbade Germany from developing military aircraft. He significantly influenced aircraft design in Japan and the United States. Mitsubishi sent Japanese engineers to Germany in December 1921. Mitsubishi-Rohrbach GmbH, was formed in Berlin in June 1925. Aircraft were assembled in Copenhagen in a new factory built with the assistance of the Imperial Japanese Navy. The personnel from Japan learned aircraft structural design from Rohrbach. One result was the Japanese A6M1 fighter, the infamous "Zeke" or "Zero" that was the scourge of the Pacific during the first half of World War II.

Rohrbach was probably the first to use the term "stressed skin." He had a major influence on American structural design because of a visit to the United States in 1926. He presented at least one lecture in Los Angeles and is credited with inspiring designers such as John K. Northrop to use stressed skin design in new airplanes, notably the Lockheed Vega.
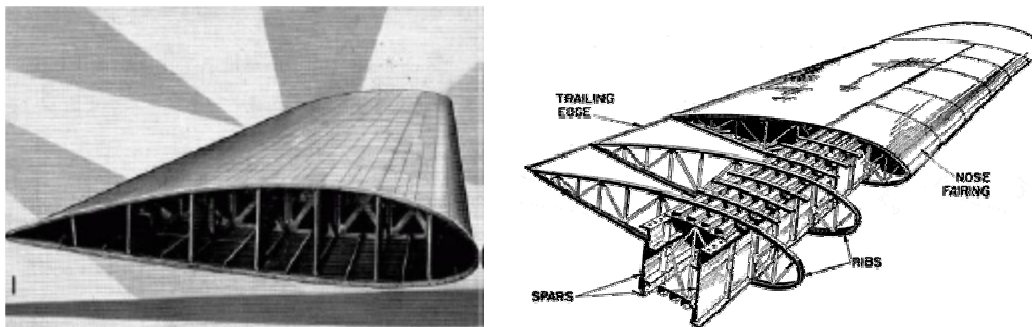
Figure 2.1.14-Northrop's cellular wing design for his Northrop Alpha was the latest in wing design in the early 1930's.(sales brochure) It was much lighter than other stressed skin designs of the time. (Introduction to Airplanes - Navy Training Courses, 1944).

The development of advanced aircraft structures came to the United States from Europe in the 1930's. The NACA championed the use of metals and stressed-skin designs. Boeing, with its model 247 pioneered advanced design and construction. The DC-3 with its clean smooth exterior aluminum stressed skin added to progress in the area.

Once designers settled on thick wings, large internal volumes became available for storage. This led to wings with the ability to carry fuel ("wet wings") and internal gun mounting, not to mention landing gear storage. By the mid-1930 the basic concept of stressed-skin construction was the *fiat accompli* for airplane wing design.
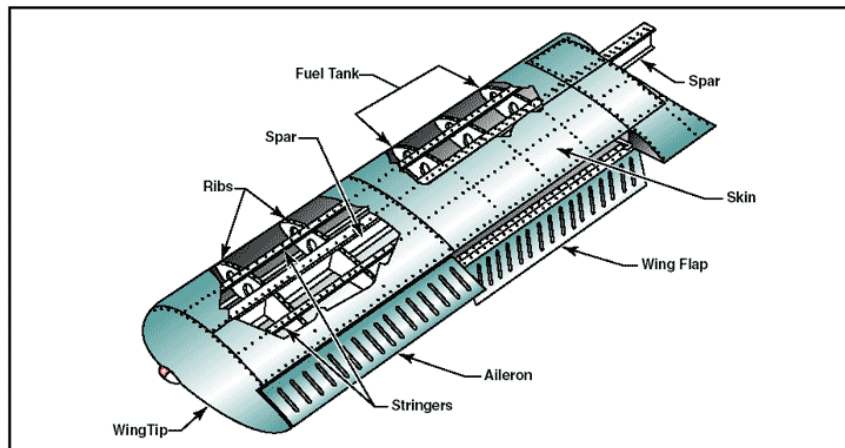
Figure 2.1.15-By the mid-1930's the basic concept of stressed-skin construction had evolved to the point where it was the choice of designers of high speed, large aircraft.

The quest for high speeds and light weight structures meant that the surfaces were flexible. Structural analysis attack two different problems, those related to stress analysis and those related to vibration and aeroelastic analysis. Stress analysis, being concerned with localized effects of loading, requires a very different model than aeroelastic analysis. Stress models are very detailed and pay attention to small internal details since they must model critical design details such as structural attachments. Aeroelastic models must only capture "macro" as opposed to "micro" structural features. These features include surface shape, both static and dynamic. Analytical odeling is the subject of the next section.

2.2 Analytical modeling

Analysis differs from *synthesis*. Synthesis involves putting things together. Analysis consists of breaking the system into parts to determine their interrelationships and interactions. Analysis requires identifying essential system details, separating the essential from the unessential, definition of models to reflect these details, and then connecting the details.[7]

Mathematical models, essential to all engineering projects, allow us to acquire information and then transform it into knowledge. Models predict outcomes and help us to decide among alternatives. Models reduce risk in making decisions and help us size critical dimensions as well as provide details for the airplane.

Aeroelastic models must be predictive; they must provide details required to allow us to understand what happens to the structure when we fly at different speeds and altitudes. Given an input or set of inputs, models provide an output. Input might be airspeed, V, while output might be wing tip deflection or load distribution. In addition to input/output predictions, analytical models provide us with understanding of how different components of a system interact. Models provide similarity parameters that show how physical parameters couple together.

A model may be physical, a wind tunnel model for instance, or the model may be analytical and simply consist of a set of equations. The model may resemble the actual engineering article very
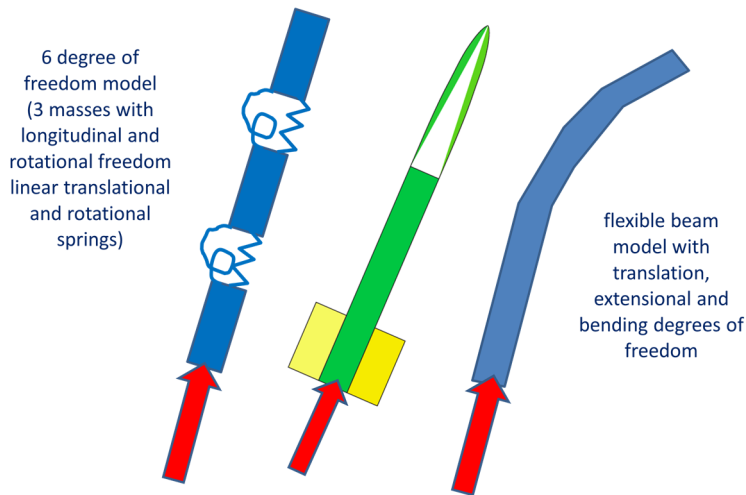
Figure 2.2.1 – Analytical models come in a wide variety of forms, applying symbolism to real configurations.

closely or it may leave out unessential features. Figures 2.1.4 and 2.1.5 are examples of analytical models that represent the dynamic behavior of a flexible aircraft, but one very closely resembles an airplane while the other does not.

Models have objectives. What are we looking for? What do we want to know? The answers to these questions determine the complexity of the model.

Models also have assumptions that simplify their development but may limit or even destroy their validity in certain circumstances.[8] Everyone remembers D'Alembert's paradox in fluid mechanics in which the exclusion of viscosity and the boundary layer gives a beautiful, simple, but incorrect result for the drag force.

Models are virtual, not real because some unnecessary details are left out of models. An example is the idealization or abstraction of a wing as a simple beam, even though the actual wing is a thin shell-like structure. This abstraction may be appropriate for estimation of wing natural frequencies but wholly inadequate for estimation of stresses in ribs. In our aeroelastic models we will begin with highly idealized abstractions that substitute springs for actual structural elements and simple wing planforms to simulate the aerodynamic features we are studying.

The two most commonly used structural models are: 1) differential equation representations of static equilibrium, either in terms of internal forces or displacements; or 2) lumped parameter models with idealizations that lead to a finite number of degrees of freedom. Differential equation models, if solved numerically, for instance by finite differences, lead to a matrix representation of structural and aerodynamic effects.

2.2.1 The typical section, the flying door and Rayleigh-Ritz idealizations

With one exception, the models in this chapter are discrete element models such as that shown in Figure 2.2.1. We will also assume that the behavior of our systems is linear, that is, output is proportional to the input.

All mathematical descriptions of aeroelastic phenomena use idealizations in which some things are emphasized and other factors are left out. The most common and popular idealization for aeroelastic phenomena are segmented models. These models, shown in two forms in Figure 2.2.2, resemble single or interconnected wing segments.

In its simplest form, the single "typical section" model resembles a wing with constant chord sandwiched between the walls of a wind tunnel. This typical section has pitching and "bending" displacement degrees of freedom; its angle of attack changes with the applied load and also deflects upward or downward. These displacements are resisted by two types of springs that are surrogates for the wing structure. The typical section model is extended to consist of a series of interconnected wing segments, elastically restrained as shown in Figure 2.2.2.

When the typical section consists only of a single wing segment the chordwise dimension is taken as the wing dimension at a position ¾ of the way out the semi-span. Similarly, other critical dimensions such as the position of a point called the shear center and the aerodynamic center are taken from the typical section at the ¾ chord.

Figure 2.2.2 – Unswept typical section models showing pitch and plunge degrees of freedom to simulate wing torsion and bending.

A second model used for static aeroelasticity studies is a variation of the unswept typical section. The so-called "semi-rigid" model, shown in Figure 2.2.3, appears in research reports from the Royal Aircraft Establishment at Farnborough in England and includes sweep as a parameter. This model is used in Chapter 3 when we discuss the effects of sweep of aeroelastic behavior. The swept wing model resembles a "flying door'" restrained at the wing root by elastic springs, but able to twist and rotate to simulate bending.

The Rayleigh-Ritz model is a third type of simple analytical model. Like the other two models the Rayleigh-Ritz model has a limited number of degrees of freedom, but these degrees of freedom are
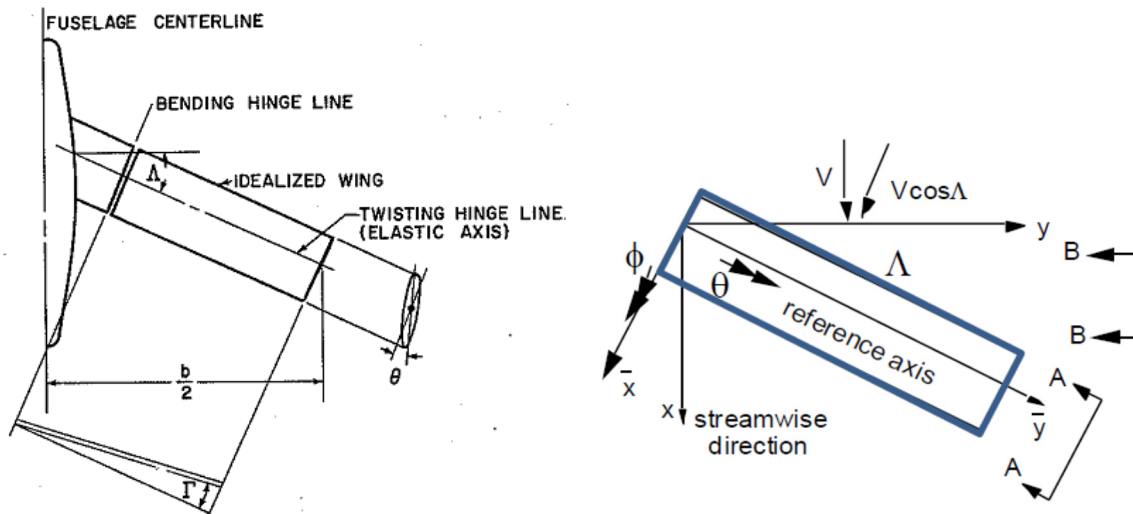
Figure 2.2.3 - Swept wing models with two degrees of freedom to simulate swept wing aeroelastic behavior.

Chapter 2

deformation shapes with unknown amplitude. These unknown amplitudes become the degrees of freedom for the model. Unlike the other models Rayleigh-Ritz models have distributed stiffness. Rayleigh-Ritz models begin as continuous structures such as beams and plate structures, with theoretically infinite numbers of degrees of freedom that are then reduced, through the use of energy methods, to a finite number of degrees of freedom. This model is discussed in an ensuing section.

2.2.2 – Functional diagrams and operators – modeling the aeroelastic feedback process

One important outcome of our aeroelasticity studies is the recognition that aeroelasticity is a feedback process in which an initial aerodynamic form, a wing surface for example, is loaded initially by placing it at an angle of attack. As a result, it deforms to produce deformation that in turn produces new loads that then produce additional loads. This load/displacement feedback process may or may not converge. The process may be viewed as a simple block diagram, as indicated in Figure 2.2.4.

Figure 2.2.4 – Wing functional diagram showing inputs and output

In addition to the inputs, the wing lift depends on the wing deformation. As a result we view the model as having two interconnected elements: 1) a wing lift generating element that takes information about the wing shape; and, a flexible structure element that takes loads information and calculates deflected shape. This wing may be represented functionally as a block diagram shown in Figure 2.2.5.
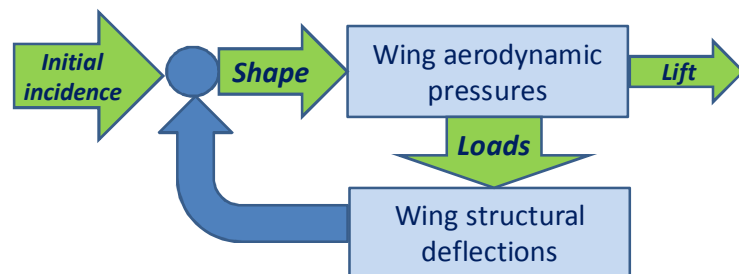
Figure 2.2.5 – Block diagram showing feedback connections between aerodynamics model and structural model

The calculation of aerodynamic pressures (and forces) requires that the wing shape and incidence are known inputs. The input angle of attack includes wing deformation. The calculation of the deformation is done in the flexible structure module and then the wing shape, incidence and aerodynamic pressures are updated. This process continues until the process converges.

In practice, this iteration is seldom necessary. We can represent what goes on in each of the modules by mathematical operators. In our case, these operators are matrix relationships, but we are getting ahead of ourselves. The point is that we need to connect aerodynamic and structural elements to create an aeroelastic feedback system. Whether the system is operating subsonically, transonically or supersonically, there is a special operator or module for the aerodynamic pressures and loads. Similarly, whether we choose to represent the wing internal structure in simple or exquisite detail, there is a structures module.

Both modules connect loads and deformations. For instance, the aerodynamic loads distributed over a surface depend on the local incidence of the surface. This incidence is due to both fixed loads $\{P_i\}$ due to known angles of attack and loads due to flexible deformations $\{x_j\}$. The loads P_i are due to initial aerodynamic loading such as an angle of attack of the aircraft input by the pilot. The expression for these forces and moments distributed over the wing, $\{L_i^{aero}\}$, is written as $\{L_i^{aero}\} = [A_{ij}]\{x_j\} + \{P_i\}$ where the matrix $[A_{ij}]$ is a collection of aerodynamic influence coefficients. The relationship between the external structural forces and moments and the same deformations $\{x_j\}$ is written as $\{L_i^{structure}\} = [K_{ij}]\{x_j\}$ where the matrix $[K_{ij}]$ is the so-called stiffness matrix, a matrix of structural influence coefficients.

Connectivity between the structures and aerodynamic modules is accomplished when we write equations of motion or, in the case of statics, equations of equilibrium, an equation that sums internal and external forces and moments and sets them to zero. This provides an equation with the form

$$\{L_i\} - \{L_i\} = 0 = [K_{ij}]\{x_j\} - [A_{ij}]\{x_j\} - \{P_i\} = 0$$

Solving for the deformations $\{x_i\}$ we have $\{L_i^{structure}\} = [K_{ij}]\{x_j\}$. The load distribution found to be $\{L_i^{aero}\} = [A_{ij}][[K_{ij}] - [A_{ij}]]^{-1}\{P_i\} + \{P_i\}$.

The aeroelastic problem is called a *statically indeterminate* problem because structural deformation creates loads that enter into the equilibrium equations. The feedback process is contained in matrix operations such as addition and inversion so we do not need to iterate. The solution procedure is similar if we have differential equations to represent the structure and the aerodynamics although the operation for inversion or "inverse operators" is somewhat different.

The next few sections discuss and develop simple structures and aerodynamic modules for aeroelasticity models. Refer back to the present section to see how the general process just outlined is applicable to these simple models.

2.3 Matrix structural analysis – stiffness matrices and strain energy
The demands for performance, efficiency and high speed for modern aircraft would be difficult were it not for high-speed computers and modern automated analysis procedures such as finite element (FEM) structural methods and aerodynamic paneling methods and computational fluid dynamics (CFD) efforts. These advanced analysis methods provide high fidelity analytical models to aid design decision-making and shorten the time required to make decisions. This section presents an overview of a structural analysis approach known as matrix methods and shows an example of how we develop them; it also introduces the *shear center* and *elastic axis* concepts.

As discussed in the previous section, the external forces and moments applied to an aircraft $\{F_i\}$ and displacements $\{u_j\}$ of the aircraft structure are related to each other. If the structural behavior is static and assumed to be linear elastic, this relationship is written as

$$\{F_i\} = [K_{ij}]\{u_j\} \tag{2.3.1}$$

where $[K_{ij}]$ is the *n x n* system stiffness matrix. The elements, K_{ij}, are called *stiffness influence coefficients*.

To develop the relationships required for the calculation of the stiffness matrix we use the finite element method. Finite element models, such as that shown in Figure 2.1.5, are collections of mathematical elements joined together at *"node points"* where displacements are computed and forces and moments are applied. A node point is a junction point connecting two or more elements. Finite element node points may or may not correspond to physical joints on the actual structure. For simple trusses, the physical node points and the mathematical node points are identical. The relationship between the structural forces and displacements on each of these elements is expressed as a set of linear (or nonlinear) algebraic equations whose coefficients are referred to as *the stiffness matrix*, a matrix of structural influence coefficients relating external forces and moments to the displacements at node points..

In reality, aircraft structural systems contain groups of discrete elements connected by rivets, welds and joints. The complex geometry and the wide variety of loads applied makes the analysis task challenging. Differential equation models with smooth continuous features are not effective for complex structures since a fundamental assumption for such equations is that the system is continuous, at least in discrete areas.

Finite element methods belong to a class of structural models called *matrix models*. Matrix method analysis development began in the aircraft industry with flutter and vibration clearance efforts. About 60 years ago, the need to accurately represent aeroelastic and vibratory interactions of geometrically complex flexible airplane structural elements at the earliest stages of design (and the ability to use electronic computers) led to the development of the finite element method (or Direct Stiffness Method) of structural analysis.

The finite element method began at the Boeing Company in the 1950's as the result of the quest for accurate analytical procedures for vibration and stress analysis on complex airplane airframes.[9] Within a few years, this idea had exploded onto the analytical scene and became the mainstay of modern structural analysis.

The finite element method has evolved rapidly over the past thirty years and led to accurate elements and large scale computer codes such as NASTRAN and ANSYS. These codes are widely used by both aerospace and non-aerospace companies.

The structural idealization of an aircraft structure and the definition of the loads on the structure require that we define degrees of freedom of structural motion. These degrees of freedom may be actual displacements (including rotation) of the structure or they may be amplitudes of assumed continuous displacement functions (shapes) or vectors that describe the structural deformation. The final result is that the actual structure, with an infinite number of displacement degrees of freedom, is replaced by an idealized model with a manageable number of unknown displacement quantities or degrees of freedom such as shown in Figure 2.1.5.

Aircraft loads are created by combinations of distributed pressures and inertia and relatively concentrated forces or inertia (such as engines). For matrix analysis, both the distributed and concentrated loads are converted into a set of equivalent discrete forces and moments associated with each of the degrees of freedom. The result is a set of generalized forces (the term generalized force can refer to *either* a force or a moment) denoted as $\{F_i\}$. Each element F_i is associated with a corresponding deflection vector element u_i (these generalized displacements can also be *either* a deflection or a rotation).

In a system without dissipative outlets such as friction, total system energy is conserved. Therefore, all of the work done by the external forces must be stored within the structure. If the structure is restrained against rigid body motion and the forces are applied slowly, the work done is stored as strain energy or potential energy. It can be recovered when the external loads are removed.
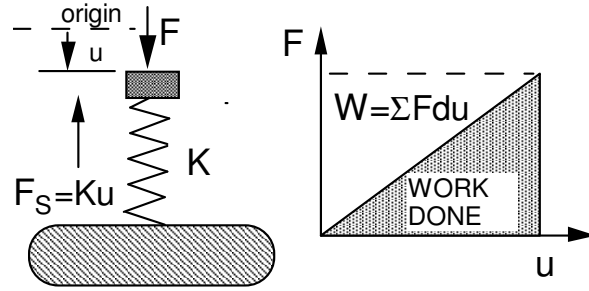
Figure 2.3.1 - Spring-mass-force system

Consider the simple spring element shown in Figure 2.3.1. If the external force is applied very slowly so that the acceleration is so small that static equilibrium is maintained approximately throughout the loading process, then the work done, W, by the force F in moving through displacement u is equal to the internal strain energy stored.

$$W = \frac{1}{2}Fu = \frac{1}{2}Ku^2 = U \qquad (2.3.2)$$

In the more general case where there are many displacements and many external forces F_i located at the *node points* where displacements u_i are measured, the work done by the external forces is

$$W = \frac{1}{2}[F_i]\{u_i\} = \frac{1}{2}\{u_i\}^T\{F_i\} \qquad (2.3.3)$$

The factor ½ appears in Eqns. 2.3.2 and 2.3.3 because the relationship between the loads and deflections is linear and the loads build slowly from zero to their final values, F_i and u_i. Substitution of Eqn. 2.3.1 into 2.3.3 provides an expression for work and strain energy done in terms of the structural displacements and the *system stiffness matrix* in Eqn. 2.3.1.

$$W = \frac{1}{2}\{u_i\}^T[K_{ij}]\{u_j\} \qquad (2.3.4)$$

The *strain energy, U, is:*

$$U = \frac{1}{2}\{u_i\}^T [K_{ij}]\{u_j\} \qquad (2.3.5)$$

When differentiated with respect to u_i the strain energy U provides force equilibrium equations

$$\frac{\partial U}{\partial u_i} = \sum K_{ij} u_j = F_i \qquad (2.3.6)$$

Differentiating Eqn. 2.3.6 with respect to u_j we recover the stiffness matrix elements for the rows and columns representing the equations of motion.

$$\frac{\partial^2 U}{\partial u_i \partial u_j} = K_{ij} = \frac{\partial^2 U}{\partial u_j \partial u_i} = K_{ji} \qquad (2.3.7)$$

since the order of differentiation in Eqn. 2.3.7 may be interchanged. The structural stiffness matrix is symmetric. The stiffness matrix elements may be positive, negative or zero when $i \neq j$, but the main diagonal elements must be positive. The determinant of the stiffness matrix is also positive.

2.4 An example - Construction of a structural stiffness matrix – the shear center concept

The idealized two-dimensional "structure" shown in Figure 2.4.1 has two linear elastic springs with stiffness K_1 and K_2 (with units lb/in or N/m). The deformation state of this model is defined by the downward deflection, h, at an arbitrary reference point chosen by the analyst, and a pitch rotation, θ, about the reference point, measured positive counterclockwise. The external force, P, computed at the reference point, is the resultant of all forces and pressures acting on the structure, while M is the resultant of the moments, about the reference point, of all forces and pressures acting on the structure. We will compute the stiffness matrix that relates P and M to h and θ.
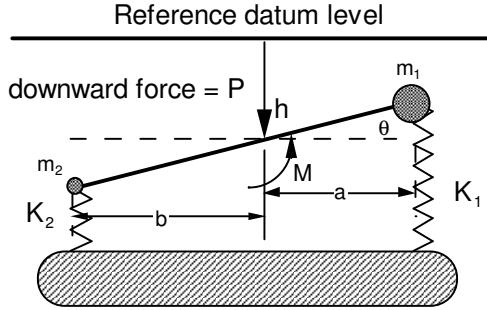
Figure 2.4.1 - Two dimensional bar and spring system
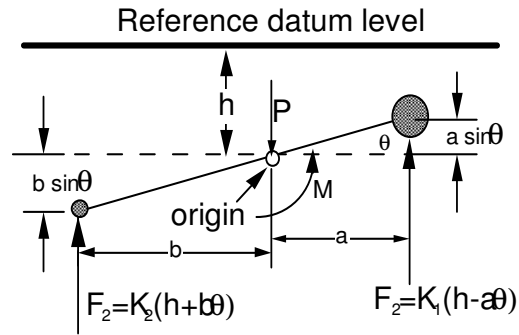
Figure 2.4.2 - Two dimensional bar free body diagram

We will use force and moment equilibrium equations to derive matrix equations of static equilibrium. Consider the free-body diagram of the deformed system (shown in Figure 2.4.2), including the forces internal to the springs. When θ is small ($\sin\theta \cong \theta$), the compression of the right hand spring K_1 is $h - a\theta$, while the compression of the left spring K_2 is $h + b\theta$. Note that the dimensions a and b measure the spring locations relative to the reference point.

The spring restoring forces are proportional to K_1, K_2, $h - a\theta$ and $h + b\theta$. Summing forces and moments about the reference point we have two equations for static equilibrium.

$$\sum F = P - K_1(h - a\theta) - K_2(h + b\theta) = 0$$

$$\sum M = M - K_2 b(h + b\theta) + K_1 a(h - a\theta) = 0$$

These two equations are written in matrix form as:

$$\begin{Bmatrix} P \\ M \end{Bmatrix} = \begin{bmatrix} (K_1 + K_2) & (K_2 b - K_1 a) \\ (K_2 b - K_1 a) & (K_2 b^2 + K_1 a^2) \end{bmatrix} \begin{Bmatrix} h \\ \theta \end{Bmatrix} \qquad (2.4.1)$$

Equation 2.4.1 relates the applied external loads (a force P and moment M) at the reference point to the deflection and rotation at this point. *Elastic or static coupling* is indicated by the non-zero *off-diagonal* terms $(K_2 b - K_1 a)$; in Eqn. 2.4.1. The force P, produces both a θ rotation and a displacement, h. The moment, M also produces both types of displacement.

We can also use an energy approach to derive this matrix also. The deflections at each spring, δ_1 and δ_2, are functions of h and θ.

$$\delta_1 = h - a\sin\theta \cong h - a\theta$$
$$\delta_2 = h + b\sin\theta \cong h + b\theta$$

The strain energies stored in each spring are

$$U_1 = \frac{1}{2}K_1\delta_1^2 = \frac{1}{2}K_1\left(h - a\theta\right)^2$$

$$U_2 = \frac{1}{2}K_2\delta_2^2 = \frac{1}{2}K_2\left(h + b\theta\right)^2$$

The total strain energy is $U = U_1 + U_2$. Differentiate the strain energy expressions with respect to h and θ to get:

$$\frac{\partial U_1}{\partial h} = K_1\left(h - a\theta\right) \qquad \frac{\partial U_1}{\partial \theta} = -aK_1\left(h - a\theta\right)$$

$$\frac{\partial U_2}{\partial h} = K_2\left(h + b\theta\right) \qquad \frac{\partial U_2}{\partial \theta} = bK_2\left(h + b\theta\right)$$

Differentiating the strain energy for a second time we have:

$$\frac{\partial^2 U_1}{\partial h^2} = K_1 \qquad \frac{\partial^2 U_1}{\partial\theta\partial h} = -aK_1 \qquad \frac{\partial^2 U_1}{\partial\theta^2} = Ka^2$$

$$\frac{\partial^2 U_2}{\partial h^2} = K_2 \qquad \frac{\partial^2 U_2}{\partial h\partial\theta} = bK_2 \qquad \frac{\partial^2 U_2}{\partial\theta^2} = K_2b^2$$

Using these expressions with Eqn. 2.4.1 we see that the stiffness elements generated using the energy approach are identical to those generated using free body diagrams and static equilibrium equations in Eqn. 2.4.1.

Elastic coupling (also called *static coupling*) depends on the coordinate system chosen. If we change the location of the reference point, the dimensions a and b will change. The size of the resultant force P (it is the sum of all the vertical forces acting on the structure) remains the same, but the size and the sign of M will change, since it represents the net external moment of a combination of external forces about the reference point. From Equation 2.4.1, if K_1a is equal to K_2b, the elastic coupling term $(K_2b - K_1a)$ is zero. Elastic coupling disappears if the ratio of dimensions a and b is:

$$\frac{a}{b} = \frac{K_2}{K_1} \qquad\qquad (2.4.2)$$

Equation 2.4.2 shows that there is a unique point on the idealized structure where a concentrated force, P, causes only a displacement, h, while a torsional moment, M, causes only rotation about that point. The first condition defines a point called *the shear center*. The second condition defines a point called *the center of twist*. For a linear elastic structure *the position of the shear center and center of twist are identical.*

The shear center is defined as "a point on a structural configuration where loading by a concentrated force will create only translational displacement but no rotation or twist." If $K_1 = K_2 = K$, Eqn. 2.4.2 shows that the center point of the bar $(a = b)$ fits our shear center definition. If the two springs have different stiffness values, the shear center is located away from the center of the structure.

We can also solve for the shear center position by first using Eqn. 2.4.1 to solve for h and θ when P and M are applied.

$$\begin{Bmatrix} h \\ \theta \end{Bmatrix} = \frac{1}{\Delta} \begin{bmatrix} (K_2 b^2 + K_1 a^2) & -(K_2 b - K_1 a) \\ -(K_2 b - K_1 a) & (K_1 + K_2) \end{bmatrix} \begin{Bmatrix} P \\ M \end{Bmatrix} \tag{2.4.3}$$

where $\Delta = K_1 K_2 (a^2 + b^2) + 2 K_1 K_2 (ab)$ is the determinant of the structural stiffness matrix. Note that the determinant is always positive.

To find the shear center we apply only the load P (we set *M*=0) and then find that

$$\begin{Bmatrix} h \\ \theta \end{Bmatrix} = \frac{P}{\Delta} \begin{Bmatrix} (K_2 b^2 + K_1 a^2) \\ -(K_2 b - K_1 a) \end{Bmatrix} \tag{2.4.4}$$

From Eqn. 2.4.4, when $K_2 b = K_1 a$ then $\theta = 0$, no matter what the size of the load P. This is the same result found in Eqn. 2.4.2. The shear center does not depend on the applied load magnitude.

2.5 Subsonic aerodynamics - fundamentals

This section reviews the fundamentals of low speed aerodynamics to the extent necessary to develop basic aeroelastic models of the types shown in Figures 2.2.2 and 2.2.3. We will review terminology and definitions only to the extent necessary to develop these models in this chapter. The review follows closely the material contained in Chapter 3 of A.C. Kermode's *Mechanics of Flight*.[10] In this section we will discuss the mathematical representation of lift and reference points such as the center of pressure and the aerodynamic center.

Analytical aerodynamic development occurred primarily in Britain and Germany before, during and shortly after World War I. Strangely the first two decades produced a great deal of discussion about the origins of lifting forces.[11] Without this understanding it was difficult to develop analytical theories. As a result the engineering world was divided into two groups, often referred to, in Britain at least, as the "mathematicians" and the practical men."[‡] In this section we will take the view of the

---

[‡] David Bloor, (*The Enigma of the Airfoil: Rival Theories in Aerodynamics 1909-1930,* University of Chicago Press, 2011) presents the history of the struggles between researchers in Britain and Germany as they sought to unravel the mysteries of aerodynamic lift.

"practical man" (with apologies to the young women who contribute to the field – much has changed since those early days when half the population was sociologically barred from entering engineering) and approach the review of aerodynamics from an empirical viewpoint.

Figure 2.2.2 shows a mathematical model of a wing composed of two different sections or segments. In our development, the term "wing segment" is used to mean a *"shaped surface, such as a three-dimensional airplane wing, tail, or propeller blade that produces lift and drag when moved through the air."[12]* Figure 2.2.2 also has a cross-section of a wing. This cross-section is referred to as an airfoil. The term *airfoil* (or aerofoil) is defined as *"the cross section of a body that is placed in an airstream … to produce a useful aerodynamic force in the most efficient manner possible."[13]* An airfoil may be thought of as a wing with infinite span. In this chapter and others to follow, the term *wing, lifting surface or wing segment* refers to three dimensional surfaces while the term *airfoil* is used to denote the two-dimensional wing cross-section.

Parameters used to define wing cross-sectional (airfoil) features and terminology are shown in Figure 2.5.1. The straight *chord line* connects the rounded leading edge with the sharp trailing edge of an airfoil designed for subsonic flow. The length of this line is denoted as the chord dimension c. The mid-point between the upper and lower wing segment boundaries is called the *mean camber line*. Wing camber is measured by calculating the ratio between the maximum distance between the mean camber line and the chord line, measured

Figure 2.5.1 – Airfoil cross- section with geometrical definitions

perpendicular to the chord line, and then dividing by the chord and multiplying by 100 to give camber as a percentage such as "5% camber". For symmetrical wing segments, the chord line and the mean camber line are identical so camber is zero.

The airfoil angle of attack, α, is shown in Figure 2.5.2, together with the lift and drag. Note that by convention the lift always acts perpendicular to the flow direction. Since a wing may be composed of many different wing sections, the angles of attack of individual wing cross-sections may not be identical.
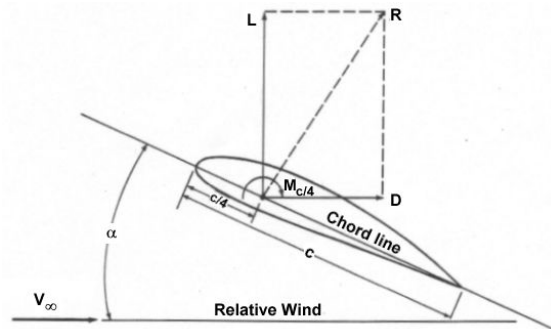
Figure 2.5.2 – Wing cross-section showing lift and drag forces and angle of attack as measured relative to the flow.

The angle of attack is sometimes confused with the *aircraft pitch angle*. As indicated in Figure 2.5.3, the pitch angle is measured from the *same* reference line as angle of attack (the chord line), but with respect to the *horizon*. Only when the aircraft is in straight and level flight are the aircraft pitch angle and wing angle of attack identical.

In subsonic flow, deflecting moving air around a surface traveling with respect to the air creates aerodynamic lift and a pitching moment, as shown in Figure 2.5.4. The aerodynamic lift, drag and pitching moments are functions of the aerodynamic pressures acting on the lifting surface. These pressures are, in turn, functions of the wing segment angle of attack.

Figure 2.5.3 – Pitch angle (shown as θ) and wing angle of attack , α, are not the same. http://www.aerospaceweb.org/

Lift is created by a phenomenon known as vorticity, a topic that we will discuss in Chapter 4. The key features of Figure 2.5.4 are: 1) the stagnation point on the leading edge where flow slows to zero; 2) the upper surface region in which flow speeds up; 3) the lower surface region
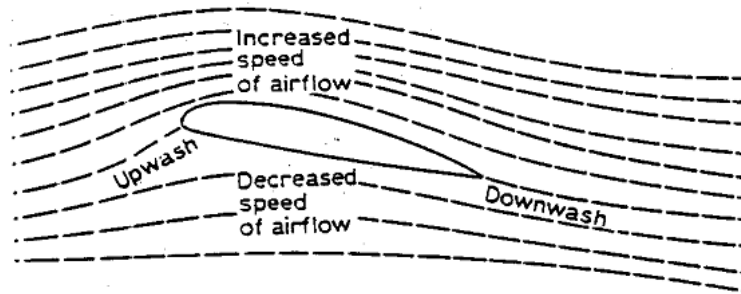
Figure 2.5.4 - Airflow around a wing section in subsonic flow. (Kermode, p. 72).

where flow slows; and 4) the trailing edge where the two flows come back together and have the same velocity.

Bernoulli's law requires that the sum of the static pressure and dynamic pressure ($\frac{1}{2}\rho V^2$, where ρ is the air density and V is the airspeed) be constant in an incompressible fluid flow. As the air speeds up over the upper surface the fluid static pressure must decrease so that a low pressure region forms there. The fluid speed is highest and the static pressure lowest near the upper surface of the forward part of the wing cross-section. On the bottom surface, the air slows, the static pressure increases and the net force upward increases to create lift.

Wing lift and drag and pitching moment depend upon: wing cross-section shape; wing planform shape; and, dynamic pressure, ½ ρV^2. The lift, drag, and pitching moment are denoted as *L, D,* and *M*, respectively; these three quantities are defined in terms of wing surface planform area, S, dynamic pressure, q, and *wing mean aerodynamic chord* $\bar{c}$ and *aerodynamic coefficients* as:

$$L = C_L q S \qquad\qquad (2.5.1a)$$

$$D = C_D q S \qquad\qquad (2.5.1b)$$

$$M = C_M q S \bar{c} \qquad\qquad (2.5.1c)$$

The force and moment *per unit length or per unit span* and are defined as:

$$l = c_l q \bar{c} \qquad\qquad (2.5.2a)$$

$$d = c_d q \bar{c} \qquad \text{(2.5.2b)}$$

$$m = c_m q \bar{c}^2 \qquad \text{(2.5.2c)}$$

These aerodynamic coefficients are functions of the wing angle of attack, Reynolds number, and Mach number.

The lift and drag coefficients for an example *airfoil* are shown in Figure 2.5.5. At angles up to 12°
this plot of the lift coefficient is almost a straight line. At about 15° the lift coefficient reaches a maximum and then declines with further increases in angle of attack as the wing segment loses lift or *stalls*.

Stall is associated with the breakdown or detachment of the streamlines around the wing. The shape of the cross-section makes little difference in the angle at which stall occurs, although it does affect the value of the maximum value of C_L (or c_l) achieved when stall occurs. Stalling is a function of angle of attack, not airspeed.
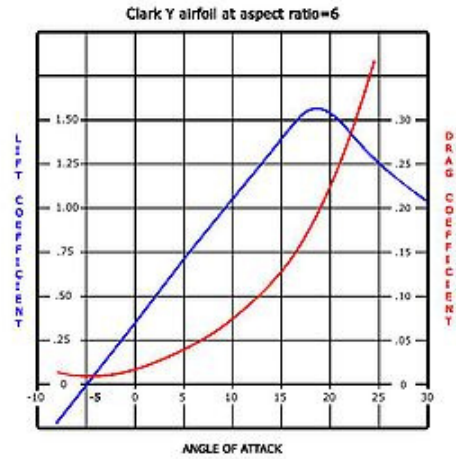
Figure 2.5.5 – Lift and drag coefficients c_L and c_D as functions of angle of attack for an example airfoil.

The linear portions of the airfoil lift and pitching moment curves are approximated by the expressions

$$c_l = c_{l_o} + \left(\frac{\partial c_l}{\partial \alpha} \right) \alpha = c_{l_o} + c_{l_\alpha} \alpha \qquad \text{(2.5.3)}$$

$$c_m = c_{m_o} + \left(\frac{\partial c_m}{\partial \alpha} \right) \alpha = c_{m_o} + c_{m_\alpha} \alpha \qquad \text{(2.5.4)}$$

The notation $(\ )_\alpha$ indicates partial differentiation with respect to angle of attack, α. The equation for c_m versus α depends upon the wing reference point location chosen to measuring the pitching moment.

Wing drag is due to friction drag on the exposed or *wetted area* of the surface (this drag is also called *parasite drag*). Drag on a wing (as opposed to an airfoil section) has an additional component called *induced drag* that depends on the lift coefficient magnitude. The analytical behavior of the drag coefficient is approximately quadratic for angles of attack within the linear region of the lift curve. This relationship is:

$$C_D = C_{D_o} + \left(\frac{\partial C_D}{\partial (\alpha^2)} \right) \alpha^2 \qquad \text{(2.5.5)}$$

where the angle α is measured from the position of zero lift. The term C_{D_o} is called the *parasite or zero lift drag coefficient*. Eqn. 2.5.5 is also written as:

$$C_D = C_{D_0} + (k)C_L^2 \qquad (2.5.6)$$

The second term in Eqns. 2.5.5 and 2.5.6 is the *induced drag* or *drag due to lift*. This induced drag only appears for wings with a finite aspect ratio (aspect ratio is defined as the span squared divided by the wing planform area) and becomes very small as the wing planform becomes more slender. If the aspect ratio is infinite, the induced drag is zero. This corresponds to the results for a two dimensional airfoil.

2.5.1 Reference points – the center of pressure

The wing segment or airfoil pitching moment is an integrated product of pressure and distance from an arbitrary reference point. Pitching moment depends on angle of attack and the point at which we measure the pitching moment. One position for measuring pitching moment is the *center of pressure*. At this point the resultant moment is zero. The pitching moment coefficient at any point x (x is measured aft of the wing leading edge) is $C_M = C_L x + C_{M_{leading\ edge}}$.

The condition $C_M(x) = 0$ defines the center of pressure position. Measured as a fraction of the wing segment chord aft of the leading edge, the center of pressure location is denoted as $\bar{x}_{cp}$ and given by the following equation,

$$\bar{x}_{cp} = \frac{x_{cp}}{c} = \frac{-C_{M_{leading\ edge}}}{C_L} \qquad (2.5.7)$$

Figure 2.5.6 plots the center of pressure position on a cambered airfoil as angle of attack changes. This plot indicates that at negative (nose down) angles of attack the center of pressure is near the rear of the airfoil. As the airfoil angle of attack increases, the center of pressure moves forward to near the 0.30 chord position and remains there until near stall when the center of pressure moves aft again as angle of attack increases. Figure 2.5.6 also shows data for a different reference point, *the aerodynamic center*.
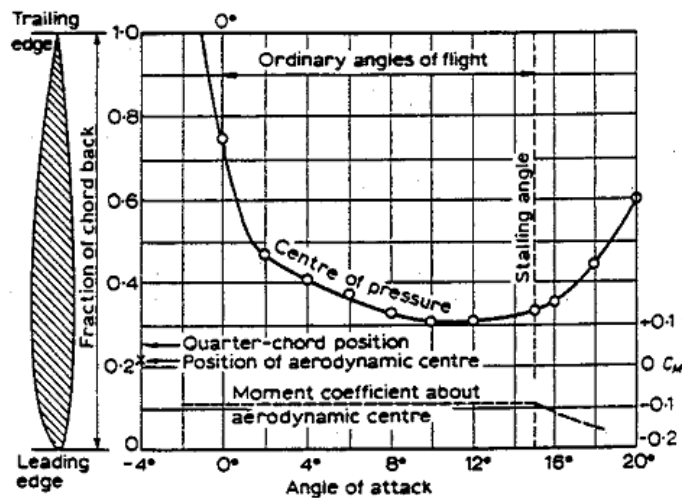
Figure 2.5.6 – Airfoil center of pressure & pitching moment coefficient at the aerodynamic center (Kermode)

Chapter 2

2.5.2 A different reference point - the aerodynamic center

There is a special point on an airfoil where the aerodynamic pitching moment does not change with angle of attack. This point is called the *aerodynamic center*. The aerodynamic center is the point on the wing chord *where the pitching moment does not change with angle of attack*. We write this relationship as:

$$\frac{\partial C_M}{\partial \alpha} = C_{M_\alpha} = 0 = \frac{\partial C_L}{\partial \alpha}\frac{x_{AC}}{c} + \frac{\partial C_{M_{leading\ edge}}}{\partial \alpha} \qquad (2.5.8)$$

Solving Eqn, 2.5.8 for $\bar{x}_{ac} = {x_{ac}}\big/{c}$ the aerodynamic center location aft (downstream) from the leading edge, as a fraction of the airfoil chord,

$$\bar{x}_{ac} = -\frac{\partial C_{M_{leading\ edge}}\big/ \partial \alpha}{\partial C_L \big/ \partial \alpha} = -\frac{C_{M_\alpha}(leading\ edge)}{C_{L_\alpha}} \qquad (2.5.9)$$

Both $C_{M_{leading\ edge}} = C_{Mo}$ and $\dfrac{\partial C_{Mo}}{\partial \alpha}$ are negative, so $\bar{x}_{ac}$ is positive.

To understand the difference between the center of pressure and the aerodynamic center, consider Figure 2.5.7 which plots the pitching moment coefficient on a cambered airfoil as its angle of attack increases. The pitching moment coefficient measured at the leading edge (the lower line) decreases as angle of attack increases. Meanwhile, measured at a point near the trailing edge, the pitching moment coefficient increases as angle of attack increases.

Figure 2.5.7 shows that the two straight lines measuring the pitching moment about both the leading edge and a point near the trailing edge intersect. This intersection point is special because it occurs at zero airfoil lift. *This special value of the pitching moment coefficient (it is not zero if the airfoil is cambered) is the pitching moment coefficient measured about the aerodynamic center position defined in Eqn. 2.5.9.* If the airfoil is symmetrical, the pitching moment at zero when the airfoil angle of attack is zero.
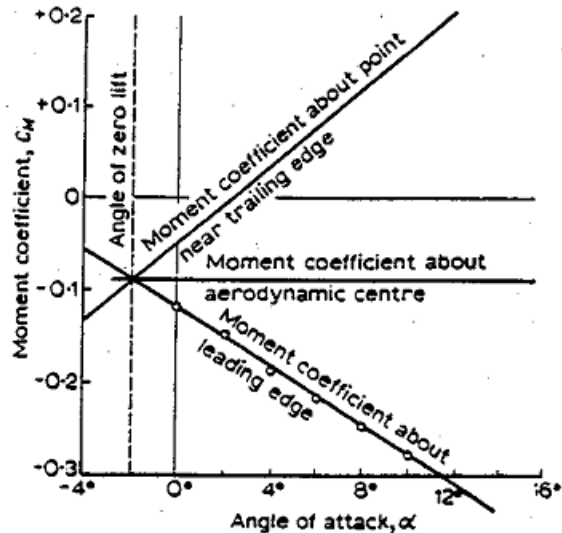
Figure 2.5.7 – Airfoil pitching moment coefficient about three reference points (Kermode).

Returning to Figure 2.5.6 we see that the aerodynamic center position for the

example airfoil is near the airfoil ¼ chord position and that, at this position, the pitching moment is slightly negative, but constant until near stall. *If the airfoil is very thin and the flow is incompressible, aerodynamic theory places the aerodynamic center exactly at the ¼ chord position.* In addition, for symmetrical airfoils, the constant pitching moment is identically zero.

The major difference between Eqn. 2.5.7, which uses the total lift and pitching moment about the leading edge, and Eqn. 2.5.9, which uses aerodynamic coefficient derivatives (rates of change with α) with respect to the angle of attack, α, is that the reference position changes when we use the center of pressure, even though we eliminate the aerodynamic moment from static equilibrium calculations. *Aeroelastic problems are concerned with the effects of changes in aerodynamic loads due to lifting surface deflections.* As a result, the early aeroelasticity researchers found using the aerodynamic center as a reference point for aerodynamic calculation more useful than the center of pressure. We will also use this point as our reference in the models developed in the next section.

2.6 Lifting surface flexibility and lift generation-the typical section model

In this section we introduce the typical section model used by aeroelasticians for at least eight decades. The model used in this book differs slightly from this historic model in that it has a finite span, as will be explained in this section.
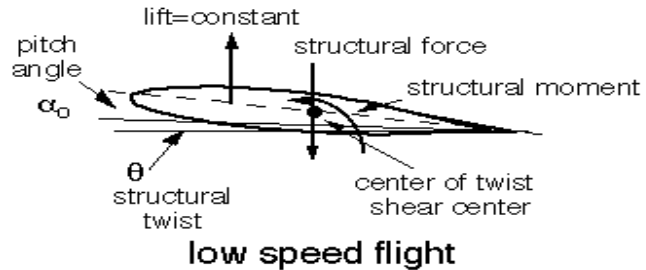
Figure 2.6.1 - Wing section twist in low speed flight

To begin, consider Figures 2.6.1 and 2.6.3 which show two cross-sections. Figure 2.6.1 shows a *symmetrical wing segment* with the lift acting at the aerodynamic center, but with no pitching moment about that point. Figure 2.6.2 shows the same segement but with camber so that the pitching moment about the aerodynamic center is not zero. Both segments have a length dimension (span) that goes into the paper; *these segments have a planform area, denoted as S*. The wings section is mounted in the wind tunnel and securely restrained by a structure that resists upward movement and twisting.
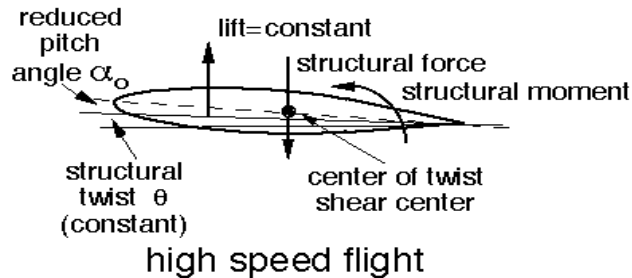
Figure 2.6.2- Wing section twist in high speed flight makes up most of the required angle of attack.

Consider the symmetrical section first. As indicated in the free body diagram shown in Figure 2.6.2, the pitching moment about the aerodynamic center is zero since the section is symmetrical, but the wing will twist because the resultant lift vector at the aerodynamic center does not pass through the shear center. The total wing segment incidence is the sum of the elastic twist angle θ and the angle of attack α_o input by the wind tunnel operator. The sum of these two angles is small, only a few degrees.

Chapter 2

If the wing lift is equal to the airplane weight then the lift is constant when the airplane weight is constant. As a result, the wing lift produces a twisting moment about the wing cross-section *shear center* that is also constant, no matter what the airspeed. If we go faster, the dynamic pressure increases and lift will increase if we do not reduce the wing angle of attack, α_o.

Let's now add wing camber and consider the idealized *unsymmetrical* wing model with planform area, *S*, in Figure 2.6.3. The structural stiffness is represented by a spring, K_h, that resists wing upward (bending) translation and a torsion spring, K_T, that resists wing twist. Historically, the bending deflection has been called *plunge* (denoted as *h* in Figure 2.6.3 and measured at the shear center) with the positive direction is downward at the shear center. *The shear center thus becomes our structural reference point.*
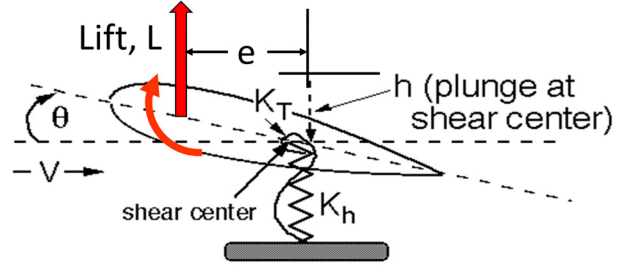
Figure 2.6.3 – Unsymmetrical wing with pitch and plunge degrees of freedom and pitch and plunge springs, showing offset distance, e, between lift and shear center and pitching moment at the aerodynamic center

This structural model is similar to the model used previously in Figure 2.4.1. Here, we model the action of the two springs in Figure 2.4.1 as a single spring to resist torsion and a single spring to resist plunge. As a result,

$$K_h = K_1 + K_2 \text{ (plunge spring)} \qquad (2.6.1)$$

$$K_T = \frac{K_1 + K_2(a+b)^2}{K_1 + K_2} \quad \text{(pitch spring)} \qquad (2.6.2)$$

When the operator gives the wing an angle of attack, α_o, this model generates aerodynamic lift *L* and a pitching moment *M* (about the shear center). *L* and *M* are functions of both the known quantity α_o and the unknown twist, θ.

$$L = qSC_{L_\alpha}(\alpha_0 + \theta) \qquad (2.6.3)$$

$$M_{SC} = M_{AC} + Le \qquad (2.6.4)$$

or

$$M_{SC} = qcSC_{MAC} + qSeC_{L_\alpha}(\alpha_0 + \theta) \qquad (2.6.5)$$

The two external loads in Eqns. 2.6.3 and 2.6.5 are written in matrix form as:

$$\begin{Bmatrix} -L \\ M_{SC} \end{Bmatrix} = qSC_{L_\alpha} \begin{bmatrix} 0 & -1 \\ 0 & e \end{bmatrix} \begin{Bmatrix} h \\ \theta \end{Bmatrix} + qSC_{L_\alpha}\alpha_o \begin{Bmatrix} -1 \\ e \end{Bmatrix} + qScC_{MAC} \begin{Bmatrix} 0 \\ 1 \end{Bmatrix} \qquad (2.6.6)$$

The static equilibrium equation that defines the relationships between the aerodynamic force and moment (L and M) and the shear center deflection, h, and the twist rotation, θ, is:

$$
\begin{bmatrix} K_h & 0 \\ 0 & K_T \end{bmatrix} \begin{Bmatrix} h \\ \theta \end{Bmatrix} = \begin{Bmatrix} -L \\ M \end{Bmatrix}
\tag{2.6.7}
$$

The loads expression in Eqn. 2.6.6 is substituted into the static equilibrium equation, Eqn.2.6.7, to give:

$$
\begin{bmatrix} K_h & 0 \\ 0 & K_T \end{bmatrix} \begin{Bmatrix} h \\ \theta \end{Bmatrix} = qSC_{L_\alpha} \begin{bmatrix} 0 & -1 \\ 0 & e \end{bmatrix} \begin{Bmatrix} h \\ \theta \end{Bmatrix} + qSC_{L_\alpha} \alpha_o \begin{Bmatrix} -1 \\ e \end{Bmatrix} + qScC_{MAC} \begin{Bmatrix} 0 \\ 1 \end{Bmatrix}
\tag{2.6.8}
$$

Gathering all of the *deflection dependent terms* on the left hand side of Eqn. 2.6.8, we have

$$
\begin{bmatrix} K_h & 0 \\ 0 & K_T \end{bmatrix} \begin{Bmatrix} h \\ \theta \end{Bmatrix} - qSC_{L_\alpha} \begin{bmatrix} 0 & -1 \\ 0 & e \end{bmatrix} \begin{Bmatrix} h \\ \theta \end{Bmatrix} = qSC_{L_\alpha} \alpha_o \begin{Bmatrix} -1 \\ e \end{Bmatrix} + qScC_{MAC} \begin{Bmatrix} 0 \\ 1 \end{Bmatrix}
\tag{2.6.9}
$$

In Eqn. 2.6.9 the right hand side contains the inputs and the left hand side has the unknown output, θ. The 2x2 matrix proportional to aerodynamic pressure, q, and the section displacements is called the *aerodynamic stiffness matrix*. While the structural stiffness matrix is symmetrical and h and θ are decoupled, the aerodynamic stiffness matrix is unsymmetrical and h and θ are coupled.

To solve for h and θ, first combine terms and then divide each term in Eqn. 2.6.9 by K_T.

$$
\begin{bmatrix} {K_h}/{K_T} & {qSC_{L_\alpha}}/{K_T} \\ 0 & 1 - {qSeC_{L_\alpha}}/{K_T} \end{bmatrix} \begin{Bmatrix} h \\ \theta \end{Bmatrix} = \frac{qSC_{L_\alpha}\alpha_o}{K_T} \begin{Bmatrix} -1 \\ e \end{Bmatrix} + \frac{qScC_{MAC}}{K_T} \begin{Bmatrix} 0 \\ 1 \end{Bmatrix}
\tag{2.6.10}
$$

The wing plunge displacement, h, and twist angle, θ, are found by inverting the matrix on the left side of Eqn. 2.6.10 and multiplying both sides by this inverse.

$$
\begin{Bmatrix} h \\ \theta \end{Bmatrix} = \frac{qSC_{L_\alpha}\alpha_o}{K_T} \begin{bmatrix} {K_T}/{K_h} & \dfrac{-qSC_{L_\alpha}/K_h}{1 - {qSeC_{L_\alpha}}/{K_T}} \\ 0 & \dfrac{1}{1 - {qSeC_{L_\alpha}}/{K_T}} \end{bmatrix} \begin{Bmatrix} -1 \\ e \end{Bmatrix} + \frac{qScC_{MAC}}{K_T} \begin{bmatrix} {K_T}/{K_h} & \dfrac{-qSC_{L_\alpha}/K_h}{1 - {qSeC_{L_\alpha}}/{K_T}} \\ 0 & \dfrac{1}{1 - {qSeC_{L_\alpha}}/{K_T}} \end{bmatrix} \begin{Bmatrix} 0 \\ 1 \end{Bmatrix}
$$

or

Chapter 2

$$\begin{Bmatrix} h \\ \theta \end{Bmatrix} = \frac{qSC_{L_\alpha}\alpha_o}{K_T} \begin{Bmatrix} -K_T/K_h - \dfrac{qSeC_{L_\alpha}/K_h}{1 - qSeC_{L_\alpha}/K_T} \\[4ex] \dfrac{e}{1 - qSeC_{L_\alpha}/K_T} \end{Bmatrix} + \frac{qScC_{MAC}}{K_T} \begin{Bmatrix} \dfrac{-qSC_{L_\alpha}/K_h}{1 - qSeC_{L_\alpha}/K_T} \\[4ex] \dfrac{1}{1 - qSeC_{L_\alpha}/K_T} \end{Bmatrix}$$

(2.6.11a)

This relationship is also written as:

$$\begin{Bmatrix} h \\ \theta \end{Bmatrix} = \begin{Bmatrix} \dfrac{-qSC_{L_\alpha}/K_h}{1 - qSeC_{L_\alpha}/K_T} \\[4ex] \dfrac{qSeC_{L_\alpha}}{K_T} \\ \dfrac{}{1 - qSeC_{L_\alpha}/K_T} \end{Bmatrix} \alpha_o + \frac{qScC_{MAC}}{K_T} \begin{Bmatrix} \dfrac{-qSC_{L_\alpha}/K_h}{1 - qSeC_{L_\alpha}/K_T} \\[4ex] \dfrac{1}{1 - qSeC_{L_\alpha}/K_T} \end{Bmatrix}$$

(2.6.11b)

The plunge displacement, h, and the wing twist angle, θ, are composed of two parts, one due to section angle of attack and the other due to wing camber:

$$h = \left(\frac{-qSC_{L_\alpha}/K_h}{1 - qSeC_{L_\alpha}/K_T} \right) \alpha_o - \frac{qScC_{MAC}}{K_T} \left(\frac{qSC_{L_\alpha}/K_h}{1 - qSeC_{L_\alpha}/K_T} \right)$$

(2.6.12)

$$\theta = \left(\frac{\dfrac{qSeC_{L_\alpha}}{K_T}}{1 - qSeC_{L_\alpha}/K_T} \right) \alpha_o + \frac{qScC_{MAC}}{K_T} \left(\frac{1}{1 - qSeC_{L_\alpha}/K_T} \right)$$

(2.6.13)

Substituting the expression for elastic twist, Eqn. 2.6.13, into the expression for lift, Eqn. 2.6.3, we have the expression for wing lift, again composed of two parts from two sources.

$$L = \left(\frac{qSC_{L_\alpha}}{1 - qSeC_{L_\alpha}/K_T} \right) \alpha_o + \left(\frac{qSC_{L_\alpha}}{1 - qSeC_{L_\alpha}/K_T} \right) \left(\frac{qScC_{MAC}}{K_T} \right)$$

(2.6.14)

Note the presence of a nondimensional "aeroelastic parameter" in Eqn. 2.6.13 and Eqn. 2.6.14. Both Eqn. 2.6.13 and Eqn. 2.6.14 have denominators that tend to zero as the nondimensional

aeroelastic parameter $qSeC_{L_\alpha} \big/ K_T$ *tends to 1.* The value of dynamic pressure at which this occurs, $q_D = K_T \big/ SeC_{L_\alpha}$, is called the *divergence dynamic pressure* and is a subject of discussion and derivation in ensuing sections. With low torsional stiffness K_T, the term in the denominator of Eqn. 2.6.14 can be small, creating large deflections, even for small angles of attack. If this is so then the wing response (plunge and twist) will be very large for small loads.

When the wing cross-section is symmetrical ($C_{MAC} = 0$) the lift expression simplifies to a single term.

$$L = \left(\frac{qSC_{L_\alpha}}{1 - qSeC_{L_\alpha} \big/ K_T} \right) \alpha_o \qquad (2.6.15)$$

The required angle of attack to generate lift equal to weight is

$$\alpha_o = \frac{L}{qSC_{L_\alpha}} \left(1 - qSeC_{L_\alpha} \big/ K_T \right) \qquad (2.6.16)$$

In this case the wing twist is constant, as discussed earlier:

$$\theta = \left(\frac{\frac{qSeC_{L_\alpha}}{K_T}}{1 - qSeC_{L_\alpha} \big/ K_T} \right) \alpha_o = \left(\frac{\frac{qSeC_{L_\alpha}}{K_T}}{1 - qSeC_{L_\alpha} \big/ K_T} \right) \left(\frac{L}{qSC_{L_\alpha}} \right) \left(1 - qSeC_{L_\alpha} \big/ K_T \right) = Le \qquad (2.6.17)$$

Notice that, from Eqn. 2.6.16) the input angle of attack is zero when $q = q_D = \dfrac{K_T}{SeC_{L_\alpha}}$. In this special case all the wing lift is generated by structural twist, θ. The reasons for this strange result will revisited when we discuss wing divergence in a later section.

A comment on the typical section model used in this text

At the beginning of this section we mentioned that the typical section used in this text is slightly different than the typical section used by early aeroelasticians. If the wing is nonuniform, with a tapered chord for instance, then aeroelasticians would go to a point located at the wing ¾ span position. They would then measure or estimate aerodynamic data for that section, in particular, the section chord, the section lift curve slope, section aerodynamic center position. The section would have a unit span so its planform area is simply S=c*1.

The difference between the historical model and the model we have discussed is that the *structural coefficients were stiffnesses per unit span*. In our case then these stiffnesses would be

$K_h \big/ b$ *and* $K_T \big/ b$ where the dimension b is the semi-span. Placing these terms into our formula

then we have $q_D = K_T \big/ becC_{L_\alpha} = K_T \big/ SeC_{L_\alpha}$. The result is the same if the wing lift curve slope and

the ¾ span lift curve slope is the same and the wing has no taper. From an educational standpoint the author prefers to see a wing slab moving in the air and supported by concentrated as opposed to distributed springs. This subject will come up again in Chapter 4 when we consider the dynamics of the wing.

A sidebar – why the ¾ semi-span position?

Why was the geometry and aerodynamic properties of the ¾ span position thought of as "typical?"
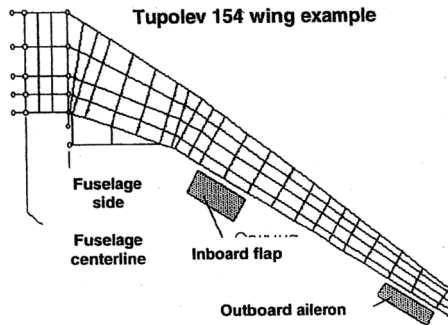
Figure 2.6.4 - Tu-154 wing structural idealization with two flaps
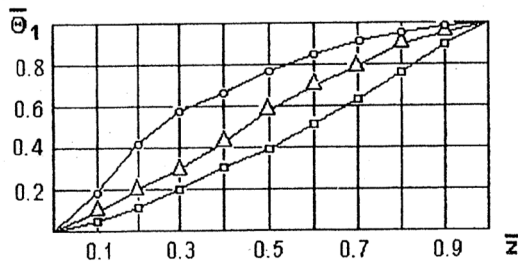
Figure 2.6.5 – Tu-154 wing twist with respect to the freestream for three loading conditions, nondimensionalized with respect to the tip twist in each case .

To determine what is special about the ¾ chord position a group of Russian researchers examined the static aeroelastic behavior of a tapered Tupolev 154 swept wing with two flaps shown in Figure 2.6.4. Three separate load conditions were used to compute three different wing twist distributions. The first condition was a one-g loading, the second was deflection of the inboard flap while the third condition was deflection of the outboard flap. The twist distributions for the load three cases are shown in Figure 2.6.5, nondimensionalized so that the maximum value in each case is 1. There is nothing remarkable about the twist values at the ¾ span position. They are all different, as we would expect.

When the wing twist in each case is divided by the integral of the twist distribution (different for each case) a distribution defined as

$$\bar{\theta}_i(z) = \frac{\theta_i(z)}{\int_0^b \theta_i(z)dz} \quad (i=1,2,3) \text{ is plotted in Figure}$$

2.6.6. The integrals are a measure of the total twist in each of the three cases and are different in all three cases. In this case the curves intersect near the ¾ span point.

Figure 2.6.6 shows similar plots and results for a low wing span supersonic transport for five different loading conditions. In this case the curves intersect near the 0.82 semi-span position.
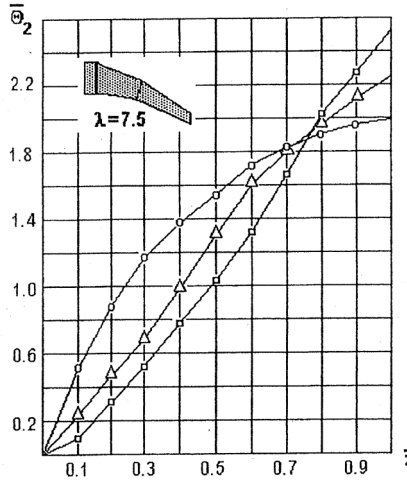
Figure 2.6.6 – Tu-154 streamwise twist for three load conditions plotted as twist divided by the integral of twist.
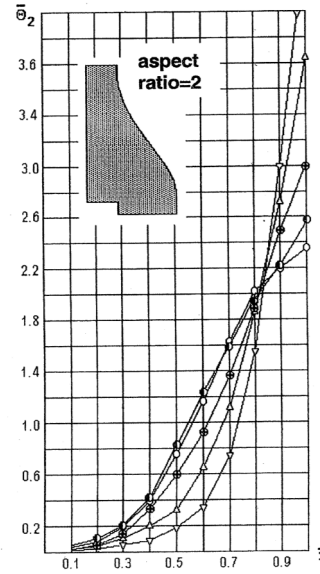
Figure 2.6.7 – Russian SST streamwise twist for five different subsonic loading conditions, nondimensionalized with respect to integral of twist.

2.7 Example problem – The effect of elastic axis offset on wing lift effectiveness and divergence

The idealized wing whose cross-section is shown in Figure 2.7.1 will be tested in the wind tunnel at several different airspeeds at sea level conditions and at such low speeds that the flow field is incompressible. The position of the wing box indicated in Figure 2.7.1 can be moved to change the wing shear center position and the offset distance between the shear center and the aerodynamic center. For instance, when the shear center is at the mid-chord, when the shear center is at the wing mid-chord the offset distance e is equal to c/4. Wind tunnel tests show that the wing divergence dynamic pressure is 100 lb / ft^2. at this wing box position.
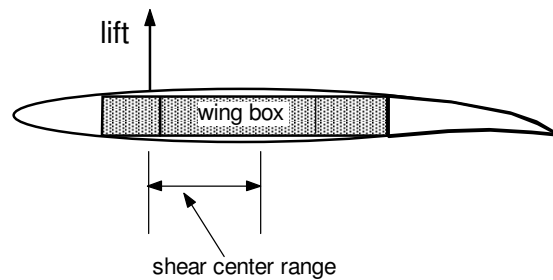
Figure 2.7.1 - Wind tunnel wing segment model cross-section

The aerodynamicist predicts that the ratio of C_{MAC} to $C_{L\alpha}$ is -0.075 and the wing lift curve slope is 4.0; the reference planform area is $S = 10$ $ft.^2$. The section angle of attack α_o for all tests will be pre-set to 3°.

Chapter 2

Problem

a) Develop the expression for the lift force when the shear center is located at the mid-chord. Find the twist angle θ as a function of wind tunnel airspeed. Plot lift and twist angle vs. airspeed.

b) Consider the same wing segment with different wing shear center locations. The offset distance $e_o = c/4$ when the shear center is located at the mid-chord in part (a) is used as the reference. We use e_i to denote the shear center/aerodynamic center offset for other shear center positions. Develop the equations for wing lift L and twist θ as functions of the ratio e_i/e_o. The divergence speed will change with changes in e_i/e_o. Plot lift and twist angle vs. airspeed for e_i/e_o values of 0, 0.25, 0.50 and 0.75.

Solution

(a) Begin by solving for the wing divergence speed. We know (by combining Eqn. 2.6.18 with given data) that the divergence speed when the shear center is at the mid-chord is:

$$q_{D0} = \frac{K_T}{Se_o C_{L_\alpha}} = 100 \, {lb}/{ft.^2}$$

(2.7.1)

From the definition of dynamic pressure, $q = \frac{1}{2}\rho V^2$

$$V_{D0} = \sqrt{\frac{2q_{D0}}{\rho_0}} = \sqrt{\frac{200}{0.0023769}} = 290.1 \, {ft.}/{sec.}$$

(2.7.2)

Using Eqns. 2.6.13 and 2.6.18 the twist angle formula becomes:

$$\theta_o = \left(\frac{q}{q_{Do}}\right)\left(\frac{\alpha_o + \left(c/e_o\right)\left(C_{MAC}/C_{L_\alpha}\right)}{1 - \left(q/q_{Do}\right)}\right) = \left(\frac{V}{V_{Do}}\right)^2 \left(\frac{\alpha_I}{1 - \left(\frac{V}{V_{Do}}\right)^2}\right)$$

(2.7.3)

where the effective initial angle of attack α_I is:

$$\alpha_I = \alpha_o + \left(\frac{c}{e_o}\right)\left(\frac{C_{MAC}}{C_{L_\alpha}}\right) = -0.2476$$

(2.7.4)

As a result the twist angle will always be negative. Substituting Eqns. 2.7.2 and 2.7.4 into Eqn. 2.7.3, the twist angle expression is

$$\theta = \left(\frac{V}{290.1}\right)^2 \left(\frac{-0.2476}{1 - \left(\frac{V}{V_{Do}}\right)^2}\right) \tag{2.7.5}$$

or
$$\theta = -0.29421x10^{-5}\left(\frac{V^2}{1 - \left(V\big/V_{Do}\right)^2}\right) \tag{2.7.6}$$

Lift is composed of two different terms, the lift due to the initial angle of attack and the twist angle due to both angle of attack and camber. The lift expression computed from Eqn. (2.6.14) is

$$L_o = \left(\frac{qSC_{L_\alpha}}{1 - \dfrac{q}{q_{D0}}}\right)\left(\alpha_o + \left(\frac{q}{q_{D0}}\right)\left(\frac{c}{e_o}\right)\frac{C_{MAC}}{C_{L_\alpha}}\right) \tag{2.7.7}$$

Substituting our data we find the lift when the shear center is at the mid-chord to be:

$$L_o = \left(\frac{qSC_{L_\alpha}}{1 - \left(\frac{V}{V_{Do}}\right)^2}\right)\left(0.05236 - 0.3\left(\frac{V}{V_{Do}}\right)^2\right) \tag{2.7.8}$$

Using the expansion $qSC_{L_\alpha} = \dfrac{q}{q_o}\left(q_o SC_{L_\alpha}\right) = \dfrac{q}{q_o}\left(100*10*4\right)$ we have

$$L_o = \left(\frac{q}{q_{Do}}\right)\left(\frac{100*10*4}{1 - \left(\frac{V}{V_{Do}}\right)^2}\right)\left(0.05236 - 0.3\left(\frac{V}{V_{Do}}\right)^2\right) \tag{2.7.9}$$

The final result is

$$L_o = \left(\frac{\left(\frac{V}{V_{Do}}\right)^2}{1 - \left(\frac{V}{V_{Do}}\right)^2}\right)\left(209.44 - 1200\left(\frac{V}{V_{Do}}\right)^2\right) \tag{2.7.10}$$

(b) Examine the effect of different shear center/aerodynamic center offsets on the amount of twist and lift generated. When the offset between the aerodynamic center and the shear center is e_i the divergence dynamic pressure is:

$$q_{Di} = \frac{K_T}{Se_iC_{L_\alpha}}$$

(2.7.11)

The reference divergence dynamic pressure is given as:

$$q_{D0} = \frac{K_T}{Se_oC_{L_\alpha}} = 100 \ psf.$$

(2.7.12)

The ratio of these two divergence dynamic pressures is

$$\frac{q_{Di}}{q_{D0}} = \frac{e_o}{e_i} = \frac{V_{Di}^2}{V_{D0}^2}$$

(2.7.13)

Using Eqns. 2.7.3 and 2.7.13, the twist angle for an arbitrary shear center position is:

$$\theta_i = \left(\frac{V}{V_{Do}}\right)^2 \left(\frac{e_i}{e_o}\right) \left(\frac{\alpha_o + \left(c/e_i\right)\left(C_{MAC}/C_{L_\alpha}\right)}{1 - \left(\frac{V}{V_{Do}}\right)^2 \left(\frac{e_i}{e_o}\right)}\right)$$

(2.7.14)

The lift on the wing is

$$L_i = qSC_{L_\alpha}\alpha_o + qSC_{L_\alpha}\left(\frac{V}{V_{Do}}\right)^2 \left(\frac{\left(\frac{e_i}{e_o}\right)\alpha_o + \left(c/e_o\right)\left(C_{MAC}/C_{L_\alpha}\right)}{1 - \left(\frac{e_i}{e_o}\right)\left(\frac{V}{V_{Do}}\right)^2}\right)$$

or (2.7.15)

$$L_i = \frac{qSC_{L_\alpha}}{1 - \left(\frac{e_i}{e_o}\right)\left(\frac{V}{V_{Do}}\right)^2}\left(\alpha_o + \left(\frac{V}{V_{Do}}\right)^2 \left(\frac{c}{e_o}\right)\left(\frac{C_{MAC}}{C_{L_\alpha}}\right)\right)$$

Plots of twist angle and lift are shown in Figures 2.7.2 and 2.7.3. Note that even though the structural twist is always negative, at low speeds wing lift increases as airspeed increases. At higher speeds lift decreases dramatically. Note however that this example does not allow the wing angle of attack to change with airspeed.
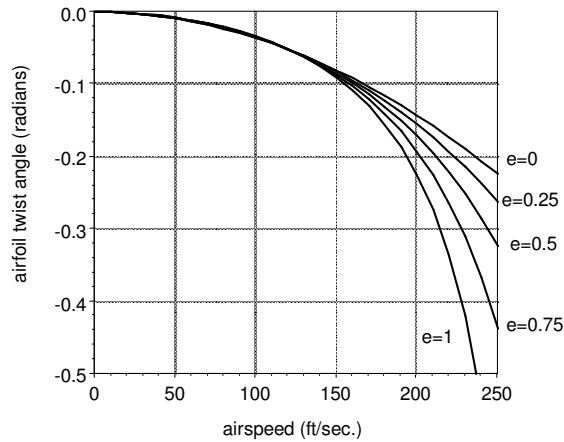
Figure 2.7.2 - Elastic twist angle vs. airspeed for 4 different ratios of elastic axis offset
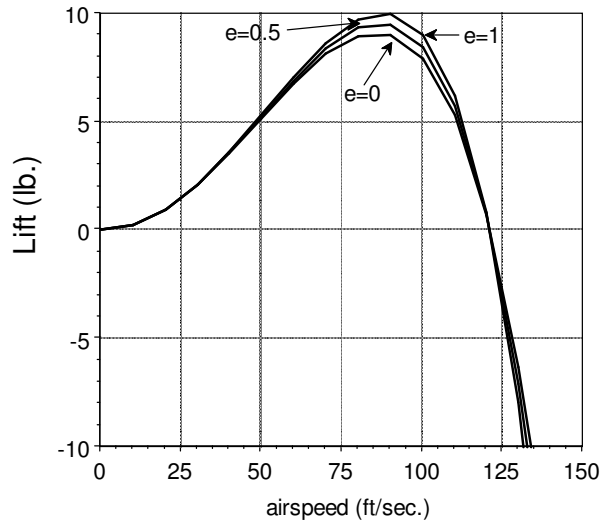
Figure 2.7.3 - Lift vs. airspeed for 3 different ratios of elastic axis offset

2.8 Using the typical section model to understand early monoplane aircraft structural failures

When $e=0$, the wing twist is $\theta = \dfrac{qScC_{MAC}}{K_T}$. The wing lift is $L = qSC_{L_\alpha}\left(\alpha_o + \dfrac{qScC_{MAC}}{K_T}\right)$. Notice that the wing lift depends on θ, but θ does not depend on the lift because there is no offset between the aerodynamic center and the shear center. This is a special case, not often encountered in aircraft designs. The Langley Aerodrome was one of these exceptions.

The first monoplane wing designs had low torsional stiffness to permit wing warping control. Their wing segment sections also had substantial camber, creating a large nose down (negative) pitching moment. The effect of the nose down pitching moment on wing twist is seen in the second term in Eqns. 2.6.14 and 2.7.15. When the angle of attack is zero, this initial twist induced angle of attack is

$$\alpha_M = \frac{qScC_{MAC}}{K_T} \tag{2.8.1}$$

The term C_{MAC} becomes more negative as camber increases. The twist due to camber becomes more negative as airspeed increases; its effect on lift is amplified by aeroelastic interaction.

Garrick and Reed[14] believe that this situation may explain why one of Langley's *Aerodrome's* crashed on take-off from its houseboat launch platform. Since the *Aerodrome* wing camber was large, a large nose-down pitching moment was placed on the torsionally flexible wings. Even though the shear center and aerodynamic center were close together so that the offset distance *e* was nearly zero, the nose-down twist placed a downward load on the wing instead of the upward load the Langley expected. Thus structural flexibility, but not aeroelastic interaction, gave the first flight prize to the Wright Brothers.

The first term in Eqn. 2.6.14 is the lift due to an input angle of attack. The effect of the lift curve slope C_{L_α} is amplified by the aeroelastic term

$$\frac{1}{1 - \dfrac{qSeC_{L_\alpha}}{K_T}} \tag{2.8.2}$$

The amplification term increases with increasing airspeed when the aerodynamic center and the shear center are offset and the AC is ahead of the shear center, the usual case for subsonic aircraft.

The wing angle of attack α_o necessary to generate lift to support one-half the airplane weight W in level flight is

$$L = \frac{W}{2} = qS\tilde{C}_{L_\alpha}\alpha_o + qS\tilde{C}_{L_\alpha}\alpha_M \tag{2.8.3}$$

where

$$\tilde{C}_{L_\alpha} = \frac{C_{L_\alpha}}{1 - \dfrac{qSeC_{L_\alpha}}{K_T}} \tag{2.8.4}$$

Solving for the wing angle of attack α_o we have

$$\alpha_o = \frac{1}{2}\left(\frac{W}{S}\right)\left(\frac{1-\bar{q}}{qC_{L_\alpha}}\right) - \alpha_M \tag{2.8.5}$$

with $\bar{q} = \dfrac{qSeC_{L_\alpha}}{K_T}$ and, as before, $\alpha_M = \dfrac{qScC_{MAC}}{K_T}$.

Equation 2.8.5 indicates that, for a wing with a symmetrical wing segment section ($\alpha_M = 0$), the pilot will have to reduce the wing attitude as dynamic pressure increases, but the angle must be increased if $\alpha_M < 0$, the case for an unsymmetrical wing cross-section.

2.9 Load factor sensitivity to aeroelastic effects-fatal changes in response

In Chapter 1 we mentioned that, in 1912, the British War Office banned Royal Flying Corps pilots from flying monoplanes after a series of accidents involving the Bristol Prier monoplane. Thurston (Reference 2) asserts that the cause of these accidents was overloading the brace wires. Even if we accept this conclusion, the cause of the overload may be aeroelastic. Some witnesses to these incidents reported in-flight explosions. Our simple model explains these incidents in which airplanes with small torsional stiffness could easily overload the wings when flying at high speed.

A slight change in wing angle of attack will increase the wing load substantially when we fly at "high" dynamic pressure. Our typical section model defines "high" in terms of the parameter $\bar{q} = qSeC_{L_\alpha}/K_T$. When $\bar{q}$ is near $\bar{q} = 1$ then the dynamic pressure is high.

To show this, differentiate the lift expression, Eqn. 2.8.3, with respect to the angle of attack α_o to obtain

$$\frac{\partial L}{\partial \alpha_o} = \frac{qSC_{L_\alpha}}{1 - \bar{q}} \qquad (2.9.1)$$

The *aircraft load factor, n*, is defined as $n = \dfrac{L}{W}$. When $n=1$ the airplane is in straight, level flight. From Eqn. 2.9.1, the change in aircraft load factor with wing angle of attack α_o is:

$$\frac{\partial \, L/W}{\partial \alpha_o} = \frac{\partial \, n}{\partial \alpha_o} = \frac{qC_{L_\alpha}}{\left(W/S\right)\left(1 - \bar{q}\right)} \qquad (2.9.2)$$

Equation 2.9.2 shows that the increased load factor due to a change in aircraft attitude from a pilot input will increase with increasing aeroelastic interaction (increasing values of $\bar{q}$). The load on an airplane wing flying close to the divergence speed $\bar{q}_D = qSeC_{L_\alpha}/K_T$ will be extremely sensitive to small changes in angle of attack.

2.10 A simple single degree of freedom (torsion only) aeroelastic model

In the last three sections we have developed a two-degree-of-freedom analytical model to demonstrate how aerodynamics and structures interact on an unswept wing. Although the typical section model has bending (plunge) freedom as well as torsional freedom, only the twisting deformation interacts with the aerodynamic loads. This interaction creates bending but the bending does no create further aerodynamic loads. We also found that there is a nondimensional aeroelastic parameter that controls the interaction process. When this parameter has a value close to unity we find that the wing deflection becomes extremely large. We called this special point "divergence."

In this section and others to follow we will examine divergence and find that it is a static aeroelastic instability. To solve for this special point we need to understand more about the mathematical

features of a general divergence problem and also understand the origins of aeroelastic stiffness related problems.

To focus on static aeroelastic stability issues we will use the modified idealized wing, with planform, S, mounted on a torsional spring, as shown in Figure 2.10.1. The translation spring K_h and the plunge degree of freedom
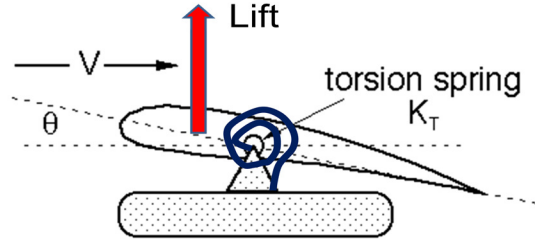
Figure 2.10.1 - Pin mounted wing segment with torsion spring restraint

are removed and replaced by a frictionless pin is inserted at the shear center. A torsion spring is inserted at the shear center to resist the aerodynamic moment. The wing has an initial angle of attack, α_0 and twist θ.

As before, the aerodynamic moment about the shear center in Figure 2.10.1 is M_a,

$$M_a = Le + M_{AC}$$

with

$$M_{AC} = qcSC_{MAC}$$

The wing lift, L, is

$$L = qSC_{L_\alpha}(\alpha_0 + \theta)$$

The elastic restoring torque of the torsion spring is M_S, defined as $M_S = K_T\theta$ in the counterclockwise direction. The unknown elastic twist angle, θ, is again found from the equation of torque static equilibrium written about the shear center. Summing moments at the pinned shear center gives

$$\sum M_{SC} = M_s - M_a = 0$$

or

$$\sum_{\substack{positive \\ clockwise}} M_{\substack{shear \\ center}} = K_T\theta - qSeC_{L_\alpha}(\alpha_o + \theta) - qScC_{MAC} = 0 \qquad (2.10.1)$$

Solving for θ, we find $\theta = \dfrac{qSeC_{L_\alpha}\left(\alpha_0 + \left(\dfrac{c}{e}\right)\left(\dfrac{C_{MAC}}{C_{L_\alpha}}\right)\right)}{K_T - qSeC_{L_\alpha}}$. Divide both the numerator and denominator by K_T to obtain

$$\theta = \frac{\left(\dfrac{qSeC_{L_\alpha}}{K_T}\right)\alpha_I}{\left(1 - \dfrac{qSeC_{L_\alpha}}{K_T}\right)} \qquad (2.10.2)$$

where

$$\alpha_I = \alpha_o + \left(\frac{c}{e}\right)\left(\frac{C_{MAC}}{C_{L_\alpha}}\right) \qquad (2.10.3)$$

Once again, the size of the aeroelastic term $\bar{q} = qSeC_{L_\alpha}\big/ K_T$ is very important because, as $\bar{q}$ approaches unity, θ will approach infinity if the angle of attack is not reduced. Aeroelastic divergence occurs when the dynamic pressure, $\bar{q}$, equals $\bar{q}_D = 1$, where

$$q_D = K_T \big/ SeC_{L_\alpha} \qquad (2.10.4)$$

The wing lift is
$$L = qSC_{L_\alpha}\left(\alpha_o + \frac{(q/q_D)\alpha_I}{1 - \dfrac{q}{q_D}}\right)$$

or

$$L = \frac{qSC_{L_\alpha}}{1-\bar{q}}\left(\alpha_o + \left(\frac{q}{q_D}\right)\left(\frac{c}{e}\right)\left(\frac{C_{MAC}}{C_{L_\alpha}}\right)\right) \qquad (2.10.5)$$

Equation 2.10.5 is identical to Eqn. 2.6.14. No matter how small the angle α_I is, the theoretical twist angle θ tends to infinity as q approaches q_D.

Stiffness is defined as the rate of change in a moment or force (in a given direction) per unit change in displacement. Displacements include translation such as plunge and angles such as θ. The aerodynamic torsional stiffness is computed differentiating Eqn. 2.10.1 with respect to θ. From this relationship we notice that there is an aerodynamic torsional stiffness term $\dfrac{\partial M_a}{\partial \theta} = -qSeC_{L_\alpha}$, and a structural stiffness term $\dfrac{\partial M_s}{\partial \theta} = K_T$. Aerodynamic stiffness resembles a negative torsion spring. Structural stiffness is always greater than zero, meaning that it resists twisting. When e is positive, the aerodynamic stiffness is negative and decreases (becomes a larger negative number) with increasing flight dynamic pressure.

The sum of the two terms $(K_T - qSeC_{L_\alpha})$

(or $\overline{K} = K_T\left(1 - q/q_D\right) = K_T\left(1 - \overline{q}\right)$) is the

wing aeroelastic torsional stiffness. As $q \to q_D$ the aeroelastic torsional stiffness declines to zero, as shown in Figure 2.10.2. At dynamic pressures larger than the divergence dynamic pressure, the aeroelastic torsional stiffness is negative; any slight increase in angle of attack of the wing will cause it to twist without limit.
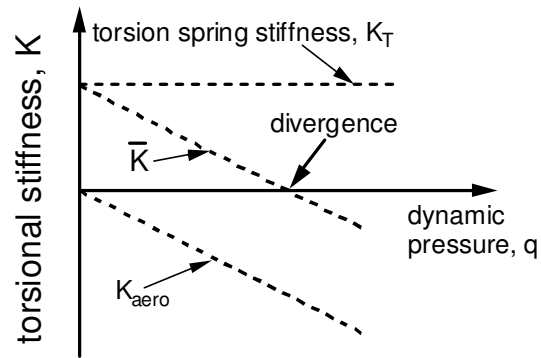
Figure 2.10.2 - Aeroelastic torsional stiffness vs. q

Unless the aeroelastic torsional stiffness is positive, there is no solution to the static equilibrium equation for this wing. A negative stiffness gives a negative twist angle for a positive angle of attack input, clearly an impossible answer.

2.10.1 Twist angle and load aeroelastic amplification, the feedback process

From 2002-2006 the Defense Advanced Research Projects Agency (DARPA) funded a project known as the Morphing Aircraft Structures Program. The purpose of this project was to design multi-role aircraft whose configurations would drastically change in flight.[15] This required complex linkages and flexible skins. One of the concerns was aeroelastic behavior, both static and dynamic. Two companies built large scale, half span model demonstrators that were tested successfully in the Transonic Wind Tunnel (TDT) at NASA Langley Research Center at simulated altitudes up to 50,000 feet and speeds up to Mach 0.93.[16,17]

Figure 2.10.3 – NEXTGEN reconfigurable aircraft prototype. This swept wing aircraft had linkages that moved a flexible skin into five different positions.

The wind tunnel tests were intended to test and to demonstrate the structural integrity of these morphing wings. This demonstration included the ability to predict stresses in a reconfigurable structure with numerous linkages and joints and to predict flutter speed. One of the two models demonstrated stress predictions to within 5% of stresses observed in the wind tunnel while the other model had larger errors of the order of 10%.

What was surprising about this 10%
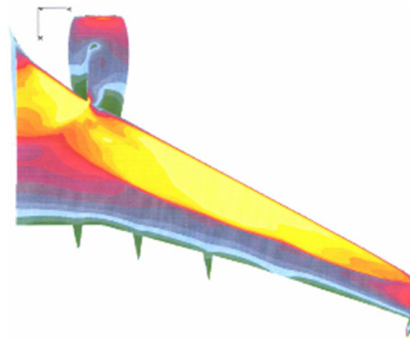
Figure 2.10.4 – Typical CFD pressure distribution detail showing color coded pressure distribution over a transport aircraft wing

difference was that the mathematical model used computational fluid dynamics (CFD) modeling to predict the external aerodynamic loads; these highly accurate loads were then incorporated into the structures finite element model. The model with the 5% errors used a less complicated aerodynamic paneling method, but demonstrated better correlation between the observed and predicted stresses.

The CFD accuracy problem was traced to the aeroelastic modeling or rather the lack of aeroelastic modeling for the static loads. The feedback between the wing surface deflections and the aerodynamic loads was nonexistent. The CFD calculations were run for the rigid wing surface, then applied to the rigid structure; the process ended there. More specifically, this procedure, involving exquisitely accurate aerodynamic loads calculation, proceeded as if there were no aerodynamic stiffness matrix like that displayed in Eqn. 2.6.9.

$$\begin{bmatrix} K_h & 0 \\ 0 & K_T \end{bmatrix} \begin{Bmatrix} h \\ \theta \end{Bmatrix} - qSC_{L_\alpha} \begin{bmatrix} 0 & -1 \\ 0 & e \end{bmatrix} \begin{Bmatrix} h \\ \theta \end{Bmatrix} = qSC_{L_\alpha}\alpha_o \begin{Bmatrix} -1 \\ e \end{Bmatrix} + qScC_{MAC} \begin{Bmatrix} 0 \\ 1 \end{Bmatrix} \qquad (2.6.9)$$

Of course the large finite element model had thousands of degrees of freedom, but the equation structure was the same. CFD aerodynamic models require exact knowledge of the wing surface geometry in Eqn. 2.6.9 this data is represented by the loads on the right hand side that are functions of the angle of attack and camber. CFD models are not efficient when used to compute aerodynamic influence coefficients that go into the aerodynamic stiffness matrix. This deficiency can be remedied by iteration, that is, computing deflections using a version of Eqn. 2.6.9 without the aerodynamic stiffness matrix:

$$\begin{bmatrix} K_h & 0 \\ 0 & K_T \end{bmatrix} \begin{Bmatrix} h_o \\ \theta_o \end{Bmatrix} = qSC_{L_\alpha}\alpha_o \begin{Bmatrix} -1 \\ e \end{Bmatrix} + qScC_{MAC} \begin{Bmatrix} 0 \\ 1 \end{Bmatrix}$$

Where the terms h_o and θ_o refer to the first estimates of deflections. We can then iterate to find the corrections to the loads by solving the equation:

$$\begin{bmatrix} K_h & 0 \\ 0 & K_T \end{bmatrix} \begin{Bmatrix} h_1 \\ \theta_1 \end{Bmatrix} = qSC_{L_\alpha}\alpha_o \left(\begin{Bmatrix} -1 \\ e \end{Bmatrix} + \begin{Bmatrix} h_o \\ \theta_o \end{Bmatrix} \right) + qScC_{MAC} \begin{Bmatrix} 0 \\ 1 \end{Bmatrix}$$

Eventually the process should converge and the deflected shape will be the sum of the series of terms generated by the iterative process. On the other hand, there is a possibility that the sum of the terms will diverge. We need to examine this possibility.

Let's return to our single degree of freedom model to examine the importance of including aeroelastic interaction effects. Equation 2.10.1 for the elastic twist can be written as

$$\theta = \frac{\bar{q}\alpha_I}{1-\bar{q}} = f\bar{q}\alpha_I \qquad (2.10.6)$$

Chapter 2

where the amplification factor, f, is $\quad f = \dfrac{1}{1-\bar{q}}\quad$ which can be expanded as an infinite series:

$$f = \frac{1}{1-\bar{q}} = 1 + \bar{q} + \bar{q}^2 + \bar{q}^3 + ... = 1 + \sum_{n=1}^{\infty} \bar{q}^n \qquad (2.10.7)$$

This infinite series convergences if $\bar{q} < 1$, but diverges if $\bar{q} \geq 1$. This explains why the deflections are infinite above the value $\bar{q} = 1$. At $\bar{q} = 1$ we have a *critical condition*.

Let's compare the size of the first 5 terms in the series in Eqn. 2.10.7 for different values of $\bar{q}$ to see how quickly the series converges and to see when aeroelastic effects are likely to be important. The first term in the series will always be equal to 1.

Figure 2.10.5 - Series terms for twist under load when $\bar{q} = 0.1$

Figure 2.10.5 shows that terms beyond $\bar{q}$ may be neglected with little inaccuracy when $\bar{q}$ is small. Aeroelastic interaction adds about 10% to the nonaeroelastic twist angle. However, in Figure 2.10.6, we see that when $\bar{q}$ is equal to 0.50, terms in the series out to $\bar{q}^4$ are important to the computation of the twist angle. Finally, as shown in Figure 2.10.7, the correction terms when $\bar{q} = 0.90$ are strong contributors to the infinite series well past the $\bar{q}^4$ term in the series.

Equations 2.10.6 and 2.10.7 are combined to get a series expression for elastic twist.

$$\theta = \frac{qSeC_{L\alpha}\alpha_I}{K_T}\left(1 + \bar{q} + \bar{q}^2 + ...\right) \qquad (2.10.8)$$

Figure 2.10.6 - Correction terms for twist when $\bar{q} = 0.5$

The first term in this series is

$$\theta_o = \frac{qSeC_{L\alpha}\alpha_I}{K_T} \qquad (2.10.9)$$

The angle θ_o is twist angle when no aeroelastic interaction or feedback is included. The second term in the series is

$$\theta_1 = \bar{q}\,\theta_o = \frac{qSeC_{L\alpha}\theta_o}{K_T} \qquad (2.10.10)$$
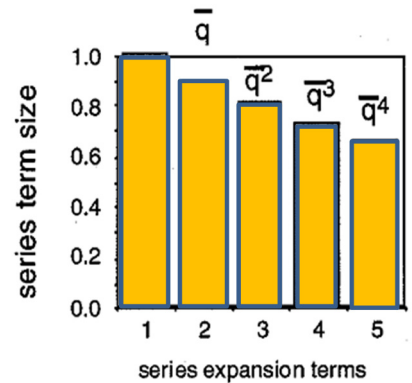
Figure 2.10.7 - Correction terms for twist when $\bar{q} = 0.90$

The term θ_1 is the wing twist in response to θ_o (not α_I). The third term in the series is

$$\theta_2 = \overline{q}^2 \theta_o = \overline{q}\,\theta_1 \qquad (2.10.11)$$

This term is the system twist in response to θ_1. Each term in the infinite series for twist is a corrector for the added moment due to the twist added by the previous term. As a result, the series for the twist including aeroelastic effects is written as

$$\theta = \theta_0 + \sum_{n=1}^{\infty} \theta_n \qquad (2.10.12)$$

where $\theta_i = \overline{q}^i \theta_o = \overline{q}\,\theta_{i-1}$ so that when $\overline{q}$ is near 1, the additional twist added to each term is nearly as large as the original input twist.

From these brief results we can see that neglecting the interaction between structural distortion and the aerodynamic loads on a wing surface can lead to underestimation of deformations and resulting stresses. This underestimation can be slight, moderate or severe depending on how close we are operating to the wing divergence speed. In Chapter 3 we will see that the divergence dynamic pressure is negative, however, it still will furnish us with a benchmark that is not to be ignored.

2.10.2   Static stability – defining the critical dynamic pressure point

For constant airplane weight, *W*, the wing supports ½ the weight so the wing angle of attack is:

$$\alpha_o = \frac{1}{2}\left(\frac{W}{S}\right)\left(\frac{1-\overline{q}}{q C_{L_\alpha}}\right) - \left(\frac{q S c C_{MAC}}{K_T}\right) \qquad (2.10.13)$$

The wing twist angle at constant weight is

$$\theta = \frac{1}{K_T}\left(\frac{eW}{2} + q S c C_{MAC}\right) \qquad (2.10.14)$$

At the theoretical divergence condition, the wing input angle of attack in Eqn. 2.10.13 is $\alpha_{oD} = -\left(\dfrac{q_D S c C_{MAC}}{K_T}\right) = -\left(\dfrac{c}{e}\right)\dfrac{C_{MAC}}{C_{L_\alpha}}$ with the wing twist angle from Eqn. 2.10.14 $\theta_D = \dfrac{eW}{2K_T} + \left(\dfrac{c}{e}\right)\dfrac{C_{MAC}}{C_{L_\alpha}}$. The wing twist angle is not infinite, as would be the case if we did not change the angle of attack.

When the lift is controlled, as it would be in flight, we cannot learn anything about stability by looking for an airspeed or dynamic pressure at which the deformation becomes unbounded (goes to infinity). Only when the wing is given a fixed angle of attack will this happen. The wing is in equilibrium, as indicated by our equations above, but it is unstable if something moves it off this equilibrium point.

Stability is the ability of a physical system to return to its original equilibrium state when disturbed or "perturbed." The stability of any structural system can be "tested" by applying "Euler's stability test" or "Euler's criterion." This is also called the *energy test*. Simply stated, *"a system in static*

equilibrium is statically stable if it returns to its original equilibrium position after being disturbed by some extraneous action." This boundary between stable and unstable occurs at a *transition point*, in our case, the divergence dynamic pressure.

The most familiar type of static structural instability is *column buckling* in which an axial force creates side deflection at a critical load called the buckling load. At buckling we encounter *"bifurcation"* in which there are multiple static equilibrium states in addition to the original equilibrium state. These states will have different structural deformation shapes. Buckling involves solving an eigenvalue problem in which the eigenvalues are related to the critical loads (in our case, critical dynamic pressure, q_D) and the eigenvectors (deformed shapes) are related to the structural shape at the critical load.

Figure 2.10.8 - Flexible wing segment perturbations in angle and load

Consider flying at a dynamic pressure so that the wing angle of attack is constant, given by Eqn. 2.10.13 and the wing twist θ is given by Eqn. 2.10.14. We disturb (in stability jargon, we "perturb") the wing twist slightly from its static equilibrium value θ (given in Eqn. 2.10.14) to a new position $\theta + \Delta\theta$, using a disturbance moment created by a force of very short duration to move the wing away from its equilibrium position.

As shown in Figure 2.10.8, the aerodynamic and structural moments about the shear center change. These changes are computed to be:

$$\Delta M_a = qSeC_{L_\alpha}(\Delta\theta)$$

and

$$\Delta M_s = K_T(\Delta\theta)$$

These two increments or "deltas" are usually not equal. The net restoring moment (the difference between the perturbation moment exerted by the spring and the perturbation moment provided by the wing aerodynamics) due to the change in twist is

$$\Delta M_R = \Delta M_S - \Delta M_a = \left(K_T - qSeC_{L_\alpha}\right)\Delta\theta \qquad (2.10.15)$$

At all values of q, except $\bar{q} = 1$, Eqn. 2.10.15 is not zero and the perturbation in the twist angle will create angular motion; the system will not be in static equilibrium.

Static structural stability analysis uses Eqn. 2.10.15 as a starting point and asks whether the *perturbed wing tends to come back* to its original equilibrium twist value *or whether it moves away. If the wing tends to move back towards its original static equilibrium position* the original static equilibrium position is stable and unique. If the wing tends to move further away from the perturbed position, then the static equilibrium position is unstable.

There is a third possibility. If Eqn. 2.10.15 is zero when the perturbation $\Delta\theta$ is very small, but non-zero, then the system also will be in static equilibrium in the perturbed state. This condition is called *neutral stability* and we are at a transition point, also called a *bifurcation point* (two equilibrium positions) or *critical point*. The arbitrary displacement angle $\Delta\theta$ can be factored out of Eqn. 2.10.15, indicating that the test for static stability does not involve the size of $\Delta\theta$.

In Eqn. 2.10.15, if $\Delta M_s > \Delta M_a$, at the wing position $\theta + \Delta\theta$ the spring torsional moment overpowers the aerodynamic moment and causes the wing to return to its original equilibrium position, θ. (Actually the wing will oscillate about the equilibrium point, as we will see in another section in the text). On the other hand, if $\Delta M_s < \Delta M_a$, the aerodynamic moment overpowers the structural moments and the wing will move away or "diverge" from the static equilibrium point.

If K_T is greater than $qSeC_{L_\alpha}$ then static aeroelastic stability is assured. If we fly at a condition where K_T is less than $qSeC_{L_\alpha}$ we will have torsional instability in which a small disturbance causes the wing to move away, uncontrollably, from its static equilibrium position.

The crossover point between stability and instability occurs at the divergence dynamic pressure q_D. This is our zero stiffness condition occurring when

$$K_T = q_D SeC_{L_\alpha}$$

so that

$$q_D = \frac{K_T}{SeC_{L_\alpha}} \tag{2.10.16}$$

This result is identical to our previous results in which we found that flying above this dynamic pressure created infinite deflection on uncontrolled wings.

2.11 Illustrative examples – doing the math

Let's consider two examples to illustrate how to solve basic static stability problems.

2.11.1 A non-aeroelastic example – static stability of a magneto-elastic device

The idealized configuration shown in Figure 2.11.1 is a "magneto-elastic" device. This involves a magnetic armature located at the end of a flexible shaft and suspended between two magnets. The magnetic field creates attraction forces on the armature; these forces depend on the distance between the magnets and the armature. This model replaces the flexible shaft with a rigid rod free to rotate about a pivot whose rotation θ is restrained by a bending spring that resists rotation θ, the "bending angle" shown in the figure.

If the armature is displaced sideways by a small angle θ the magnetic forces change. The forces are given by the
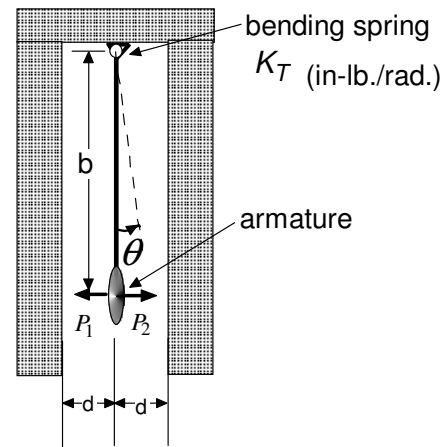
Figure 2.11.1 – Magnetic device model

expressions $P_1 = \dfrac{a}{(d+y)^2}$ and $P_2 = \dfrac{a}{(d-y)^2}$ where a is a field strength parameter, d is the gap distance when θ is zero and $y = b\sin\theta$ is the lateral displacement of the end of the rigid. Only when θ is zero are the forces equal.

Problem

Find the value of the magnetic field parameter a that makes this configuration neutrally statically stable. For your calculations, restrict deflections to be small so that $\sin\theta \approx \theta$ and $\theta << \dfrac{d}{b}$. Note that $(d-y)^2 (d+y)^2 = \left(d^2 - y^2\right)^2$.

Solution

Perturb the device an amount θ and then sum moments about the pivot point. Use the counter-clockwise direction as positive

$$\sum M_p = P_2\, b - P_1\, b - K_T\, \theta = 0 \qquad (2.11.1)$$

Substitute expressions for P_1, P_2 (and note that $y \cong b\theta$) into Eqn. 2.11.1 to get following equation.

$$\sum M_p = \frac{ab}{(d-b\theta)^2} - \frac{ab}{(d+b\theta)^2} - K_T\theta$$

$$\sum M_p = \left(\frac{ab(4db)}{(d^2 - b^2\theta^2)^2} - K_T \right)\theta \qquad (2.11.2)$$

Since $\theta << \dfrac{d}{b}$ we can neglect higher order terms in θ and simplify Eqn. 2.11.2.

$$\sum M_p = \left(\frac{4ab^2}{d^3} - K_T \right)\theta \qquad (2.11.3)$$

Equation 2.11.3 is the negative of the system stiffness. There are two ways to solve this problem. The first is by computing the value of a at which the system stiffness becomes zero. This leads us to the neutrally statically stable condition, written as

$$\frac{\partial M}{\partial \theta} = 0 \qquad (2.11.4)$$

From Eqn. 2.11.3 we get

$$\frac{\partial M}{\partial \theta} = 0 = \frac{4ab^2}{d^3} - K_T \qquad (2.11.5)$$

Solving for a

$$a_{crit} = \frac{K_T}{4}\left(\frac{d^3}{b^2} \right) \qquad (2.11.6)$$

The second method of obtaining the solution is to set Eqn. 2.11.3 equal to zero.

$$\sum M_p = \left(\frac{4ab^2}{d^3} - K_T \right)\theta = 0 \qquad (2.11.7)$$

The result is the same, $a_{crit} = \frac{K_T}{4}\left(\frac{d^3}{b^2} \right)$

2.11.2   Example – a flexible aircraft in steady turning flight

An idealized aircraft is shown in Figure 2.11.2 flying at an angle of attack α_o with its idealized, uncambered "wings" twisted an amount θ. The wing lift for each of its two, idealized, wing segments is $L_w = qSC_{L_\alpha}(\alpha_o + \theta)$ where

> α_o = wing angle of attack
> θ = wing elastic twist
> S = wing area (per wing segment)

During a banked, constant altitude turn this airplane develops a load factor n, is defined as

Figure 2.11.2 - Aircraft and wing free body diagram

$$n = \frac{Total\ Lift}{Total\ Weight}$$

where $Total\ lift = 2qSC_{L_\alpha}(\alpha_o + \theta)$.

The total aircraft weight is $W = (2m + M)g$, where m=wing mass (per wing segment) and M=fuselage mass (plus everything else). With these definitions, the load factor is:

$$n = \frac{2qSC_{L\alpha}(\alpha_o + \theta)}{(2m + M)g} \qquad (2.11.7)$$

We will solve for the aircraft angle of attack α_o and the wing segment twist angle θ as functions of n. We will also solve for the divergence dynamic pressure.

Equilibrium requires that

$$L = nW = 2L_w \qquad (2.11.8)$$

In this problem, n is the independent variable with α_o determined from Eqn. 2.11.8.

The restoring torque, M_S, on each wing segment is $M_S = K_T\theta$. When we sum moments (with $L_w = qSC_{L_\alpha}(\alpha_o + \theta)$) about either wing shear center we get the following static equilibrium equation:

$$\sum M_{spring} = 0 = K_T\theta - L_W e - nmgd \qquad (2.11.9)$$

$$K_T\theta = L_W e + nmgd \qquad (2.11.10)$$

From Eqns. 2.11.8 and 2.11.10 we get

$$K_T\theta = L_W\left(e + \frac{2mgd}{W}\right) \qquad (2.11.11)$$

Defining the new parameter $\mu = \dfrac{2mgd}{W}$ we have

$$K_T\theta = L_W(e + \mu) = \left(qSC_{L_\alpha}(\alpha_o + \theta)\right)(e + \mu) \qquad (2.11.12)$$

Solving for the twist angle:

$$\theta = \frac{qSC_{L_\alpha}\alpha_o(e + \mu)}{K_T - qSC_{L_\alpha}(e + \mu)} \qquad (2.11.13)$$

From Eqn. 2.11.13 it appears that the twist angle θ becomes infinite when the denominator approaches zero. This implies that aircraft weight ratio μ (and dimension *d*) determines the divergence dynamic pressure. However, α$_o$ is a function of dynamic pressure so we need to explore Eqn. 2.11.13 further.

The divergence dynamic pressure for the restrained wing (with α$_o$ held constant) is $q_{D_{fixed}} = \dfrac{K_T}{SeC_{L_\alpha}}$.

Rewrite Eqn. 2.11.13 as

$$\theta = \frac{\dfrac{q}{q_{D_{fixed}}}\left(1 + \dfrac{\mu}{e}\right)\alpha_o}{1 - \dfrac{q}{q_{D_{fixed}}}\left(1 + \dfrac{\mu}{e}\right)} \qquad (2.11.14)$$

The lift force acting on each wing segment is L$_w$,

$$L_W = qSC_{L_\alpha}\alpha_o\left(1 + \frac{\dfrac{q}{q_{D_{fixed}}}\left(1 + \dfrac{\mu}{e}\right)}{1 - \dfrac{q}{q_{D_{fixed}}}\left(1 + \dfrac{\mu}{e}\right)}\right) \qquad (2.11.15)$$

Rewriting Eqn. 2.11.15 with a common denominator, we get

$$L_W = qSC_{L_\alpha}\alpha_o \left(\cfrac{1}{1 - \cfrac{q}{q_{D_{fixed}}}\left(1+\cfrac{\mu}{e}\right)} \right) \qquad (2.11.16)$$

The angle of attack of the two wing segments, α_o, is found by setting each wing segment lift equal to ½ the aircraft weight, W, so that $L_w = \dfrac{nW}{2}$. Solving for α_o, using Eqn. 2.11.16, we get

$$\alpha_o = \cfrac{nW}{2}\left(\cfrac{1 - \cfrac{q}{q_{D_{fixed}}}\left(1+\cfrac{\mu}{e}\right)}{qSC_{L_\alpha}} \right) \qquad (2.11.17)$$

Now substitute Eqn. 2.11.17 into Eqn. 2.11.14. This gives an expression for the wing segment twist angle θ in terms of *n*.

$$\theta = \left(\cfrac{nW}{2}\right)\cfrac{\left[1 - \cfrac{q}{q_{D_{fixed}}}\left(1+\cfrac{\mu}{e}\right)\right]\left[\cfrac{q}{q_{D_{fixed}}}\left(1+\cfrac{\mu}{e}\right)\right]}{qSC_{L_\alpha}\left[1 - \cfrac{q}{q_{D_{fixed}}}\left(1+\cfrac{\mu}{e}\right)\right]} \qquad (2.11.18)$$

Equation 2.11.18 reduces to

$$\theta = \left(\cfrac{nW}{2}\right)\left(\cfrac{e}{K_T}\right)\left(1+\cfrac{\mu}{e}\right) \qquad (2.11.19)$$

Although the twist angle θ is a function of the load factor, it is not a function of airspeed once we take into account that the wing angle of attack must change with airspeed. It is not possible to determine anything about wing static instability by simply examining the denominator in Eqn. 2.11.19.

The reason that the static equilibrium value of θ does not become infinite as airspeed increases is that we are constantly reducing the angle of attack to keep the lift on the wing segments equal to the aircraft weight. As we fly faster, we get enough lift with reduced α_o and constant θ. A static stability analysis using perturbations from the static equilibrium state is necessary to find the divergence dynamic pressure.

To examine the effects of increased dynamic pressure on torsional stiffness, we re-write the torsional equilibrium equation as

$$K_T\theta = qSeC_{L\alpha}(\alpha_0 + \theta) + nmgd \qquad (2.11.20)$$

Combine θ terms to get

$$\left(K_T - qSeC_{L_\alpha}\right)(\theta) = qSeC_{L_\alpha}\alpha_o + nmgd \qquad (2.11.21)$$

If we perturb that wing we transform Eqn. 2.11.1 into

$$\left(K_T - qSeC_{L_\alpha}\right)(\theta + \Delta\theta) = qSeC_{L_\alpha}\alpha_o + nmgd \qquad (2.11.22)$$

This leaves us with two separate parts

$$\left(K_T - qSeC_{L_\alpha}\right)(\theta) + \left(K_T - qSeC_{L_\alpha}\right)(\Delta\theta) = qSeC_{L_\alpha}\alpha_o + nmgd \qquad (2.11.23)$$

From Eqn. 2.11.23, we see that for two solutions for static equilibrium to exist we must have

$$\left(K_T - qSeC_{L_\alpha}\right) = 0 \quad or \quad K_T = qSeC_{L_\alpha} \qquad (2.11.24)$$

The load factor does not appear in Eqn. 2.11.24 so that the divergence q for this example is the same as found from our fixed wing stability analysis. We conclude that inertia loads (or gravity) don't change the divergence speed.

2.12 Linear analysis vs. nonlinear analysis-divergence with a nonlinear aerodynamic load

The onset of static structural instability is predicted by locating the *bifurcation point* at which two or more structural deformation forms are possible for the same external, applied loading. In this section we will show that nonlinear theory predicts the appearance of multiple equilibrium states, but with finite, not infinite, deformations. The purpose of this section is to show how linear system stability concepts are related to nonlinear system behavior. The problem we will solve is one for which the structural restoring moment is linear but the aerodynamic load is nonlinear.

Our previous static equilibrium analyses assumed that there was a linear relationship between the structural and aerodynamic loads and the twist deflection. These analyses predicted that, at the divergence speed, the wing twist and the aerodynamic load become infinite no matter how small the external applied load. Linear analysis also predicts that the aeroelastic stiffness becomes negative once the system becomes statically unstable.
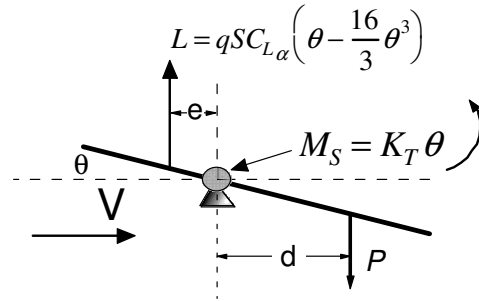
Figure 2.12.1 - Single degree of freedom airfoil with nonlinear aerodynamic load and linear structural spring

Consider the single degree of freedom uncambered wing with the cross-section shown in Figure 2.12.1. A concentrated load P is applied aft of the shear center (represented as a pin in Figure 2.12.1) to create a moment Pd about the shear center to create twist θ. The wing has no initial incidence angle. Twist, θ, is resisted by a linear torsion spring, but the aerodynamic lift is a nonlinear function of θ (measured in radians) with lift coefficient C_L given as:

$$C_L = C_{L_\alpha}\left(\theta - \frac{16}{3}\theta^3\right) \qquad (2.12.1)$$

The effects of θ on the moment arms e and d are ignored (in fact, these moment arms are $e\cos\theta$ and $d\cos\theta$, respectively). The torsional equilibrium equation is:

$$\sum M_{SC} = 0 = Le - K_T\theta + Pd \qquad (2.12.2)$$

Substituting the lift expression in Eqn. 2.12.1, the torsional equilibrium equation in terms of twist angle θ is:

$$\left(K_T - qSeC_{L_\alpha}\right)\theta + \frac{16}{3}qSeC_{L_\alpha}\theta^3 = Pd \qquad (2.12.3)$$

Dividing all terms in Eqn. 2.12.3 by K_T (with the notation $\bar{q} = \dfrac{qSeC_{L\alpha}}{K_T}$) we obtain the nondimensional torsional equilibrium equation:

$$(1 - \bar{q})\theta + \frac{16}{3}\bar{q}\theta^3 = \frac{Pd}{K_T} = \bar{P} \qquad (2.12.4)$$

The parameter $\bar{P} = \dfrac{Pd}{K_T}$ is the elastic twist that would occur if no aerodynamic load acted on the section.

The effective torsional stiffness K_e for this single degree of freedom system is defined as:

$$K_e = \frac{\partial Pd}{\partial\theta} \qquad (2.12.5)$$

Flexibility is the inverse of stiffness:

$$flexibility = \frac{1}{K_e} = \frac{\partial\theta}{\partial(Pd)} \qquad (2.12.6)$$

From Eqns. 2.12.3 and 2.12.4, the effective torsional stiffness of the nonlinear system is

$$K_e = \left(K_T - qSeC_{L_\alpha}\right)\theta + 16qSeC_{L_\alpha}\theta^2 \qquad (2.12.7)$$

Divide the effective stiffness in Eqn. 2.12.7 by K_T to obtain the *nondimensional effective torsional stiffness*:

Chapter 2

$$\overline{K}_e = \frac{K_e}{K_T} = \frac{\partial \overline{P}}{\partial \theta} = \left(1 - \overline{q} + 16\overline{q}\,\theta^2\right) \qquad (2.12.8)$$

The effective torsional stiffness is a nonlinear function of twist θ. A stable system will resist the applied torque; the effective stiffness of a stable system is positive. The effective stiffness expression in Eqn. 2.12.8 has *hardening* features. As twist angles increase the system becomes more resistant to twist.

A plot Eqn. 2.12.8 at four different values of $\overline{q}$: 0, 0.5, 1 and 1.5, is shown in Figure 2.12.2. The expression for effective stiffness is symmetrical with respect to θ. When θ is zero the linear and nonlinear expressions for effective stiffness are identical. The figure indicates that

Figure 2.12.2 - Effective torsional stiffness vs. twist angle θ
(Eqn. 2.12.8) at four different dynamic pressures.

effective stiffness has a value of unity at zero dynamic pressure and then declines, becoming zero at divergence and negative at dynamic pressures above divergence.

When $\overline{q} = 0.5$ (50% of the divergence dynamic pressure parameter), the system is stable because the effective stiffness is positive; the effective torsional stiffness increases as the section twists and the effective stiffness increases (hardens).

When $\overline{q} = 1$ (the curve marked *divergence*) the effective stiffness at $\theta = 0$ is zero. The linear system model predicts neutral stability, divergence, at this point. However, as load increases the wing twists; the effective torsional stiffness becomes positive and thus stable, but not with zero deflection. This indicates that the section is stable when $\theta \neq 0$ and will resist further twist, even when $\overline{q} = 1$. This is a major difference between the nonlinear model and the linear model

When $\overline{q} = 1.5$ (the curve marked 150% divergence) we have a negative effective torsional stiffness at $\theta = 0$; the system is statically unstable. Figure 2.12.2 shows that the effective stiffness of the nonlinear system does not become positive until the section twists about 0.14 radians, a fairly large displacement. The linear and the nonlinear systems are unstable (the effective torsional stiffness is negative) for a small range of twist angles when $\overline{q} = 1.5$, but the nonlinear system will restabilize if it rotates more than 0.14 radians.

Figure 2.12.3 shows the plot of the static equilibrium twist angle as a function of applied load Pd/K_T given in Eqn. 2.12.4. When there is no aerodynamic load, the relationship between load parameter and twist angle is linear, as indicated by the line marked *linear system*. At dynamic

pressures below the divergence speed, for a fixed value of Pd/K_T, there is only one unique value of θ. When operating at the divergence dynamic pressure, Figure 2.12.3 indicates that, while the solution for twist angle is unique, the region near $\theta = 0$ is very sensitive to small changes in applied torque; a small change in Pd/K_T creates large changes in θ.

At divergence, with $\theta = 0$, $\partial Pd/\partial\theta$ is zero indicating that the stiffness is zero at this point (the flexibility is infinite). As a result, large twist angles result from small changes in applied torque Pd.

Figure 2.12.3 – A plot of static equilibrium twist angle θ vs. load parameter $\bar{P}$ (Eqn. 2.12.4) showing multiple equilibrium states when operating above divergence where the wing is statically unstable.

When the system is neutrally statically stable, as predicted by linear theory, there are an infinite number of nearby, but undetermined, equilibrium states, Euler's so called *proximate* states, at the same value of load. For the nonlinear system, a slight load change produces more deflection but there are no infinite deflections and the load deformation relationship is unique.

From Figure 2.12.3, when $\bar{q} = 1.5$, linear system analysis predicts that the effective torsional stiffness of the section is always negative and, as a result, statically unstable. A positive applied torque produces in a negative twist - a physically unacceptable result. In fact, the nonlinear analysis predicts that, when a small positive torque is applied, *three possible equilibrium states exist*, one of them zero but two relatively far away from zero twist.

The two nonzero equilibrium states shown in Figure 2.12.3 when $\bar{q} = 1.5$ are stable because the slopes of the curves, the effective torsional stiffness, have positive slopes. The third static equilibrium angle at $\theta = 0$ is unstable because the effective stiffness is negative. The conclusion is that, above the neutral stability point identified by linear analysis, there are multiple equilibrium twist angles; the equilibrium state depends not only on the equilibrium equations but on which direction the system is perturbed after the load is applied. *While the wing will not undergo infinite deformation, the nonlinear analysis predicts a finite, but large deflection that is most likely unacceptable*.

Homework problem-nonlinear torsional spring stiffness
The single degree of freedom wing model shown previously in Figure 2.12.1 has a linear aerodynamic applied load given as $L = qSC_{L_\alpha}\theta$ but it resists applied torque by developing a nonlinear structural restoring moment given by the relationship:
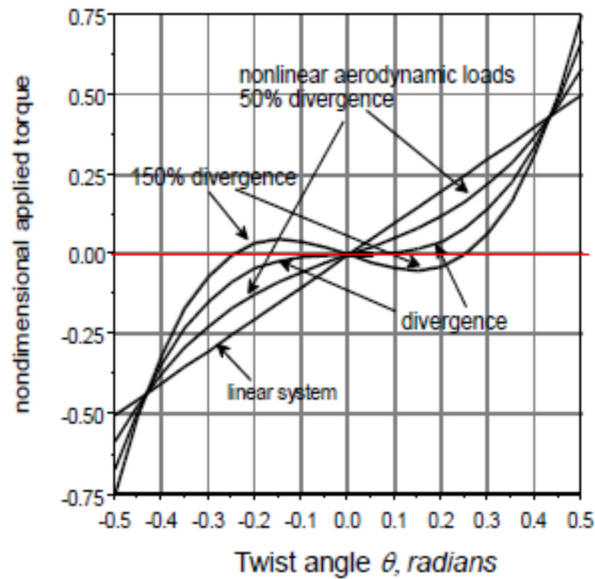
Chapter 2

$$M_S = K_T \theta + K_{T1} \theta^3$$

K_{T1} can be either positive or negative. When K_{T1} is positive we have a so-called "hardening spring." When K_{T1} is negative the spring is called a "softening spring." When K_{T1} is zero, we have the usual linear spring relationship.

a) When $K_{T1}/K_T = 0.2$ derive the nonlinear equations of static equilibrium when an initial

moment $M_o = qSeC_{L\alpha}\alpha_o$ is applied at a flight dynamic pressure q. Plot M_o/K_T vs. θ for

four different values of dynamic pressure parameter: $\bar{q} = \dfrac{q}{q_D} = 0.1,\ 0.5,\ 1.0,\ 1.1$, with

$q_D = \dfrac{K_T}{SeC_{L\alpha}}$ for $-0.5 \le \theta \le 0.5$

Answer - $\dfrac{M_o}{K_T} = (1 - \bar{q})\theta + 0.2\theta^3$

b) The *effective torsional stiffness* is defined as the change in M_o with respect to θ

$K_{eff} = \dfrac{\partial M_o}{\partial \theta}$. The normalized effective torsional stiffness is defined as

$K_e = \dfrac{K_{eff}}{K_T} = \dfrac{1}{K_T}\dfrac{\partial M_o}{\partial \theta}$ so that $K_e = (1 - \bar{q}) + 0.6 * \theta^2$ Using the same values of dynamic

pressure parameter as in part (a) plot normalized effective stiffness as a function of θ for $-0.5 \le \theta \le 0.5$.

c) Remove the external load and verify that the static equilibrium equation becomes

$\theta^3 + \dfrac{K_T}{K_{T_1}}(1 - \bar{q})\theta = 0$. This equation has three solutions $\theta = 0$ *or* $\theta = \pm\sqrt{\dfrac{K_T}{K_{T_1}}(\bar{q} - 1)}$.

When $q \le q_D$ then there is only one equilibrium point $\theta_e = 0$ because the term under the

radical is negative. Plot these solutions as a function of $0 \le \dfrac{K_{T_1}}{K_T} \le 1$ (note that this is the

inverse of the term in the twist solution above and is a measure of the spring nonlinearity.

2.13 The effect of Mach number on divergence-the match point

Flow compressibility introduces added complexity to aerodynamic calculations. The importance of flow compressibility is judged by computing the airstream Mach number. Mach number is defined as the ratio of the airspeed divided by the local speed of sound. Flow compressibility effects are subdivided into four different regions: 1) the subsonic regime $0 < M < 0.8$; 2) the transonic regime $0.8 < M < 1.2$; 3) the supersonic regime $1.2 < M < 5$; and 4) the hypersonic regime $M > 5$. In this section we will briefly examine how flow compressibility affects the divergence speed in the subsonic flow regime. We will define and identify the importance of the "match point."

Airstream compressibility begins to become important above M = 0.3. As discussed in Section 2.5, wing lift (and the aerodynamic coefficients) depends on the local flow velocities at points above and below the wing surface. The Mach number at some points on the wing itself may be considerably larger than the airstream ahead of the wing.

Consider the airfoil shown in Figure 2.13.1.[18] The static air pressure, *p*, at points on the airfoil section decreases on the upper surface so that it is lower than the freestream static pressure. The static pressure measured on the lower surface may also decrease, but not as much as it does on the upper surface. The difference between the two pressures defines the lift coefficient.
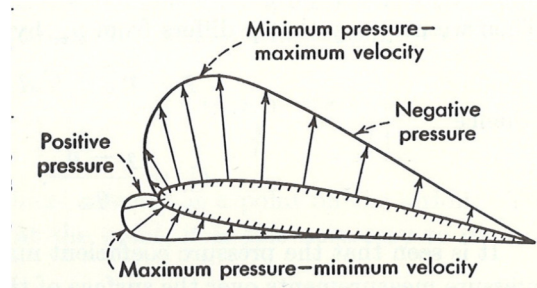
Figure 2.13.1 – Typical pressure distribution on an airfoil surface. (Reference 18)

The static pressure, *p*, on the upper or lower wing surface is:

$$p = p_o + \Delta p \qquad (2.13.1)$$

where p_o is the airstream static pressure ahead of the wing and Δp is defined as:

$$\Delta p = \frac{1}{2}\rho V_o^2 C_p = qC_p \qquad (2.13.2)$$

C_p is the local pressure coefficient on the upper or lower wing surface, written as

$$C_p = 1 - \left(\frac{V^2}{V_o^2}\right) \qquad (2.13.3)$$

V is the local flow velocity at any point on the wing surface and V_o is the wing airspeed. This expression is only valid for incompressible flow. At a stagnation point where the flow speed is zero, (for instance, on the nose of the airfoil), the C_p is equal to 1, its maximum value in incompressible flow. At wing surface positions where the flow speeds increases $V > V_o$; the pressure coefficient is negative.

The lift coefficient is computed by integrating the differences between the pressure distributions over the upper and lower wing surface

$$c_l = \frac{1}{c}\int_{\substack{leading\\edge}}^{\substack{trailing\\edge}} \left(C_{p_{lower}} - C_{p_{upper}}\right)dx \qquad (2.13.4)$$

When the flow is compressible, it is shown that the maximum value of C_p is greater than 1; the values of C_p are larger those computed for incompressible flow. Prandtl and Glauert[§] independently

---

[§] "Science and aeronautics have suffered a severe loss through the fatal accident to Mr. Hermann Glauert on August 4. Mr. Glauert was walking with his brother and his three children, and stopped to watch the blowing-up of a tree-stump; a large piece of wood, projected nearly 100 yards, struck him on the temple and killed him instantly. Born in Sheffield on October 2, 1892, Mr. Glauert was educated at King Edward VII School and

suggested a pressure coefficient *compressibility correction factor* to account for flow compressibility (now known as the *Prandtl-Glauert transformation*):

$$C_p = \frac{C_{p_{incomp}}}{\sqrt{1-M^2}} \qquad (2.13.5)$$

This approximation is accurate up to about M= 0.8. Since wing aerodynamic coefficients are integrals of the pressure coefficient, they will be modified by the same transformation given in Eqn. 2.13.5. The same is true of the lift curve slope. For instance, the lift curve slope for a two-dimensional airfoil in incompressible flow is $c_{l_\alpha} = 2\pi$. The lift curve slope, corrected for compressibility, is $c_{l_\alpha} = \frac{2\pi}{\sqrt{1-M^2}}$.

We can now use the relationship $C_{L_\alpha} = \frac{C_{L_{\alpha 0}}}{\sqrt{1-M^2}}$ in the equation for the divergence dynamic pressure so that

$$q_D = \frac{1}{2}\rho V_D^2 = \frac{1}{2}\rho\left(\frac{V_D^2}{a^2}\right) = \frac{1}{2}\rho a^2 M_D^2 = \frac{K_T}{SeC_{L_\alpha}} = \frac{K_T\sqrt{1-M_D^2}}{SeC_{L_{\alpha 0}}} \qquad (2.13.6)$$

The parameter "a" is the local speed of sound which changes with altitude. The divergence Mach number appears on both sides of Eqn. 2.13.6. The torsional stiffness coefficient, K_T, does not depend on Mach number or altitude unless there is significant aerodynamic heating.

The equation on the left hand side of Eqn. 2.13.6 $q = \frac{1}{2}\rho a^2 M^2$ is called the *atmosphere line*. The airspeed computed from the left side of Eqn. 2.13.6 must match that computed for the right hand side. The divergence dynamic pressure on the right hand side of Eqn. 2.13.6 is written as the product of an incompressible term times a Mach number term.

$$q_D = \frac{K_T\sqrt{1-M^2}}{SeC_{L_{\alpha 0}}} = q_{Do}\sqrt{1-M^2} \quad \text{with} \quad q_{Do} = \frac{K_T}{SeC_{L_{\alpha 0}}} \qquad (2.13.7)$$

The intersection point between the curve defined in Eqn. 2.13.7 and the atmosphere line is called the *match point*.

The match point changes with altitude. An example of this change is plotted in Figure 2.13.2 for a wing with a computed divergence dynamic pressure of 250 *psf* in incompressible flow. Three different atmosphere lines are plotted in Figure 2.13.2 for three different altitudes. The intersection

Trinity College, Cambridge." A similar notice was given in Flight on August 9, 1934. "The British aviation world was shocked to read in the news of the untimely accident which caused the death of Mr. H. Glauert near Aldershot last Saturday. Hermann Glauert was Principal Scientific papers Officer at the Royal Aircraft Establishment, Farnborough, Mr. Glauert, his wife and three children were watching the Royal Engineers blowing up tree stumps, and a piece of wood hit Mr. Glauert on the temple. He was a well-known authority on aerodynamics. Among his works the best known is, perhaps, "The Elements of Aerofoil and Airscrew Theory." Mr. Glauert was 42 years of age."

point moves to the right as altitude increases so divergence occurs at a higher Mach number at altitude.

Write the equation for the match point as:

$$q_D = q_{Do}\sqrt{1-M_D^2} = \frac{1}{2}\rho a^2 M_D^2 = q_{ref}M_D^2 \quad (2.13.8)$$

with $q_{ref} = \frac{1}{2}\rho a^2$

Figure 2.13.2 - Match point Mach number for divergence

The reference dynamic pressure q_{ref} is a known function of altitude. Now, square both sides of Eqn. 2.13.10 to get a quadratic expression for M_D^2, the divergence Mach number

$$M_D^4 + \left(\frac{q_{Do}}{q_{ref}}\right)^2 M_D^2 - \left(\frac{q_{Do}}{q_{ref}}\right)^2 = 0 \quad (2.3.9)$$

so that

$$M_D^2 = \frac{-\left(\frac{q_{Do}}{q_{ref}}\right)^2 + \sqrt{\left(\frac{q_{Do}}{q_{ref}}\right)^4 + 4\left(\frac{q_{Do}}{q_{ref}}\right)^2}}{2} \quad (2.3.10)$$

Figure 2.13.3 plots divergence speed as a function of altitude for the example wing. Also shown is the result of the calculation of divergence speed when the effect of Mach number is ignored. The computed divergence speed is smaller if compressibility effects are included.

Figure 2.13.3 - Altitude vs. divergence Mach number ($q_{do} = 250$ psf.)

2.14 Divergence of multi-degree of freedom systems

The objective of this section is to expand our study of aeroelastic stability to a two degree of freedom system in which both degrees of freedom affect the result. We will also show that this leads to an eigenvalue problem. We will use a two-degree-of-freedom model shown in Figure 2.14.1, with semi-span, b, and wing chord, c, to develop the static stability solution. This model consists of two wing sections mounted on a rigid shaft that excludes
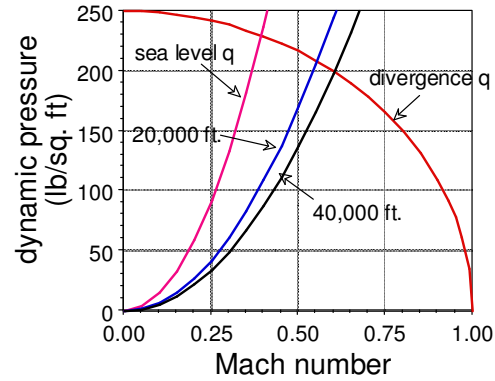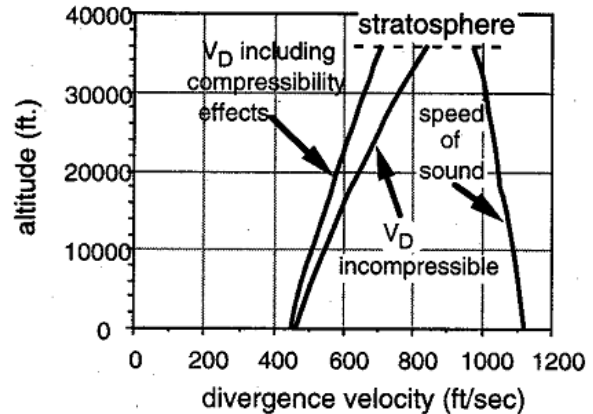

Figure 2.14.1 - Two degree of freedom wing showing definition of twist angles (degrees of freedom).

wing plunge but permits torsional rotation. Each section is uncambered and has the same initial angle of attack, α_o. Two torsion springs model the wing structure resistance between the inboard and outboard wing sections and between the wind tunnel wall and the inner section.

View A-A in Figure 2.14.1 shows the two wing twist degrees of freedom measured and the initial angle of attack α_o. The lift on each wing segment acts at its aerodynamic center and is calculated to be
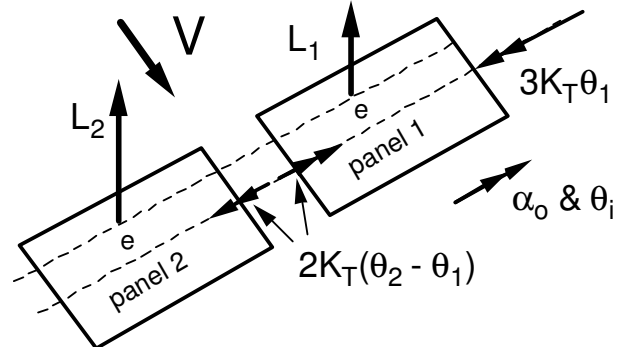
Figure 2.14.2 - Free body diagram of the wing segments.

$$L_1 = qSC_{L_\alpha}\left(\alpha_o + \theta_1\right)$$
$$L_2 = qSC_{L_\alpha}\left(\alpha_o + \theta_2\right)$$

(2.14.1 a,b)

Figure 2.14.2 shows a free-body diagram of each of the two wing sections, together with the external and internal forces and moments for a deformed position of the system in which the outer section is rotated more than the inboard section. The shear forces in the rod are not shown. Summing twisting moments about the rod support for each section in the positive, nose-up pitch, direction, we have:

$$\sum M_1 = 0 = 2K_T(\theta_2 - \theta_1) - 3K_T\theta_1 + L_1 e$$

(2.14.2)

$$\sum M_2 = 0 = -2K_T(\theta_2 - \theta_1) + L_2 e$$

(2.14.3)

Substituting for L_1 and L_2 in terms of α_o, θ_1 and θ_2 we create the following two equations.

$$5K_T\theta_1 - 2K_T\theta_2 = qSeC_{L_\alpha}(\alpha_o + \theta_1)$$

(2.14.4)

$$-2K_T\theta_1 + 2K_T\theta_2 = qSeC_{L_\alpha}(\alpha_o + \theta_2)$$

(2.14.5)

Collecting like terms, these equations are written in matrix form as:

$$K_T\begin{bmatrix} 5 & -2 \\ -2 & 2 \end{bmatrix}\begin{Bmatrix} \theta_1 \\ \theta_2 \end{Bmatrix} + qSeC_{L_\alpha}\begin{bmatrix} -1 & 0 \\ 0 & -1 \end{bmatrix}\begin{Bmatrix} \theta_1 \\ \theta_2 \end{Bmatrix} = qSeC_{L_\alpha}\alpha_o\begin{Bmatrix} 1 \\ 1 \end{Bmatrix}$$

(2.14.6)

Summing forces does not provide useful aeroelastic information because these equations only relate the lift forces to the shear reactions in the rod support.

In Eqn. 2.14.6 we have taken the portion of the aerodynamic loads proportional to deformations θ_1 and θ_2 from the right hand side and moved it to the left side of the equation with the structural stiffness matrix. As written in Eqn. 2.14.6, the matrix contribution from the aerodynamic loads is referred to as the *aerodynamic stiffness matrix*. Divide Eqn. 2.14.6 by K_T and define a nondimensional parameter $\overline{q}$ as

$$\overline{q} = \frac{qSeC_{L_\alpha}}{K_T} \qquad (2.14.7)$$

(note that this nondimensional parameter is identical to that used for the single degree of freedom wing) The equations of static equilibrium become:

$$\begin{bmatrix} 5-\overline{q} & -2 \\ -2 & 2-\overline{q} \end{bmatrix} \begin{Bmatrix} \theta_1 \\ \theta_2 \end{Bmatrix} = \overline{q}\alpha_o \begin{Bmatrix} 1 \\ 1 \end{Bmatrix} \qquad (2.14.8)$$

The 2x2 matrix in Eqn. 2.14.8 is the **_aeroelastic stiffness matrix._** The solutions for the unknown static torsional deformations, θ_1 and θ_2, are

$$\begin{Bmatrix} \theta_1 \\ \theta_2 \end{Bmatrix} = \overline{q}\frac{\alpha_o}{\Delta} \begin{Bmatrix} 4-\overline{q} \\ 7-\overline{q} \end{Bmatrix} \qquad (2.14.9)$$

The term, Δ, is the determinant of the *aeroelastic stiffness matrix.*

$$\Delta = \overline{q}^2 - 7\overline{q} + 6 \qquad (2.14.10)$$

The values for θ_1 and θ_2 (divided by α_o) are plotted as a function of the parameter $\overline{q}$ and shown in Figure 2.14.3. From Eqn. 2.14.10 we see that $\Delta \to 0$ as $\overline{q} \to 1$ or $\overline{q} \to 6$ so that both θ_1 and θ_2 approach infinity as $\overline{q} \to 1$ or $\overline{q} \to 6$.

The two dynamic pressure conditions, $\overline{q}=1$ and $\overline{q}=6$, are associated with large torsional deformations and loss of stiffness in this two wing segment system. These large values occur because the determinant of the total system stiffness matrix (structural plus aerodynamic) in Eqn. 2.14.10 is zero. For the single-degree-of-freedom example, when the single aeroelastic torsional stiffness term became zero, divergence occurred. It appears that the divergence condition for the two degree of freedom system is (we will prove this in Section 2.14.1):
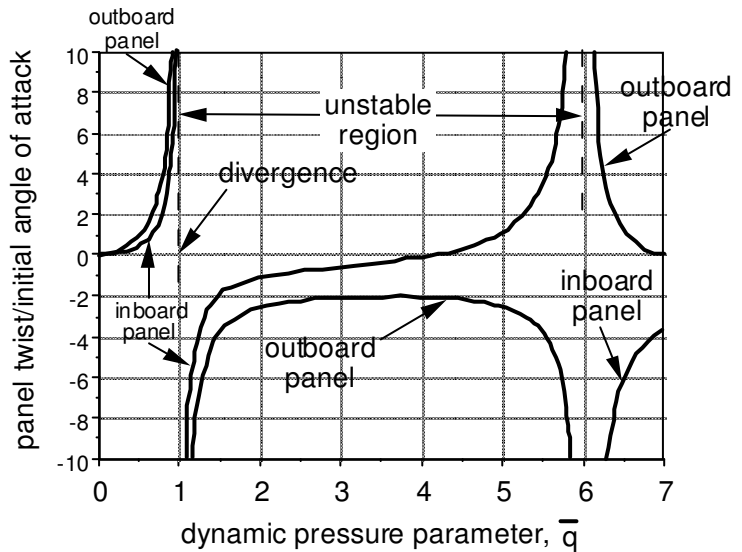

Figure 2.14.3 – Calculated twist angles θ_1 and θ_2 vs. dynamic pressure.

$$\Delta = 0 \qquad (2.14.11)$$

Combining the panel lift force expressions in Eqns. 2.14.1 a,b with the solutions for the static torsional deformations, θ_1 and θ_2, Eqn. 2.14.9, the lift on each segment is:

$$\begin{Bmatrix} L_1 \\ L_2 \end{Bmatrix} = qSC_{L_\alpha}\alpha_o \left\{ \begin{Bmatrix} 1 \\ 1 \end{Bmatrix} + \frac{\bar{q}}{\Delta} \begin{Bmatrix} 4-\bar{q} \\ 7-\bar{q} \end{Bmatrix} \right\} = \frac{3qSC_{L_\alpha}\alpha_o}{(\bar{q}-1)(\bar{q}-6)} \begin{Bmatrix} 2-\bar{q} \\ 2 \end{Bmatrix} \tag{2.14.12}$$

The total lift is $L_1 + L_2$. Let's say that this two degree of freedom system is required to produce a constant lift so that $L = L_1 + L_2 = \frac{W}{2}$ (this wing segment is one of two wings lifting an aircraft with weight W.) The wing angle of attack required to produce constant lift equal to W/2 is:

$$\alpha_o = \left(\frac{W}{2}\right) \frac{(\bar{q}-1)(\bar{q}-6)}{3qSC_{L_\alpha}(4-\bar{q})} \tag{2.14.13}$$

Combining Eqns. 2.14.12 and 2.14.13 we find the panel section lift forces:

$$\begin{Bmatrix} L_1 \\ L_2 \end{Bmatrix} = \frac{W}{2(4-\bar{q})} \begin{Bmatrix} 2-\bar{q} \\ 2 \end{Bmatrix} \tag{2.14.14}$$

The lift on each section changes with dynamic pressure. As dynamic pressure increases the outboard panel carries a larger fraction of the total weight. The angle of attack becomes zero at $\bar{q} = 1$ and . On the other hand, the lift on each segment is finite at $\bar{q} = 1$ and $\bar{q} = 6$. It does become infinite at $\bar{q} = 4$, but as we shall see, this outside the operational envelope because the wing is statically unstable at this point.

2.14.1 Static aeroelastic stability of multi-degree-of-freedom systems

The two-degree-of-freedom aeroelastic wing static equilibrium equations are written in general as:

$$\left[[K_S] - q[K_A] \right] \begin{Bmatrix} \theta_1 \\ \theta_2 \end{Bmatrix} = \begin{Bmatrix} Q_1 \\ Q_2 \end{Bmatrix} \tag{2.14.15}$$

where $\begin{Bmatrix} Q_1 \\ Q_2 \end{Bmatrix}$ are input loads. The vector $\begin{Bmatrix} \theta_1 \\ \theta_2 \end{Bmatrix}$ is the wing deformed system equilibrium state.

A statically stable linear system has a unique equilibrium state. But, when a system is in a state of neutral stability, more than one equilibrium state exists. This is the so-called bifurcation point. Let's see what special set of conditions must be present to obtain not one, but two solutions to Eqn. 2.14.15.

Define $\begin{Bmatrix} \theta_1 \\ \theta_2 \end{Bmatrix} = \begin{Bmatrix} \theta_1^{(S)} \\ \theta_2^{(S)} \end{Bmatrix} + \begin{Bmatrix} \delta\theta_1 \\ \delta\theta_2 \end{Bmatrix}$ where $\begin{Bmatrix} \delta\theta_1 \\ \delta\theta_2 \end{Bmatrix}$ is the vector of perturbation twist angles and $\begin{Bmatrix} \theta_1^{(S)} \\ \theta_2^{(S)} \end{Bmatrix}$ is the vector of original equilibrium twist angles. Use the notation $\left[\bar{K}_{ij} \right] = [K_S] - q[K_A]$ to denote the aeroelastic stiffness matrix. Then Eqn. 2.14.15 becomes

$$\left[\bar{K}_{ij} \right] \{\theta_j^{(S)}\} + \left[\bar{K}_{ij} \right] \{\delta\theta_j\} = \{Q_j\} \tag{2.14.16}$$

By definition $\{Q_i\} = \left[\bar{K}_{ij}\right]\{\theta_j^{(s)}\}$ so we have the following requirement for the existence of the perturbed equilibrium state.

$$\left[\bar{K}_{ij}\right]\{\delta\theta_j\} = \{Q_j\} - \left[\bar{K}_{ij}\right]\{\theta_j^{(S)}\} = \{0\} \qquad (2.14.17)$$

The condition for the existence of the perturbed static equilibrium state is:

$$\left[\bar{K}_{ij}\right]\{\delta\theta_j\} = \{0\} \qquad (2.14.18)$$

Equation 2.14.18 is simply the wing static equilibrium equation, Eqn. 2.14.15, with all external, non-deformation dependent loads removed, set to zero. As a result, static stability analysis is simply a by-product of our usual static equilibrium analysis.

When we drop the notation $\delta\theta$ in Eqn. 2.4.18 we can write this equation as:

$$q[K_A]\begin{Bmatrix}\theta_1 \\ \theta_2\end{Bmatrix} = [K_S]\begin{Bmatrix}\theta_1 \\ \theta_2\end{Bmatrix} \quad \text{or} \quad q\begin{Bmatrix}\theta_1 \\ \theta_2\end{Bmatrix} = [K_A]^{-1}[K_S]\begin{Bmatrix}\theta_1 \\ \theta_2\end{Bmatrix} \qquad (2.14.19)$$

with the understanding that the displacements θ_i are perturbations, not real displacements. In these equations we clearly identify the critical dynamic pressure as an eigenvalue and the displacement vector $\begin{Bmatrix}\theta_1 \\ \theta_2\end{Bmatrix}$ as an eigenvector.

For our example the eigenvalue problem is, from Eqn. 2.14.6:

$$\left(\frac{qSeC_{L_\alpha}}{K_T}\right)\begin{bmatrix}-1 & 0 \\ 0 & -1\end{bmatrix}\begin{Bmatrix}\theta_1 \\ \theta_2\end{Bmatrix} = \begin{bmatrix}5 & -2 \\ -2 & 2\end{bmatrix}\begin{Bmatrix}\theta_1 \\ \theta_2\end{Bmatrix}$$

or

$$\bar{q}\begin{bmatrix}-1 & 0 \\ 0 & -1\end{bmatrix}\begin{Bmatrix}\theta_1 \\ \theta_2\end{Bmatrix} = \begin{bmatrix}5 & -2 \\ -2 & 2\end{bmatrix}\begin{Bmatrix}\theta_1 \\ \theta_2\end{Bmatrix} \qquad (2.14.20)$$

From Eqn. 2.14.8 this eigenvalue problem can also be written as:

$$\bar{q}\begin{Bmatrix}\theta_1 \\ \theta_2\end{Bmatrix} = \begin{bmatrix}5 & -2 \\ -2 & 2\end{bmatrix}\begin{Bmatrix}\theta_1 \\ \theta_2\end{Bmatrix} \qquad (2.14.21)$$

2.14.2   Divergence eigenvalues

One obvious solution to Eqns. 2.14.18, 2.14.20, 2.14.21 is $\{\delta\theta_i\} = \{0\}$, but this solution simply defines the original, undisturbed equilibrium state since it means that we have no perturbation of the system; $\{\delta\theta_i\} = \{0\}$ is called the *trivial solution*. As mentioned previously, the existence of a non-zero perturbation solution is known as *Euler's criteria* for neutral static stability. The neutral stability condition involves finding a set of self-equilibrating deformations that do not require

external inputs such as α_o. At neutral stability the system is able to remain in a specially shaped deformed state without external loading.

Linear algebra tells us that the perturbations $\delta\theta_1$ and $\delta\theta_2$ can be nonzero only if the determinant of the aeroelastic stiffness matrix $\left[\,\overline{K}_{ij}\,\right]$ is zero.

$$\left|\overline{K}_{ij}\right| = \Delta = 0 \tag{2.14.22}$$

Equation 2.14.22 is identical to the neutral stability condition we found in Eqn. 2.14.11; Δ is called the *stability determinant.* It provides us with the *characteristic equation for stability*, a polynomial function of dynamic pressure.

Dynamic pressure is an *eigenvalue* of the aeroelastic stiffness matrix. When q is equal to an eigenvalue, two static equilibrium states will be possible. This special value of dynamic pressure is called a *bifurcation point*; Eqn. 2.14.22 is a formal mathematical condition for neutral static stability of a linear, multi-degree-of-freedom aeroelastic system.

In general, a structural system with n independent displacement degrees of freedom (the present example has $n=2$) has n eigenvalues. The eigenvalue that yields the lowest positive value of q usually has the most physical importance. (Note that there might be negative eigenvalues or even imaginary eigenvalues which would not make sense physically). For our example, the eigenvalues $\overline{q}_1$ and $\overline{q}_2$ for Eqn. 2.14.16 are $\overline{q}_1 = 1$ and $\overline{q}_2 = 6$.
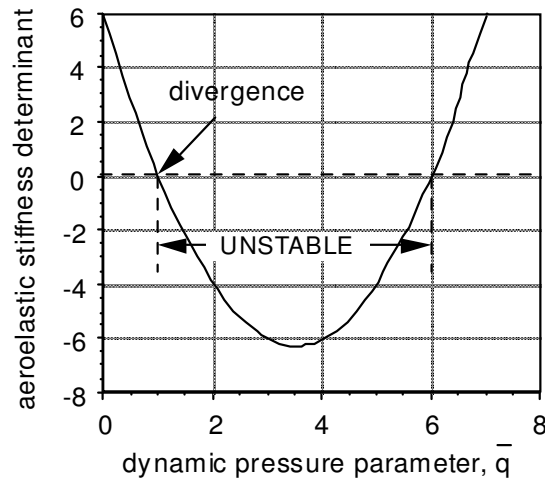
Figure 2.14.4- Aeroelastic stiffness matrix determinant Δ vs. $\overline{q}$.

The strain energy stored in the springs is always positive so the determinant of the aeroelastic stiffness matrix is positive when the dynamic pressure is zero. As shown in Figure 2.14.4, the determinant decreases as the dynamic pressure increases.

At $\overline{q} = 1$ the total energy stored as the result of wing torsion is just equal to the work done for some specific combinations of panel deformations (eigenvectors). At this condition, we lose the ability to resist additional aerodynamic moments. Further increases in airspeed will cause the determinant to become negative, alerting us to the fact that static equilibrium is impossible and that any additional loads will cause motion. This motion is divergent motion that we will examine later.

At values of dynamic pressure above $\overline{q} = 6$ the determinant is again positive, indicating that the system appears to be able to store energy. While this may be so theoretically, the result is meaningless because divergence has already occurred and we have moved well beyond the initial equilibrium position.

All solutions to Eqns. 2.14.11 and 2.14.22 are associated with neutral static equilibrium. On the other hand, from Figure 2.14.4, some solutions to Eqn. 2.14.11 are associated with entry into an instable region while others are associated with exit from the instability. The test of entry or exit from static stability is whether or not the determinant becomes positive or negative when the dynamic pressure increases.

The plot of the stability determinant in Figure 2.14.4 shows that the divergence dynamic pressure is the lower of these two values.

$$q_D = \bar{q}_1 \frac{K_T}{SeC_{L_\alpha}} = \frac{K_T}{SeC_{L_\alpha}} \qquad (2.14.23)$$

Note that if we change the value of one of the two torsion spring stiffnesses, say from $3K_T$ to $5K_T$, the eigenvalue in Eqn. 2.14.23 will change.

2.14.3   Divergence eigenvectors

Wing divergence eigenvectors are found by substituting, one at a time, the values of divergence dynamic pressure $\bar{q}_i$ into the equilibrium equations in Eqn. 2.14.18 and then solving for $\delta\theta_1$ and $\delta\theta_2$. We will eliminate the deltas from the $\delta\theta_1$ and $\delta\theta_2$ notation in the discussion that follows to simplify notation. When $\bar{q} = 1$, the two homogeneous equilibrium equations in Eqn. 2.14.18 become

$$4\theta_1 - 2\theta_2 = 0 \qquad (2.14.24)$$

$$-2\theta_1 + \theta_2 = 0 \qquad (2.14.25)$$

When $\bar{q} = 1$, we find from either Eqn. 2.14.24 or 2.14.25 that

$$\theta_1 = \frac{\theta_2}{2} \qquad (2.14.26)$$

Notice that any twist displacement vector with the ratio $\frac{\theta_2}{\theta_1} = 2$ satisfies Eqns. 2.14.24 and 2.14.24. We arbitrarily set $\theta_2 = 1$ and write the expression for the divergence "*mode shape*" associated with eigenvalue $\bar{q}_1 = 1$ as the vector

$$\begin{Bmatrix} \theta_1 \\ \theta_2 \end{Bmatrix}^{(1)} = \begin{Bmatrix} 0.5 \\ 1.0 \end{Bmatrix} \qquad (2.14.27)$$

Equation 2.14.27 also can be expressed as

$$\begin{Bmatrix} \theta_1 \\ \theta_2 \end{Bmatrix}^{(1)} = C_1 \begin{Bmatrix} 0.5 \\ 1.0 \end{Bmatrix} \qquad (2.14.28)$$

Since any arbitrary constant C_1 either positive or negative, can be used and still have the wing twist angles satisfy the perturbation equilibrium equations in Eqns. 2.14.24 and 2.14.25. Equation 2.14.27 (or Eqn. 2.14.28) is called a *divergence mode shape* corresponding to the eigenvalue $\bar{q}_1 = 1$.

With $\bar{q} = 6$, the perturbed static equilibrium equations become

$$-\theta_1 - 2\theta_2 = 0 \qquad (2.14.29)$$

$$-2\theta_1 - 4\theta_2 = 0 \qquad (2.14.30)$$

The solution is

$$\theta_1 = -2\theta_2 \qquad (2.14.31)$$

With $\theta_2 = 1$, the mode shape (eigenvector) for $\bar{q} = 6$ is written as

$$\left\{\begin{matrix} \theta_1 \\ \theta_2 \end{matrix}\right\}^{(2)} = \left\{\begin{matrix} -2 \\ 1 \end{matrix}\right\} \quad or \quad C_2 \left\{\begin{matrix} -2 \\ 1 \end{matrix}\right\} \qquad (2.14.32)$$

Look again at Figure 2.14.3, where the static response $\left\{\begin{matrix} \theta_1/\alpha_o \\ \theta_2/\alpha_o \end{matrix}\right\}$ is plotted as a function of $\bar{q}$, When $\bar{q} \to 1$, the ratio θ_1/θ_2 tends to 0.5; this is the first eigenvector. Similarly, as $\bar{q} \to 6$, the ratio θ_1/θ_2 is negative and approaches -2.0, the second eigenvector.

Let's compare the strain energy stored when the system is deformed in the *divergence mode shapes*. The strain energy, U, stored by torsion springs is:

$$U = \frac{1}{2}\left(3K_T\theta_1^2 + 2K_T\left(\theta_2 - \theta_1\right)^2\right) \qquad (2.14.33)$$

When deformed into the first *divergence mode* (with $C_1 = 1$), the strain energy is:

$$U_1 = \left(\frac{3}{2}K_T\left(\frac{1}{4}\right) + K_T\left(\frac{1}{4}\right)\right)\theta_2^2 = \frac{5}{8}K_T\theta_2^2 \qquad (2.14.34)$$

When deformed in the second divergence mode (with $C_2 = 1$), the strain energy is:

$$U_2 = \left(\frac{3}{2}K_T\left(4\right) + K_T\left(9\right)\right)\theta_2^2 = 15K_T\theta_2^2 \qquad (2.14.35)$$

The strain energy stored in divergence mode 2 is 24 times larger than that in divergence mode 1 because it takes more work by aerodynamic forces to deform the system into mode 2; this requires a much larger divergence dynamic pressure to generate these forces.

2.14.4   Summary - divergence of multi-degree of freedom systems

To construct the eigenvalue problem for static aeroelastic stability we first assume that the flexible structure is in a deformed equilibrium state. We then develop static equilibrium equations in terms

of the system deformation. Then, all terms on the right hand side of the equation (for instance, those depending on α_o) are set to zero. This gives us the static equilibrium equations for the neutrally stable perturbation states in terms of perturbation displacements.

We can either directly expand the determinant of the resulting matrix equation in terms of parameters such as q, K_T and then solve for q_D or, if we know the numerical values of K_T and other problem parameters, we can let the computer find numerical values of q_D.

In general, the eigenvalue problem for static stability of an nth order wing system is:

$$[K_S]\{\theta\} = q[K_A]\{\theta\} \qquad (2.14.36)$$

This equation has the form

$$[A]\{x\} = \lambda[B]\{x\} \qquad (2.14.37)$$

The eigenvalues, λ_i, are related to values of dynamic pressure for which the system has neutral static stability.

2.15 Example - Two degree of freedom wing divergence

A side view of a two segment wing idealization is shown in Figure 2.15.1. These segments are connected by two springs, one with spring constant k *lb/inch* and the other with spring constant 2k. Each wing segment has planform area S.
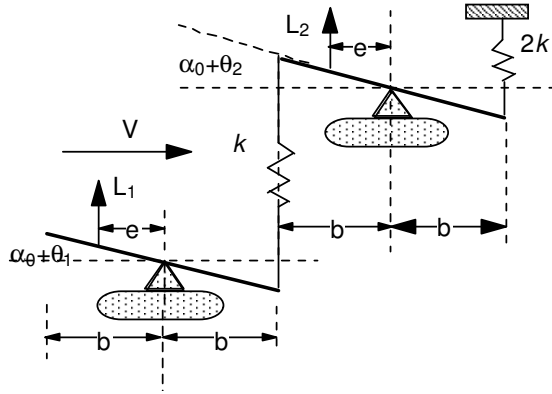
Figure 2.15.1 - Tandem wing geometry
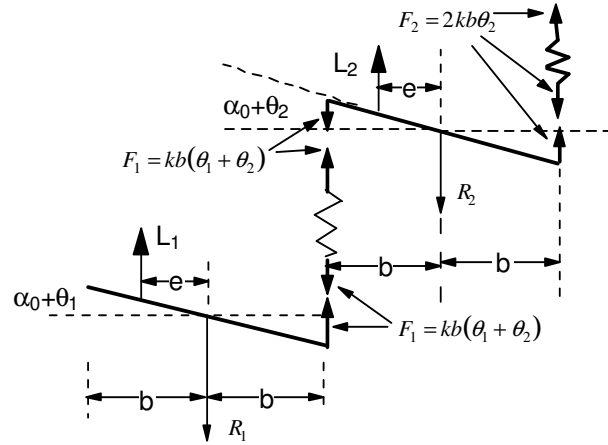
Figure 2.15.2 - Free body diagram of configuration

Each spring develops internal forces in response to relative deflection between its ends. The lift on each of the wing segments is given by

$$L_1 = qSC_{L\alpha}(\theta_1 + \alpha_o)$$
$$L_2 = qSC_{L\alpha}(\theta_2 + \alpha_o) \qquad (2.15.1)$$

where α_o is an initial angle of attack common to both segments and θ_1 and θ_2 are additional angles of incidence caused by lift on each wing segment. The free-body diagram for this configuration is shown in Figure 2.15.2.

Moment equilibrium gives the following (assuming small angles)

Sum clockwise about pin 1

$$\sum M_1 = 0 = L_1 e - kb^2 \left(\theta_1 + \theta_2 \right) \tag{2.15.2}$$

Sum clockwise about pin 2

$$\sum M_2 = 0 = L_2 e - kb^2 \left(\theta_1 + \theta_2 \right) - 2kb^2 \theta_2 \tag{2.15.3}$$

Substituting L_1 and L_2 from Eqns. 2.15.1 and 2.15.2 into Eqns. 2.15.3 and 2.15.4, we get

$$kb^2 \theta_1 + kb^2 \theta_2 - qSeC_{L_\alpha} \theta_1 = qSeC_{L_\alpha} \alpha_o$$
$$kb^2 \theta_1 + 3kb^2 \theta_2 - qSeC_{L_\alpha} \theta_2 = qSeC_{L_\alpha} \alpha \tag{2.15.4}$$

Equation 2.15.4 is written in matrix form as

$$kb^2 \begin{bmatrix} 1 & 1 \\ 1 & 3 \end{bmatrix} \begin{Bmatrix} \theta_1 \\ \theta_2 \end{Bmatrix} + qSeC_{L_\alpha} \begin{bmatrix} -1 & 0 \\ 0 & -1 \end{bmatrix} \begin{Bmatrix} \theta_1 \\ \theta_2 \end{Bmatrix} = qSeC_{L_\alpha} \alpha_o \begin{Bmatrix} 1 \\ 1 \end{Bmatrix} \tag{2.15.5}$$

Using the nondimensional pressure parameter

$$\bar{q} = \frac{qSeC_{L_\alpha}}{kb^2} \tag{2.15.6}$$

Then Eqn. 2.15.5 becomes

$$\begin{bmatrix} 1 & 1 \\ 1 & 3 \end{bmatrix} \begin{Bmatrix} \theta_1 \\ \theta_2 \end{Bmatrix} + \bar{q} \begin{bmatrix} -1 & 0 \\ 0 & -1 \end{bmatrix} \begin{Bmatrix} \theta_1 \\ \theta_2 \end{Bmatrix} = \bar{q} \alpha_o \begin{Bmatrix} 1 \\ 1 \end{Bmatrix} \tag{2.15.7}$$

Checking the stiffness matrix
Before continuing, let's use the strain energy method discussed in Section 2.3 to check to see if our structural stiffness matrix is correct. First we form the strain energy expression.

$$U = \frac{1}{2} kb^2 \left(\theta_1 + \theta_2 \right)^2 + \frac{1}{2} 2kb^2 \left(\theta_2 \right)^2$$

We then differentiate this result, using Eqn. 2.3.7 as the guide.

$$\frac{\partial U}{\partial \theta_1} = \frac{2}{2} kb^2 \left(\theta_1 + \theta_2 \right)(1) = kb^2 \left(\theta_1 + \theta_2 \right) \qquad \frac{\partial^2 U}{\partial \theta_1^2} = kb^2 \qquad \frac{\partial^2 U}{\partial \theta_1 \partial \theta_2} = kb^2$$

and

$$\frac{\partial U}{\partial \theta_2} = \frac{2}{2}kb^2 \left(\theta_1 + \theta_2\right)(1) + \frac{2}{2}2kb^2 \left(\theta_2\right) = kb^2\theta_1 + 3kb^2 \left(\theta_2\right) \quad \frac{\partial^2 U}{\partial \theta_2 \partial \theta} = kb^2 \quad \frac{\partial^2 U}{\partial \theta_2^2} = 3kb^2$$

Comparing these expressions with the structural stiffness matrix in Eqn. 2.15.5, we see that the stiffness matrix matches.

Note also that we have developed the stiffness matrix from the equilibrium equations in Eqns. 2.15.2 and 2.15.3. In these equations the structural stiffness terms are negative. We chose to take these terms to the left side of the equations so that they became positive. No matter how we solve these equations we will get the correct result. However, *it is always better to organize the equilibrium equations so the diagonal elements of the structural stiffness matrix are positive.* Then the equilibrium equation results will match the energy method results.

The divergence dynamic pressure

The divergence dynamic pressure is found by writing the homogeneous static equilibrium equations using Eqn. 2.15.7 in the following eigenvalue form (note again that the displacements in Eqn. 2.15.8 are perturbation displacements):

$$\bar{q}\begin{Bmatrix} \theta_1 \\ \theta_2 \end{Bmatrix} = \begin{bmatrix} 1 & 1 \\ 1 & 3 \end{bmatrix}\begin{Bmatrix} \theta_1 \\ \theta_2 \end{Bmatrix} \tag{2.15.8}$$

Equation 2.15.9 can also be written as

$$\begin{bmatrix} (1-\bar{q}) & 1 \\ 1 & (3-\bar{q}) \end{bmatrix}\begin{Bmatrix} \theta_1 \\ \theta_2 \end{Bmatrix} = \begin{Bmatrix} 0 \\ 0 \end{Bmatrix} \tag{2.15.9}$$

Calculating the determinant of the aeroelastic stiffness matrix in Eqn. 2.15.9 and setting it equal to zero, we have

$$\Delta = \bar{q}^2 - 4\bar{q} + 2 = 0 \tag{2.15.10}$$

Equation 2.15.10 has two roots. $\bar{q}_{D1} = 0.5858$ and $\bar{q}_{D2} = 3.4142$

The stability determinant in Eqn. 2.15.9 is positive between $\bar{q} = 0$ and $\bar{q}_D = 0.5858$ but becomes negative at larger values. This means that the divergence dynamic pressure is:

$$q_D = 0.5858\frac{kb^2}{SeC_{L_\alpha}} \tag{2.15.10}$$

2.16 *Example – the shear center, center of twist and divergence*

A wind tunnel test article consists of a thin, relatively rigid shell supported on a relatively flexible support mechanism consisting of three beams, as shown in Figures 2.16. As a result, the wing surface can only rotate with respect to the wind tunnel airstream and move upward or downward. The structural stiffness effects of these flexible beams are idealized to be three springs, K_1, K_2 and
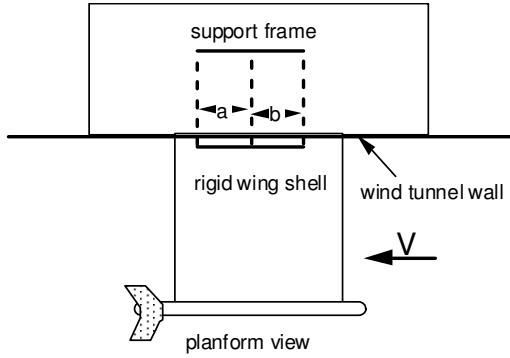
Figure 2.16.1 – Example-wind tunnel model with frame support

Figure 2.16.2 – Two-dimensional idealization
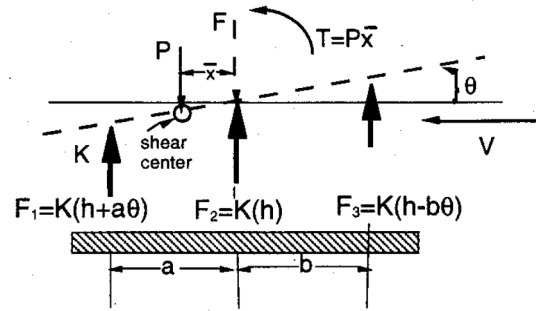
Figure 2.16.3 – Free body diagram showing spring forces and shear center position.

K_3 as indicated in Figure 2.16.2. In our case, measurements indicate that the support beams are of equal size so that the three spring constants are all equal to K (lb/in.) ($K_1 = K_2 = K_3 = K$).

The upward or downward wing displacement is represented by the displacement, h, at the center beam (positive downward). The wing rotation is due to wing elastic twist, θ, as indicated in Figure 2.16.2.

A free body diagram showing the deflected springs is shown in Figure 2.16.3. This free body diagram shows the deflections due to h and θ create restoring forces and a moment about the arbitrary reference point we have chosen at the center spring. Also shown in Figure 2.16.3 is the unknown position of the shear center. We cannot at present use this position for our reference point because we don't know where it is. Finding this position is one of our objectives.

The structural stiffness matrix of this model is developed using strain energy methods. From the deflections shown in Figure 2.16.3 we conclude that the strain energy due to deformation of the three springs is:

$$U = \frac{1}{2} K \left(h + a\theta \right)^2 + \frac{1}{2} K \left(h \right)^2 + \frac{1}{2} K \left(h - b\theta \right)^2$$

Using our relationships for the elements of the structural stiffness matrix (differentiating with respect to h and θ) we find

$$\begin{bmatrix} K_{11} & K_{12} \\ K_{12} & K_{22} \end{bmatrix} = \begin{bmatrix} 3K & K\left(a-b\right) \\ K\left(a-b\right) & K\left(a^2+b^2\right) \end{bmatrix}$$

When a downward force F (downward forces are positive, upward forces are negative because of the fact that we chose, arbitrarily, the downward displacement h to be positive) and a nose-up (measured at the reference point at the center beam and positive counter-clockwise) torque T are applied to this idealized wing model, the relationship between F, T, h and θ is represented as follows:

$$\left\{ \begin{array}{c} F \\ T \end{array} \right\} = \left[\begin{array}{cc} K_{11} & K_{12} \\ K_{12} & K_{22} \end{array} \right] \left\{ \begin{array}{c} h \\ \theta \end{array} \right\} \qquad (2.16.1)$$

Solving Eqn. 2.16.1 for h and θ,

$$\left\{ \begin{array}{c} h \\ \theta \end{array} \right\} = \frac{1}{\Delta} \left[\begin{array}{cc} K\left(a^2 + b^2\right) & K\left(b - a\right) \\ K\left(b - a\right) & 3K \end{array} \right] \left\{ \begin{array}{c} F \\ T \end{array} \right\} \qquad (2.16.2)$$

where $\Delta = |K| = 2K^2\left(a^2 + ab + b^2\right)$ is the determinant of the stiffness matrix. Note that since there are no aerodynamic forces (yet) this determinant is always positive.

2.16.1 Locating the model shear center

The wing sectional shear center is defined as a point on the wing section where a concentrated force may be applied without creating rotation. Suppose that the shear center is located at a distance $\bar{x}$ to the left of the center spring as indicated in Figure 2.16.3 (if we find that the shear center is to the right then $\bar{x}$ will be a negative number). When we apply the downward force P at the position $\bar{x}$ to the left of the center spring in Figure 2.16.3 we create external loads $F = P$ $and\,T = P\bar{x}$. Equation 2.16.2 becomes:

$$\left\{ \begin{array}{c} h \\ \theta \end{array} \right\} = \frac{1}{\Delta} \left[\begin{array}{cc} K_{22} & -K_{12} \\ -K_{12} & K_{11} \end{array} \right] \left\{ \begin{array}{c} P \\ P\bar{x} \end{array} \right\} \qquad (2.16.3)$$

From this equation we see that $\theta = \dfrac{P}{\Delta}\left(-K_{12} + K_{11}\bar{x}\right)$ and that this twist angle is a function of both P and $\bar{x}$. The size of the load is known because we are free to choose it. The distance $\bar{x}$ is unknown. If the value of $\bar{x}$ is the shear center then $\theta = 0$. Using Equation 2.16.3, we find the relationship between P, $\bar{x}$ and the stiffness matrix elements when P is placed at the shear center.

$$\theta = \frac{P}{\Delta}\left(-K_{12} + K_{11}\bar{x}\right) = 0 \qquad (2.16.4)$$

Solving for $\bar{x}$ we find

$$\bar{x} = \frac{K_{12}}{K_{11}} = \frac{Ka - Kb}{3K} = \frac{a - b}{3} \qquad (2.16.5)$$

Note that the size of the load P does not affect the shear center position. Although the rotation is zero, the displacement, h, is not zero, but depends on the size of P.

$$h = \frac{P}{\Delta}\left(K_{22} - \bar{x}K_{12}\right) = \frac{2}{3}\left(\frac{PK}{\Delta}\right)\left(a^2 + ab + b^2\right) = \frac{P}{3K} \qquad (2.16.6)$$

2.16.2 Locating the center of twist

The center of twist is defined as the point about which the wing section appears to rotate when only a torque is applied. To find the center of twist, we apply only a torque T. From Eqn. 2.16.2, the torque will cause *both* twist θ and deflection h:

$$h = \frac{K(b-a)}{\Delta}T \tag{2.16.7}$$

and

$$\theta = \frac{3K}{\Delta}T \tag{2.16.8}$$

The downward deflection of a point y a located a distance x *(to the left of the center spring)* is:

$$y = h + x\theta = \frac{K}{\Delta}(b-a+3x)T \tag{2.16.9}$$

We set $y = 0$, to find the point where the wing displacement is zero due to an applied torque:

$$x = \frac{a-b}{3} \tag{2.16.10}$$

Comparing Eqn. 2.16.10 with Eqn. 2.16.5, we see that the shear center and center of twist are located at the same point.

2.16.3 Wing divergence

To find the divergence dynamic pressure for this model, we apply an aerodynamic force $L = qSC_{L_\alpha}\alpha_o + qSC_{L_\alpha}\theta$ at the aerodynamic center located at a distance d to the right of the middle spring. In this case, the force and moment are $F = -L$ and $T=Ld$. The aerodynamic force is negative because we took the positive displacement direction downward and the lift force is directed upward. Similarly the lift causes a positive counter-clockwise torsional moment. The static equilibrium matrix equation is:

$$\begin{Bmatrix} -L \\ Ld \end{Bmatrix} = \begin{bmatrix} K_{11} & K_{12} \\ K_{12} & K_{22} \end{bmatrix} \begin{Bmatrix} h \\ \theta \end{Bmatrix} \tag{2.16.11}$$

The static equilibrium equation becomes

$$qSC_{L_\alpha}\alpha_o \begin{Bmatrix} -1 \\ d \end{Bmatrix} = \begin{bmatrix} K_{11} & (K_{12} + qSC_{L_\alpha}) \\ K_{12} & (K_{22} - qSC_{L_\alpha}d) \end{bmatrix} \begin{Bmatrix} h \\ \theta \end{Bmatrix} \tag{2.16.12a}$$

or

$$qSC_{L_\alpha}\alpha_o \begin{Bmatrix} -1 \\ d \end{Bmatrix} = \begin{bmatrix} K_{11} & \overline{K}_{12} \\ K_{12} & \overline{K}_{22} \end{bmatrix} \begin{Bmatrix} h \\ \theta \end{Bmatrix} \tag{2.16.12b}$$

The notation $\bar{K}_{ij}$ is applied to only the two stiffness terms with q in them. The deflections are:

$$\begin{Bmatrix} h \\ \theta \end{Bmatrix} = \frac{qSC_{L\alpha}\alpha_o}{\Delta} \begin{bmatrix} \bar{K}_{22} & -\bar{K}_{12} \\ -K_{12} & K_{11} \end{bmatrix} \begin{Bmatrix} -1 \\ d \end{Bmatrix} \qquad (2.16.13)$$

where $\Delta = K_{11}\bar{K}_{22} - \bar{K}_{12}K_{12}$.

To solve for divergence we set the determinant equal to zero.

$$\Delta = K_{11}\bar{K}_{22} - \bar{K}_{12}K_{12} = 0 \qquad (2.16.14)$$

Expanding the determinant,

$$K_{11}K_{22} - q_D SC_{L\alpha}K_{11}d - K_{12}^2 - q_D SC_{L\alpha}K_{12} = 0 \qquad (2.16.15)$$

We find that the divergence dynamic pressure is

$$q_D = \frac{1}{SC_{L\alpha}} \left(\frac{K_{22} - \dfrac{K_{12}^2}{K_{11}}}{d + \dfrac{K_{12}}{K_{11}}} \right) \qquad (2.16.16)$$

The shear center location is $\bar{x} = \dfrac{K_{12}}{K_{11}}$, so that

$$q_D = \left(\frac{K_{22} - K_{12}\bar{x}}{d + \bar{x}} \right) \cdot \frac{1}{SC_{L\alpha}} \qquad (2.16.17)$$

Notice that when $d = -\bar{x}$ (aerodynamic center coincident with the shear center), divergence will not occur. Substituting for $\bar{x}$, K_{22} and K_{12}, we have:

$$q_D SC_{L\alpha} = \frac{K_{11}K_{22} - K_{12}^2}{K_{11}d + K_{12}} = \frac{3K^2(a^2 + b^2) - K^2(a-b)^2}{3Kd + K(a-b)}$$

or
$$q_D = \frac{\dfrac{2}{3}K[a^2 + b^2 + ab]}{SC_{L\alpha}\left(d + \dfrac{a-b}{3}\right)} \qquad (2.16.18)$$

Notice that the distance $e = d + \dfrac{a-b}{3}$ is the distance between the shear center and the aerodynamic center, so that Eqn. 2.16.17 is similar to the expression we found from the analysis of our typical section, single degree of freedom system.

2.17 Example - Divergence of a three-degree-of-freedom system

A wind tunnel model shown in Figure 2.17.1 consists of three rigid wing sections mounted to a shaft so that they are free to rotate about the shaft. The gaps in the figure are accentuated for illustrative purposes. Three torsion springs restrain relative motion of the wing sections with respect to each
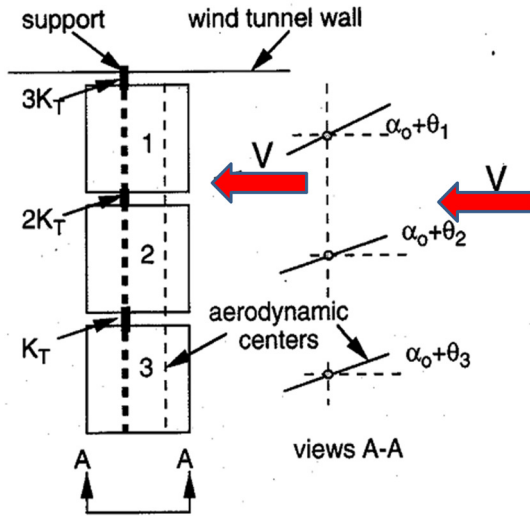

Figure 2.17.1 - Three degree of freedom wing planform and side view
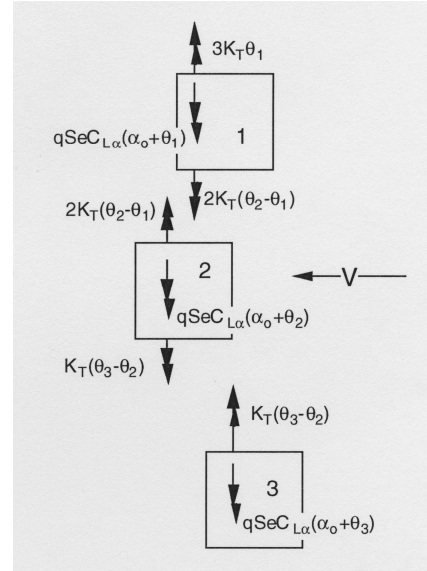
Figure 2.17.2 - Three degree of freedom free-body diagrams

other and the wind tunnel wall. The spring connecting wing section 1 to the wind tunnel wall has spring constant $3K_T$ lb-in/radian. The other springs have spring constants $2K_T$ and K_T, respectively. Each wing section has equal aerodynamic and geometric parameters given as S, e and C_{L_α}.

The wind tunnel is operating at a simulated altitude of 35,000 feet when the system is given an initial angle of attack α_o at airspeed, V. The angles of incidence of the three wing sections are shown in Figure 2.17.2.

Problem

1) Find the divergence airspeed assuming incompressible flow; 2) find the divergence speed in compressible flow. We are given that $\dfrac{K_T}{SeC_{L_\alpha}} = 1500 \; lb/ft^2$.

Solution

First develop the equations of static equilibrium in matrix form and then find the polynomial characteristic equation to calculate the divergence dynamic pressure when $\dfrac{K_T}{SeC_{L_\alpha}} = 1500 \; lb/ft^2$, where

$C_{L_{\alpha_o}}$ is the incompressible flow lift curve slope for each of the three sections, uncorrected for Mach number.

Summing torsional moments for each of the three wing sections shown in Figure 2.17.2 produces the following equations.

$$\Sigma M_1 = 0 = L_1 e - 3K_T \theta_1 + 2K_T (\theta_2 - \theta_1)$$

$$\Sigma M_2 = 0 = L_2 e - 2K_T (\theta_2 - \theta_1) + K_T (\theta_3 - \theta_2)$$

$$\Sigma M_3 = 0 = L_3 e - K_T (\theta_3 - \theta_2)$$

These three moment equilibrium equation, written in matrix form, become

$$\begin{bmatrix} (5K_T - qSeC_{L_{\alpha_o}}) & -2K_T & 0 \\ -2K_T & (3K_T - qSeC_{L_{\alpha_o}}) & -K_T \\ 0 & -K_T & (K_T - qSeC_{L_{\alpha_o}}) \end{bmatrix} \begin{Bmatrix} \theta_1 \\ \theta_2 \\ \theta_3 \end{Bmatrix} = qSeC_{L_{\alpha_o}} \alpha_o \begin{Bmatrix} 1 \\ 1 \\ 1 \end{Bmatrix} \qquad (2.17.1)$$

Arbitrarily define a nondimensional dynamic pressure $\bar{q} = \dfrac{q}{\dfrac{2K_T}{SeC_{L_{\alpha_o}}}} = \dfrac{qSeC_{L_{\alpha_o}}}{2K_T}$. Eqn. 2.17.1

becomes

$$\begin{bmatrix} 5 - 2\bar{q} & -2 & 0 \\ -2 & 3 - 2\bar{q} & -1 \\ 0 & -1 & 1 - 2\bar{q} \end{bmatrix} \begin{Bmatrix} \theta_1 \\ \theta_2 \\ \theta_3 \end{Bmatrix} = 2\bar{q}\alpha_o \begin{Bmatrix} 1 \\ 1 \\ 1 \end{Bmatrix} \qquad (2.17.2a)$$

Setting the external loads to zero the divergence eigenvalue problem is

$$\bar{q} \begin{Bmatrix} \theta_1 \\ \theta_2 \\ \theta_3 \end{Bmatrix} = \frac{1}{2} \begin{bmatrix} 5 & -2 & 0 \\ -2 & 3 & -1 \\ 0 & -1 & 1 \end{bmatrix} \begin{Bmatrix} \theta_1 \\ \theta_2 \\ \theta_3 \end{Bmatrix} \qquad (2.17.2b)$$

The divergence dynamic pressure for incompressible flow is found by forming the determinant of the aeroelastic stiffness matrix in Eqn. 2.17.2a and then setting it to zero to solve for q_{Do}. This gives the following characteristic equation.

$$\Delta = -8\bar{q}^3 + 36\bar{q}^2 - 36\bar{q} + 6 = 0 \qquad (2.17.3a)$$

Dividing by 2

$$4\bar{q}^3 - 18\bar{q}^2 + 18\bar{q} - 3 = 0 \qquad (2.17.3b)$$

The three roots of the characteristic equation, Eqn. 2.17b are $\bar{q}_1 = 0.2079 \quad \bar{q}_2 = 1.147 \quad \bar{q}_3 = 3.145$ The same results are found from a MATLAB eigenvalue calculation using Eqn. 2.17.2b.. Divergence occurs at the lowest value of $\bar{q}_D$ so the divergence dynamic pressure is

$$\bar{q}_{D_0} = 0.2079 \quad so \ that \quad q_{D_0} = 0.4158 \frac{K_T}{SeC_{L_\alpha}}$$

When the wind tunnel is operating at a simulated altitude of 35,000 feet, the speed of sound and air density are, respectively, $a_\infty = 973 \frac{ft}{s}$ $\rho = 7.365 \times 10^{-4} \frac{lb - \sec^2}{ft^4}$. The incompressible flow divergence speed V_o is $V_o^2 = \frac{2q_D}{\rho}$ so that $V_o^2 = 2\left(\frac{0.4158}{7.365 \times 10^{-4}}\right)\frac{K_T}{SeC_{L_{\alpha_o}}} = 1129 \frac{K_T}{SeC_{L_{\alpha_o}}} \left. ft^2 \middle/ sec^2 \right.$ so that the airspeed predicted with incompressible flow data is

$$V_o = 33.6\left(\frac{K_T}{SeC_{L\alpha}}\right)^{\frac{1}{2}} = 33.6(1500)^{\frac{1}{2}} = 1301 \; ft / sec \qquad (2.17.4)$$

The divergence Mach number is

$$M_o = \frac{V_o}{a_\infty} \; \text{ or } \; M_{Do} = 1.34$$

This Mach number is supersonic; the assumption of incompressibility is not valid.

With compressibility included, the divergence dynamic pressure q_D is found by using the Prandtl-Glauert transformation $C_{L_\alpha} = \frac{C_{L_{\alpha_o}}}{\sqrt{1 - M^2}}$ and then solving Eqn. 2.13.8

$$q_D = \overline{q}_D \left(\frac{2K_T}{SeC_{L_{\alpha_o}}}\right)\sqrt{1 - M_D^2} = \frac{1}{2}\rho a_\infty^2 M_D^2 \qquad (2.17.5)$$

Squaring both sides of Eqn. 2.17.5 gives

$$\left(\frac{4\overline{q}_D}{\rho a_\infty^2}\frac{K_T}{SeC_{L_{\alpha_o}}}\right)^2 (1 - M_D^2) = M_D^4 \qquad (2.17.6)$$

This equation is rewritten as

$$M_D^4 + A^2 K^2 M_D^2 - A^2 K^2 = 0 \qquad (2.17.7)$$

with $A = \left(\frac{4\overline{q}_{D_0}}{\rho a_\infty^2}\right)$ $K = \left(\frac{K_T}{SeC_{L_{\alpha_o}}}\right)$. The two solutions for M_D^2 in Eqn. 2.17.7 are

$$M_D^2 = \frac{-A^2 K^2 \pm \sqrt{A^4 K^4 + 4A^2 K^2}}{2} \qquad (2.17.8)$$

One of these values is negative. The positive value of M_D^2 is:

$$M_D^2 = \frac{-A^2 K^2 + \sqrt{A^4 K^4 + 4A^2 K^2}}{2} \qquad (2.17.9)$$

Taking the positive square root of Eqn. 2.17.9 (Mach number must be positive) we find the expression for the divergence Mach number at the match point.

$$M_D = AK\sqrt{\frac{-1+\sqrt{1+\dfrac{4}{A^2K^2}}}{2}}$$

(2.17.10)

With the values of $\bar{q}_{D_0}$, ρ. and a_∞ inserted into A and K we have:

$$M_D = 0.84\times10^{-3}\left(\frac{K_T}{SeC_{L_{\alpha_o}}}\right)\left[-1+\sqrt{1+2.83\times10^6\left(\frac{SeC_{L_{\alpha_o}}}{K_T}\right)^2}\right]^{\frac{1}{2}}$$

(2.17.11)

The divergence velocity V_c, with flow compressibility, is

$$V_c = a_\infty M_D$$

(2.17.12)

so that

$$V_c = 0.817(1500)\left[-1+\sqrt{1+2.83\times10^6\left(\frac{1}{1500}\right)^2}\right]^{\frac{1}{2}}$$

(2.17.13)

When we divide V_c by V_o we get

$$\frac{V_c}{V_o} = 0.02439(1500)^{\frac{1}{2}}\left[-1+\sqrt{-1+2.83\times10^6\left(\frac{1}{1500}\right)^2}\right]^{\frac{1}{2}} = 0.67$$

(2.17.14)

so $V_c = (0.67)(1301) = 871.7$ *fps.* and $M_D = 0.898$. This result is transonic and a bit larger than recommended for the validity of the Prandtl-Glauert transformation, but shows that divergence for this configuration is not supersonic.

The divergence mode shapes are found using 2.17.2b with each of the eigenvalues, taken one at a time, to solve the following equation.

$$\begin{bmatrix} 5-2\bar{q}_{D_0} & -2 & 0 \\ -2 & 3-2\bar{q}_{D_0} & -1 \\ 0 & -1 & 1-2\bar{q}_{D_0} \end{bmatrix}\begin{Bmatrix} \theta_1 \\ \theta_2 \\ \theta_3 \end{Bmatrix} = \begin{Bmatrix} 0 \\ 0 \\ 0 \end{Bmatrix}$$

For the first eigenvalue, $\bar{q}_{D_0} = 0.208$, these equations become:

$$
\begin{bmatrix} 4.584 & -2 & 0 \\ -2 & 2.584 & -1 \\ 0 & -1 & 0.584 \end{bmatrix} \begin{Bmatrix} \theta_1 \\ \theta_2 \\ \theta_3 \end{Bmatrix} = \begin{Bmatrix} 0 \\ 0 \\ 0 \end{Bmatrix} \tag{2.17.15}
$$

Because the 3 x 3 matrix is singular (we made it so when we formed the characteristic equation) we have only two independent equations. If we arbitrarily let $\theta_3 = 1$, the divergence mode shape for the wing is

$$
\begin{Bmatrix} \theta_1 \\ \theta_2 \\ \theta_3 \end{Bmatrix} = \begin{Bmatrix} 0.2549 \\ 0.5842 \\ 1 \end{Bmatrix} \tag{2.17.16}
$$

Note that we could have arbitrarily set any of the three displacements equal to 1 or any other number we might choose.

2.18 Example - Divergence of 2 DOF offset wing segment sections

In this section we will work a problem three different ways to show that how we choose the coordinate system and develop equations may change parts of the analysis, but does not change the result. A swept flexible lifting surface is modeled as the two interconnected, uncambered wing sections shown in Figure 2.18.1. This model simulates wing sweep by positioning the outer wing segment at a distance $h \tan \Lambda$ aft of the inner section (here the term h is a dimension, not the plunge displacement). The relative rotation of these sections with respect to each other and with respect to the wing root connection is restrained by two linear elastic torsion springs with equal spring constants K_T. These springs develop a restoring torque proportional to the twist angles θ_1 and θ_2, as shown in Figure 2.18.1.

The elastic axis of each section is located a distance e downstream of the section aerodynamic center (the ¼ chord line). Each wing section has a planform area equal to $S = hc$. The lift curve slope for each section is equal to C_{L_α}.
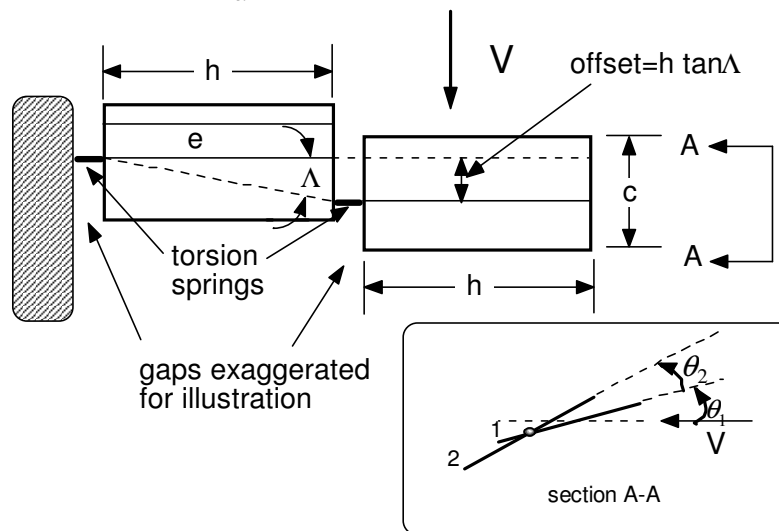

Figure 2.18.1 - Staggered wing section model

Problem

(a)   Develop the equations necessary to determine the divergence speed for this configuration.

(b)   Determine the divergence dynamic pressure q_D when $h/e = 10$ Plot q_D vs. angle Λ.

Solution

Begin by finding the equations for the twist deflection of each section. Because divergence is a self-equilibrating condition, we examine the system with no initial angle of attack so that the twist angles are perturbations from system static equilibrium. The Free Body Diagram for this problem is shown in Figure 2.18.2.
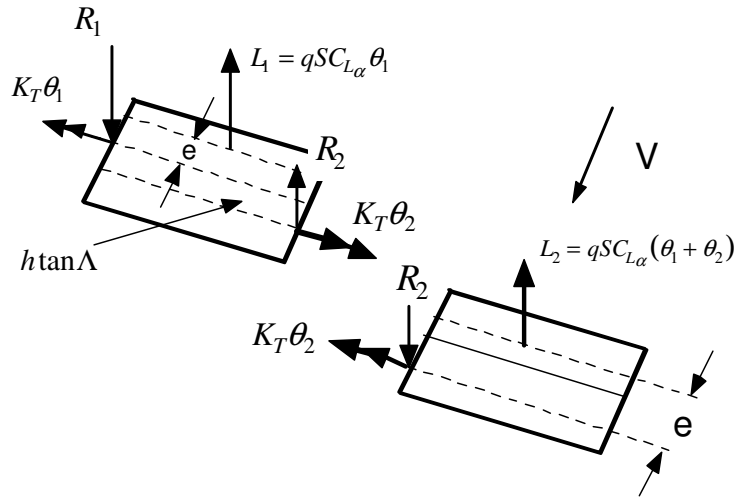

Figure 2.18.2 - Free body diagrams for inboard panel (segment 1) and outboard panel (segment 2)

Static torque equilibrium and shear equilibrium are written at and about the torsion springs as follows.

Section 2- Equilibrium at/about the outer rod (elastic axis)

Force equilibrium $\qquad\qquad\qquad\qquad\qquad R_2 = L_2$ $\qquad\qquad\qquad\qquad\qquad$ (2.18.1a)

Torque equilibrium (+ c-clockwise) $\qquad L_2 e - K_T \theta_2 = 0$ $\qquad\qquad\qquad\qquad$ (2.18.1b)

Section 1- Equilibrium about/at the inner rod (elastic axis)

Force equilibrium $\qquad\qquad\qquad -R_1 + L_1 + R_2 = 0 = -R_1 + L_1 + L_2$ $\qquad\quad$ (2.18.2a)

Torque equilibrium

(+ c-clockwise) $\qquad\qquad\qquad L_1 e - R_2 \left(h \tan \Lambda \right) + K_T \theta_2 - K_T \theta_1 = 0$

Substituting Eqn. 2.18.1a we get $\qquad L_1 e - L_2 \left(h \tan \Lambda \right) + K_T \theta_2 - K_T \theta_1 = 0$ $\qquad$ (2.18.2b)

Note that Eqns. 2.18.1b and 2.18.2b are elastically coupled and the stiffness matrix will be unsymmetrical. We could remove this coupling and asymmetry by using Eqn. 2.18.1b to change

Eqn. 2.18.2b to $L_1 e - L_2 (h \tan \Lambda) + L_2 e - K_T \theta_1 = 0$. However, we will use Eqns. 2.18.1b and 2.18.2b as our building blocks for this part of the example.

Note that the shear force equilibrium equations for R_1 and R_2 are required because the shear forces enter into the torque equilibrium equations. Substituting for the wing segment lift in terms of twist angles θ_1 and θ_2 in Eqn. 2.18.2b becomes

$$qSeC_{L_\alpha}\theta_1 - qSh \tan \Lambda C_{L_\alpha}(\theta_1 + \theta_2) - K_T\theta_1 + K_T\theta_2 = 0$$
$$or \quad K_T\theta_1 - K_T\theta_2 - qSeC_{L_\alpha}\theta_1 + qSh \tan \Lambda C_{L_\alpha}(\theta_1 + \theta_2) = 0$$

(2.18.3)

While Eqn. 2.18.1b becomes

$$qSeC_{L_\alpha}(\theta_1 + \theta_2) - K_T\theta_2 = 0$$
$$or \quad K_T\theta_2 - qSeC_{L_\alpha}(\theta_1 + \theta_2) = 0$$

(2.18.4)

Define the nondimensional parameter $\bar{q} = \dfrac{qSeC_{L\alpha}}{K_T}$ and divide Eqns. 2.18.3 and 2.18.4 by K_T to get

$$\left(1 - \bar{q} + \bar{q}\frac{h}{e}\tan\Lambda\right)\theta_1 - \left(-1 + \bar{q}\frac{h}{e}\tan\Lambda\right)\theta_2 = 0$$

(2.18.5)

$$-\bar{q}\theta_1 + (1 - \bar{q})\theta_2 = 0$$

(2.18.6)

Equations 2.18.5 and 2.18.6 are written in matrix form as

$$\begin{bmatrix} \left(1 - \bar{q} + \bar{q}\dfrac{h}{e}\tan\Lambda\right) & \left(-1 + \bar{q}\dfrac{h}{e}\tan\Lambda\right) \\ (-\bar{q}) & (1 - \bar{q}) \end{bmatrix} \begin{Bmatrix} \theta_1 \\ \theta_2 \end{Bmatrix} = 0$$

(2.18.7)

When $\dfrac{h}{e} = 10$ the divergence dynamic pressure is found by forming the determinant of aeroelastic stiffness matrix in Eqn. 2.18.7 and setting it to zero to get the characteristic equation for divergence.

$$\bar{q}_D^2 + \bar{q}_D(10\tan\Lambda - 3) + 1 = 0$$

(2.18.8)

The divergence dynamic pressure from this polynomial is

$$\bar{q}_D = \frac{\left(3 - 10\tan\Lambda \pm \sqrt{100\tan^2\Lambda - 60\tan\Lambda + 5}\right)}{2}$$

(2.18.9)

The plot of $\bar{q}_D$ versus Λ is shown in Figure 2.18.3. Notice that there are 2 solutions to Eqn. 2.18.9 and that these two roots bound an instability region for which the characteristic equation is negative,

$$\bar{q}_D^2 + \bar{q}_D \left(10\tan\Lambda - 3\right) + 1 < 0 .$$

When the term under the radical in Eqn. 2.18.9 is negative, the divergence dynamic pressure is a complex number; there will be no real divergence speed. These values occur to the right of the value $\Lambda = 5.71^\circ$ ($\tan\Lambda = 1/10$).
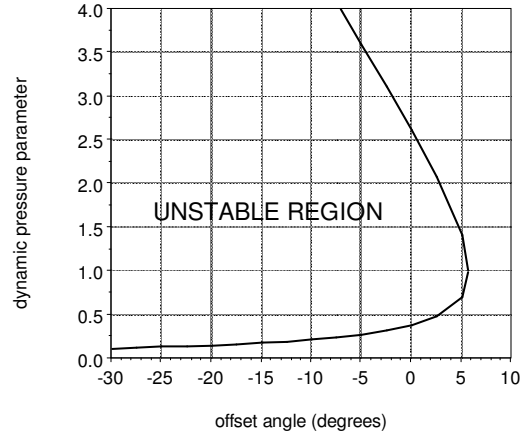

Figure 2.18.3 - Divergence parameter $\bar{q}$ as a function of angle Λ

When $\Lambda = 5.71^\circ$ the divergence dynamic pressure parameters found from Eqn. 2.18.9 are equal; above $\Lambda = 5.71^\circ$, no real divergence speed exists. At $\Lambda = 26.57^\circ$ the term under the radical is again zero. When $\Lambda > 26.57^\circ$ Eqn. 2.18.9 gives real, but negative, divergence dynamic pressure parameter values that are real, but negative. The plot of Eqn. 2.18.9 is entirely in the lower, negative region for these sweep angles.

The physical explanation for these "divergence impossible" values of sweep is that, when $\Lambda > 5.71^\circ$, the twist from the outer wing segment twists the inner wing segment nose-down so much that the configuration will not diverge.

2.18.1 Solution using a different coordinate system

Changing the wing segment coordinate system changes the equilibrium equations but cannot change the divergence speed. Let's illustrate this by considering the same example with a slightly different wing segment twist definition. For the outer wing segment (wing segment 2), the angle of attack is re-defined as shown in Figure 2.18.4 so that both wing segment twist angles are measured as rotations from a common line parallel to the airstream. This changes the equation for L_2 and the equation for the torsional reaction between the two wing segments.
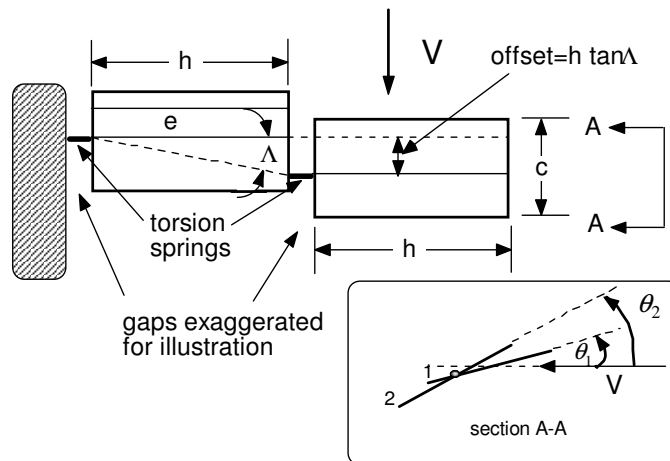

Figure 2.18.4 - Re-definition of wing segment elastic twist angles

The torsional moment equilibrium equations for this configuration are developed using the free body diagram shown in Figure 2.18.5.
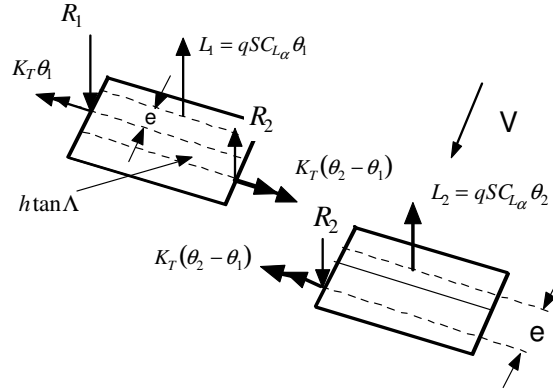

Figure 2.18.5 - Free body diagram with new twist angle coordinates

These equations are

$$-K_T\theta_1 + L_1 e + K_T(\theta_2 - \theta_1) - L_2 h\tan\Lambda = 0 \qquad (2.18.10)$$

$$-K_T(\theta_2 - \theta_1) + L_2 e = 0 \qquad (2.18.11)$$

Lift L_2 is now written as

$$L_2 = qSC_{L_\alpha}\theta_2 \qquad (2.18.12)$$

Substituting the lift expressions into Eqns. 2.18.10 and 2.18.11 results in the following two equations for torsional equilibrium

$$K_T\theta_1 - qSeC_{L_\alpha}\theta_1 + K_T\theta_1 - K_T\theta_2 + qSC_{L_\alpha}e\left(\frac{h}{e}\tan\Lambda\right)\theta_2 = 0 \qquad (2.18.13)$$

$$K_T(\theta_2 - \theta_1) - qSC_{L_\alpha}e\theta_2 = 0 \qquad (2.18.14)$$

Equations 2.18.13 and 2.18.14 are written in matrix form as

$$\begin{bmatrix} 2K_T & -K_T \\ -K_T & K_T \end{bmatrix}\begin{Bmatrix} \theta_1 \\ \theta_2 \end{Bmatrix} - qSeC_{L_\alpha}\begin{bmatrix} 1 & -\frac{h}{e}\tan\Lambda \\ 0 & 1 \end{bmatrix}\begin{Bmatrix} \theta_1 \\ \theta_2 \end{Bmatrix} = \begin{Bmatrix} 0 \\ 0 \end{Bmatrix} \qquad (2.18.15)$$

The stiffness matrix is symmetrical. With $\bar{q} = \dfrac{qSeC_{L_\alpha}}{K_T}$ we write Eqn. 2.18.15 as

$$\begin{bmatrix} (2-\bar{q}_D) & \left(-1+\bar{q}_D\dfrac{h}{e}\tan\Lambda\right) \\ (-1) & (1-\bar{q}_D) \end{bmatrix}\begin{Bmatrix} \theta_1 \\ \theta_2 \end{Bmatrix} = \begin{Bmatrix} 0 \\ 0 \end{Bmatrix} \qquad (2.18.16)$$

Copyright Terrence A. Weisshaar

The divergence dynamic pressure is computed by forming the determinant of the aeroelastic stiffness matrix in Eqn. 2.18.16, setting it to zero and solving for $\overline{q}_D$. The determinant is

$$(2 - \overline{q}_D)(1 - \overline{q}_D) + \left(-1 + \overline{q}_D \frac{h}{e} \tan\Lambda \right) = 0 \qquad (2.18.17)$$

With $\dfrac{h}{e} = 10$ the equations became

$$2 - 3\overline{q}_D + \overline{q}_D^2 - 1 + \overline{q}_D \frac{h}{e} 10 \tan\Lambda = 0 \qquad (2.18.18)$$

or

$$\overline{q}_D^2 - (3 - 10\tan\Lambda)\overline{q}_D + 1 = 0 \qquad (2.18.19)$$

Equation 2.18.19 is identical to Eqn. 2.18.8. We have shown, by example, that the divergence dynamic pressure is independent of coordinate system definition.

2.18.2 Equation development using the Principle of Virtual Work

Analytical mechanics provides an alternative way of developing static and dynamic equilibrium equations. Also referred to as Hamilton's Principle and the Principle of Virtual Work, these methods use work and energy concepts, together with variational calculus to methodically develop the equations necessary to find divergence. Some readers will be familiar with energy method formulations while others will not. The purpose here is not to give a tutorial, but to outline the solution in a way that is at least understandable at a low level.

A statement of the Principle of Virtual Work for a static system such as tose we have been considering is:

*"If a body is in static equilibrium under the action of prescribed external forces (in our case the two lift forces acting on the two sections) the **virtual work** done by these forces due to small compatible displacements (called **virtual displacements**) is equal to the change in the strain energy of the system."*

There are two new terms, virtual displacement and virtual work in this definition. If we have an infinitesimal displacement, say $d\theta_1$ then the inboard section actually rotates an infinitesimal amount so that some force must be applied to move it. A virtual displacement $\delta\theta_1$ is an infinitesimally small rotation, but this rotation is hypothetical or imaginary. The notation $\delta(\ )$ is an operator used for variational calculus, much like the operator $d(\ )$ used for calculus so that, for instance, $\delta\left(\theta_1^2\right) = 2\theta_1\delta\theta_1$.

Virtual work is the product of a force times a virtual displacement. For instance, when the inboard section rotates a small amount, the upward deflection of the aerodynamic center is $d_1 = e\theta_1$. If the lift were held constant during this actual displacement the work done would be $W_e = L_1 d_1 = L_1 e\theta_1$.

During a virtual displacement the lift is held constant so that the virtual work is $\delta W_e = L_1 \delta d_1 = L_1 e \delta \theta_1 = qSC_{L_\alpha} \theta_1 e \delta \theta_1 = qSeC_{L_\alpha} \theta_1 \delta \theta_1$. (Notice that the lift is a function of the twist angle but we require that the lift remain fixed even as the twist angle changes. The virtual work $\delta W_e \neq \delta L_1 d_1 = \delta q SeC_{L_\alpha} e \theta_1^2 = 2qSeC_{L_\alpha} e \theta_1 \delta \theta_1$.)

Return to the original coordinate system shown in Figure 2.18.1. When we give the wing segments virtual displacements $\delta \theta_1$ and $\delta \theta_2$, the lift vectors move upward as indicated in Figure 2.18.6
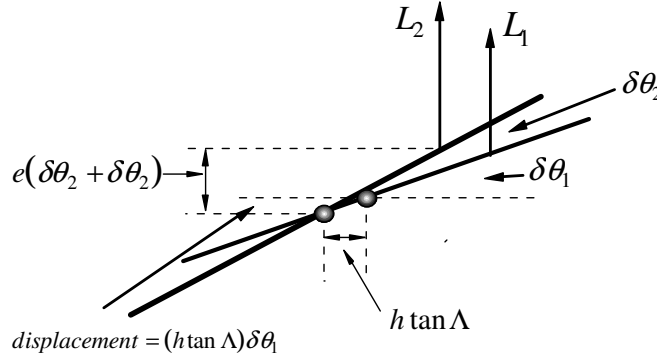

Figure 2.18.6 - Lift vector virtual displacements for wing segment sections

The virtual work δW done by the two aerodynamic loads is:

$$\delta W = L_1 \delta d_1 + L_2 \delta d_2 \qquad (2.18.20)$$

The virtual displacements δd_1 and δd_2 are the virtual displacements of the aerodynamic centers of the wing segments due to virtual torsional displacements $\delta \theta_1$ and $\delta \theta_2$

$$\delta d_1 = e \delta \theta_1 \qquad (2.18.21)$$

and

$$\delta d_2 = (e - h \tan \Lambda) \delta \theta_1 + e \, \delta \theta_2 \qquad (2.18.22)$$

Equation 2.18.20 becomes

$$\delta W = L_1 e \delta \theta_1 + L_2 (e - h \tan \Lambda) \delta \theta_1 + L_2 e \delta \theta_2 \qquad (2.18.23)$$

or

$$\delta W = \left(qSeC_{L_\alpha} \theta_1 + qSeC_{L_\alpha} (\theta_1 + \theta_2) - qSeC_{L_\alpha} (\theta_1 + \theta_2) \left(e \frac{h}{e} \tan \Lambda \right) \right) \delta \theta_1$$
$$+ qSeC_{L_\alpha} (\theta_1 + \theta_2) \delta \theta_2 \qquad (2.18.24)$$

The potential energy of the two springs is:

$$U = \frac{1}{2} K_T (\theta_1)^2 + \frac{1}{2} K_T (\theta_2)^2 \qquad (2.18.25)$$

The virtual work done by the springs is equal to the variation δU, the result of the variational operator $\delta(\ )$.

$$\delta U = K_T \theta_1 \delta\theta_1 + K_T \theta_2 \delta\theta_2 \qquad (2.18.26)$$

The virtual work of the lift forces (Eqn. 2.18.24) must equal the variation of the internal forces in the springs.

$$\delta W = \delta U$$

or

$$\left(qSeC_{L_\alpha}\theta_1 + qSeC_{L_\alpha}\left(\theta_1 + \theta_2\right) - qSeC_{L_\alpha}\left(\theta_1 + \theta_2\right)\left(e\frac{h}{e}\tan\Lambda \right) \right)\delta\theta_1$$
$$+ qSeC_{L_\alpha}\left(\theta_1 + \theta_2\right)\delta\theta_2 = K_T\theta_1\delta\theta_1 + K_T\theta_2\delta\theta_2 \qquad (2.18.27)$$

Gather like terms in Eqns. 2.18.27 and write these two equations in matrix form.

$$\begin{bmatrix} K_T & 0 \\ 0 & K_T \end{bmatrix}\begin{Bmatrix} \theta_1 \\ \theta_2 \end{Bmatrix} = qSeC_{L_\alpha}\begin{bmatrix} \left(2 - \dfrac{h}{e}\tan\Lambda\right) & \left(1 - \dfrac{h}{e}\tan\Lambda\right) \\ 1 & 1 \end{bmatrix}\begin{Bmatrix} \theta_1 \\ \theta_2 \end{Bmatrix} \qquad (2.18.28)$$

With $\bar{q} = \dfrac{qSeC_{L_\alpha}}{K_T}$ Eqn. 2.18.28 becomes

$$\begin{bmatrix} \left(1 - 2\bar{q} + \bar{q}\dfrac{h}{e}\tan\Lambda\right) & \left(-\bar{q} + \bar{q}\dfrac{h}{e}\tan\Lambda\right) \\ -\bar{q} & \left(1 - \bar{q}\right) \end{bmatrix}\begin{Bmatrix} \theta_1 \\ \theta_2 \end{Bmatrix} = \begin{Bmatrix} 0 \\ 0 \end{Bmatrix} \qquad (2.18.29)$$

Calculating the determinant of the aeroelastic stiffness matrix in Eqn. 2.18.29 and setting it to zero gives the characteristic equation:

$$\bar{q}_D^2 + \bar{q}_D\left(10\tan\Lambda - 3\right) + 1 = 0 \qquad (2.18.30)$$

This characteristic equation for divergence is identical to Eqns. 2.18.8 and 2.18.19 developed previously.

As mentioned previously, the matrix relationship in Eqn. 2.18.29 is different than Eqn. 2.18.7 even though the same twist coordinates are used. Note also that when $\bar{q} = 0$, Eqn. 2.18.29 is symmetric, while Eqn. 2.18.7 is not. A stiffness matrix found using the Principle of Virtual Work will always yield a symmetrical stiffness matrix.

2.19 Torsional divergence of an unswept flexible wing - differential equation model

So far we have limited our static aeroelastic models to one, two or three degrees of freedom in which the aerodynamic surfaces and structures were lumped into wing segments with interconnected torsional springs. The interaction between aerodynamic loads and twisting deformation of slender wings can be idealized so that equilibrium conditions are represented with differential equations. In this case the structure is uniformly distributed along the wing so that any deformation will be continuously distributed along the wing. In this section we will use this classic model (discussed routinely in all aeroelasticity texts)
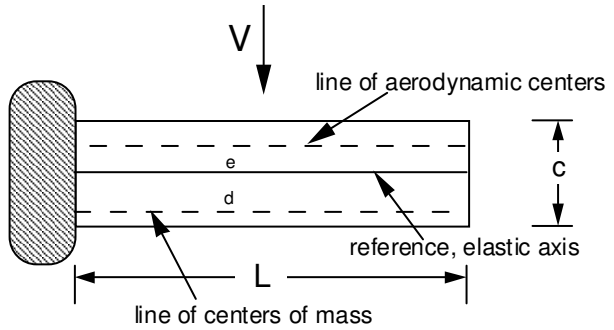

Figure 2.19.1 - Unswept wing planform

to discover the effects of aeroelasticity on a higher fidelity wing model. In particular, the model allows us to predict how the airloads redistribute themselves because of aeroelasticity.

The continuous flexible wing structure, shown in a planform view in Figure 2.19.1, has only twisting freedom, despite the fact that the wing will also bend under the distributed aerodynamic loads. The structure extends continuously
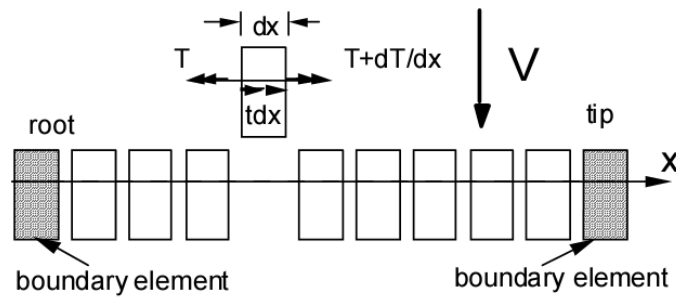

Figure 2.19.2 Unswept wing torsion idealization showing a typical torsion element

from the root to the tip and is embedded within a wing with constant chord. The model has a reference line of aerodynamic centers and a line of *shear centers* (called the *elastic axis*) so that there is a constant distance, e, between the two. In addition the wing mass is accounted for by distributing a constant mass per unit length along the wing at a distance *d* behind the elastic axis.

Figure 2.19.2 shows the continuous wing structure subdivided into infinitesimally small sections with lengths *dx* together with a typical free body diagram. Lift forces $l(x)$ are distributed, directed upward from the page, along the line of aerodynamic centers. Lift forces produce a torque about the wing elastic axis. The lift per unit length, in terms of the initial angle of attack and the distributed twist, $\theta(x)$, is:

$$l(x) = qc\,c_{l_\alpha}\alpha = qca_o(\alpha_o + \theta)$$

(2.19.1)

The notation a_o is used as shorthand for the local lift curve slope c_{l_α}. In reality the local lift curve slope is not constant but changes with wing location, but this model ignores this feature. This aerodynamic representation is often referred to as ***strip theory*** in which the aerodynamic interaction between elements is ignored.

In addition, an aerodynamic pitching moment is distributed along the span at the aerodynamic center.

$$m_{ac} = qc^2 c_{mac} \tag{2.19.2}$$

where c_{mac} is the sectional moment coefficient (also assumed constant along the wing) about the aerodynamic centerline. Finally, the distributed wing weight w creates a torque, t_w.

$$t_w = nwd \tag{2.19.3}$$

where n is the load factor normal to the wing surface. Combining these loads, the distributed torque, shown in Figure 2.19.2, and positive as shown, is:

$$t(x) = qcea_o(\alpha_o + \theta) + qc^2 c_{mac} + nwd$$
$$(note \ a_o = c_{l_\alpha}) \tag{2.19.4}$$

The relationship between the twist deformation along the length of this structure and an internal cross-sectional resultant torque, $T(x)$, shown in Figure 2.19.2, is given by the relationship:

$$T(x) = GJ \frac{d\theta}{dx} \tag{2.19.5}$$

GJ is the effective torsional stiffness of the wing cross-section.

Equilibrium of internal and external torques about the x-axis gives:

$$\Sigma M_x = 0 = T - tdx - \left(T + \frac{dT}{dx} dx \right) = \left(-t - \frac{dT}{dx} \right) dx \tag{2.19.6}$$

or

$$\frac{dT}{dx} = -t(x) \tag{2.19.7}$$

By using Eqn. 2.19.7, we can derive a relation between the torsional deformation θ and the applied external torque $t(x)$. This is

$$\frac{dT}{dx} = \frac{d}{dx} \left(GJ \frac{d\theta}{dx} \right) = -t(x) \tag{2.19.8}$$

Substituting the expressions for the distributed torque, Eqn. 2.19.8, becomes:

$$\frac{d}{dx} \left(GJ \frac{d\theta}{dx} \right) + qcea_o \theta = -\left(qcea_o \alpha_o + qc^2 c_{mac} + nwd \right) \tag{2.19.10}$$

$K = \left(qcea_o \alpha_o + qc^2 c_{mac} + nwd \right) / GJ$. With GJ constant along the wing, Eqn. 2.19.10 is $\frac{d^2\theta}{dx^2} + \left(\frac{qcea_o}{GJ} \right) \theta = -K$. Define an aeroelastic parameter, $\lambda^2 = \frac{qcea_o}{GJ}$; Eqn. 2.19.10 is:

$$\theta'' + \lambda^2 \theta = -K \tag{2.19.11}$$

The solution to Eqn. 2.19.11 is:

$$\theta(x) = A\sin\lambda x + B\cos\lambda x - K/\lambda^2 \tag{2.19.12}$$

where A and B are unknown constants. At the wing root, $x=0$, we have a boundary condition.

$$\theta(0) = 0 = B - \frac{K}{\lambda^2}$$

that gives $B = \dfrac{K}{\lambda^2}$. The expression for $\theta(x)$ becomes:

$$\theta(x) = A\sin\lambda x - \frac{K}{\lambda^2}(1-\cos\lambda x) \tag{2.19.13}$$

At the wing tip, $x=L$, the torque $T(L)$ is zero because it is a free end. From Eqn. 2.19.5,

$$T(L) = GJ\theta'(L) = 0 = GJ\left[A\lambda\cos\lambda L - \frac{K}{\lambda}\sin\lambda L\right] \tag{2.19.14}$$

Solving for A and substituting it into Eqn. 2.19.13, we have:

$$\theta(x) = \frac{-K}{\lambda^2}\left[1-\cos\lambda x - (\tan\lambda L)(\sin\lambda x)\right]$$

$$\tag{2.19.15a,b}$$

$$\theta(x) = -\left(\alpha_o + \left[\frac{c}{e}\right]\left[\frac{c_{mac}}{a_o}\right] + \left[\frac{nwd}{qcea_o}\right]\right)\left[1-\cos\lambda x - (\tan\lambda L)(\sin\lambda x)\right]$$

Equations 2.19.15(a) and (b) describe the twist distribution along the wing from root to tip. We should not forget that the wing also has bending deflection, but bending deflection does not affect unswept wing airloads.

Equation 2.19.15(a) shows that the $\tan\lambda L$ term has a big effect on wing twist. A plot of $\tan\lambda L$ vs. λL is shown in Figure 2.19.3. At $\lambda L = \dfrac{\pi}{2}$, $\tan\lambda L$ becomes infinite. If $\lambda = \dfrac{\pi}{2L}$, small initial wing loads produce (theoretically) infinite torsional deformations. Physically, this cannot happen because structural and/or aerodynamic nonlinear effects would make our model assumptions invalid.
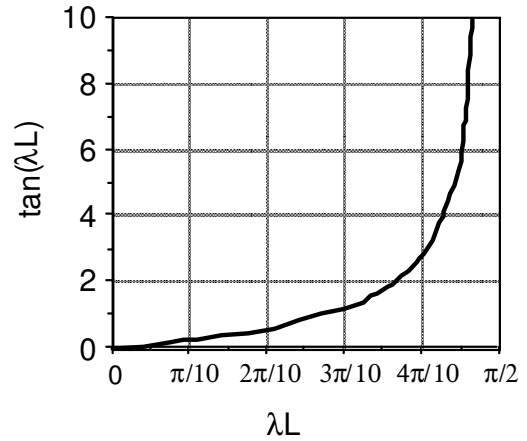

Figure 2.19.3- Twist amplification coefficient tan λL

We suspect (and will prove in the next section) that torsional divergence of this wing model occurs when

$$\lambda^2 = \frac{qcea_o}{GJ} = \left(\frac{\pi}{2L}\right)^2 \tag{2.19.16}$$

or

$$q_D = \left(\frac{\pi}{2L}\right)^2 \left(\frac{GJ}{cea_o}\right) = \left(\frac{\pi}{2}\right)^2 \left(\frac{GJ}{L}\right)\left(\frac{1}{Sec_{l_\alpha}}\right) \tag{2.19.17}$$

The typical section idealization predicted the divergence dynamic pressure to be $q_D = {K_T}/{SeC_{L\alpha}}$,

the dynamic pressure at divergence is directly proportional to the stiffness parameter ${GJ}/{L}$ and inversely proportional to wing area S; the greater the wing semi-span, the lower the divergence q. Notice also that the sectional lift curve slope $c_{l_\alpha} = a_o$ has replaced the wing lift curve slope in the equation for $q_D = {K_T}/{SeC_{L\alpha}}$.
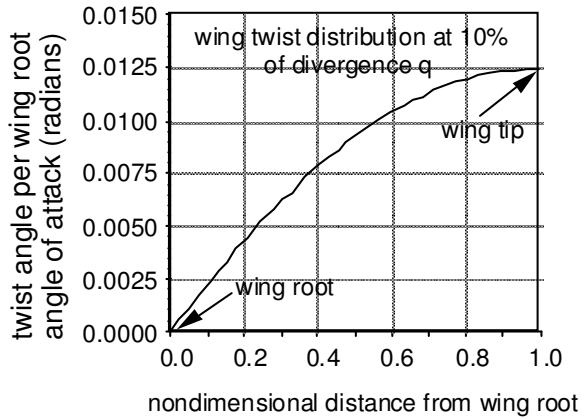

Figure 2.19.4 plots Eqn. 2.19.15(b) when K=1 (the plot is θ/K) and q equal to 10% of the divergence dynamic pressure. This twist distribution is very close to that found when aeroelastic effects are ignored.

Figure 2.19.4 - Twist angle (radians) vs. distance from root at 10% divergence q

2.19.1 The perturbation solution for differential equation divergence dynamic pressure

Stability is determined by considering perturbations away from a static equilibrium position. We develop the perturbation equilibrium equation by taking Eqn. 2.19.10 and setting the right hand side to zero.

$$\frac{d^2\theta}{dx^2} + \left(\frac{qcea_o}{GJ}\right)\theta = 0 \tag{2.19.18}$$

In this case, θ represents the perturbation twist distribution along the wing. The is

$$\theta(x) = A\sin\lambda x + B\cos\lambda x \tag{2.19.19}$$

with the constants A and B undetermined. The boundary conditions are

$$\theta(0) = 0 \tag{2.19.20}$$

and

$$T(L) = GJ\theta'(L) = 0 \tag{2.19.21}$$

Substituting Eqn. 2.19.20 into Eqn. 2.19.19, we have

$$\theta(0) = A\sin\lambda * 0 + B\cos\lambda * 0 = 0 \qquad (2.19.22)$$

or
$$A(0) + B(1) = 0 \qquad (2.19.23)$$

The wing free end torque condition, Eqn. 2.19.21, becomes

$$\theta' = A\lambda\cos\lambda L - B\lambda\sin\lambda L \qquad (2.19.24)$$

$$A(\lambda\cos\lambda L) + B(-\lambda\sin\lambda L) = 0 \qquad (2.19.25)$$

Equations 2.19.23 and 2.19.25 are written in matrix form as

$$\begin{bmatrix} 0 & 1 \\ (\lambda\cos\lambda L) & (-\lambda\sin\lambda L) \end{bmatrix} \begin{Bmatrix} A \\ B \end{Bmatrix} = \begin{Bmatrix} 0 \\ 0 \end{Bmatrix} \qquad (2.19.26)$$

This is an eigenvalue problem. The determinant of the 2 x 2 matrix in Eqn. 2.19.27 must be zero if A and B are to be nontrivial. This leads to the condition for neutral stability at divergence.

$$\Delta = \lambda\cos\lambda L = 0 \qquad (2.19.27)$$

This equation has the following solutions

$$\lambda^2 L^2 = \frac{n^2\pi^2}{4} = \frac{q_D cec_{l\alpha}L^2}{GJ} \qquad (2.19.28)$$

where n is an odd number so that

$$\lambda L = \frac{\pi}{2}, \frac{3\pi}{2}, \dots \frac{(2n+1)\pi}{2} \qquad (2.19.29)$$

The lowest value in Equation 2.19.28 (*n=1*) defines the divergence dynamic pressure. This leads to the divergence condition when *n = 1*.

$$\lambda^2 L^2 = \frac{\pi^2}{4} = \frac{q_D cec_{l\alpha}L^2}{GJ} \qquad (2.19.30)$$

Equations. 2.19.30 and 2.19.16 are identical.

When the eigenvalue in Eqn. 2.19.28 and the boundary conditions are inserted into the solution for the eigenfunction, Eqn. 2.19.19 we get the divergence mode shape.

$$\theta(x) = A \sin \lambda x = A \sin\left(\frac{\pi}{2}\frac{x}{L}\right)$$

This is the mode shape for divergence of this continuous wing model. It has an arbitrary amplitude, A, and is a half sine wave.

Figure 2.19.5 shows the effect of increasing the value of the nondimensional dynamic pressure to 75% of the divergence dynamic pressure. The same plot for the 10% divergence dynamic pressure was previously presented in Figure 2.19.4 and is barely visible in Figure 2.19.5. An increase in dynamic pressure from 10% to 50% and 75% of the divergence dynamic pressure creates a substantial increase in twist (and lift) if the angle of attack is not changed.
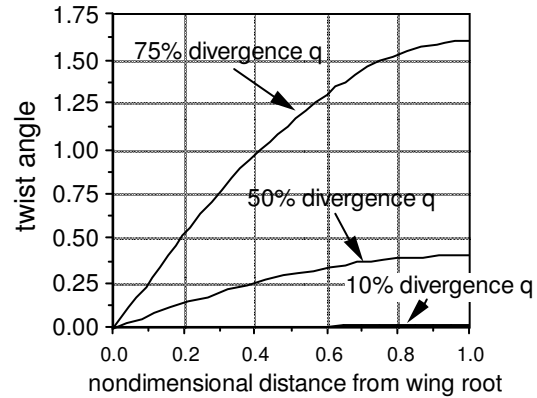

Figure 2.19.5- Twist angle parameter, θ/K vs. distance from root for three different dynamic pressures

2.19.2 Example - Divergence of a wing with flexible wing/fuselage attachment

The wing root attachment to an aircraft fuselage is fairly rigid. However, to investigate the effect of a flexible wing root/fuselage connection we will use the differential equation model. The planform of our uniform cross-section, uncambered, unswept wing is shown in Figure 2.19.6 (the wing semi-span is the dimension b instead of L and the independent coordinate is now y, not x). The wing-fuselage attachment joint is torsionally flexible; a torsional spring with spring stiffness K_T (in-lb./rad.) is attached between the wing root and the fuselage so that the attachment restoring moment is $K_T\theta(0)$ when the wing root twists an amount $\theta(0)$. In the previous example, the root was restrained so that $\theta(0) = 0$.

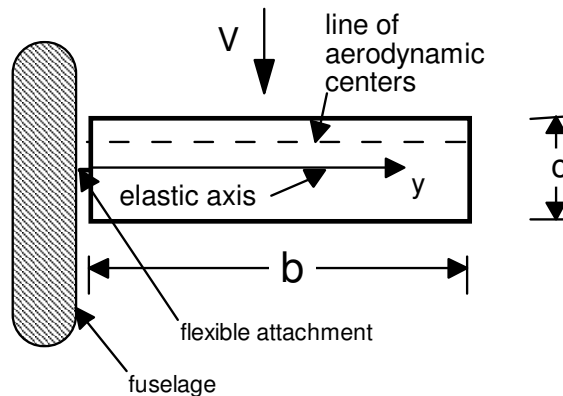

Figure 2.19.6 - Continuous wing with flexible wing/fuselage attachment

The purpose of this example is to investigate how wing attachment flexibility changes the divergence speed of this wing model. To do this we will:

- develop the boundary conditions for wing divergence and show that the value of the dimensionless stiffness ratio $\beta = GJ/K_T b$ determines the wing divergence speed.
- develop the characteristic equation for wing divergence and solve this equation for several values of β.

The equilibrium equation for the continuous wing does not change. From Eqn. 2.19.18, the homogenous torsional equilibrium equation for the wing perturbed twist distribution, $\theta(y)$, at divergence, is $\theta'' + \lambda^2 \theta = 0$ *with* $\lambda^2 = \dfrac{qcec_{l_\alpha}}{GJ}$.
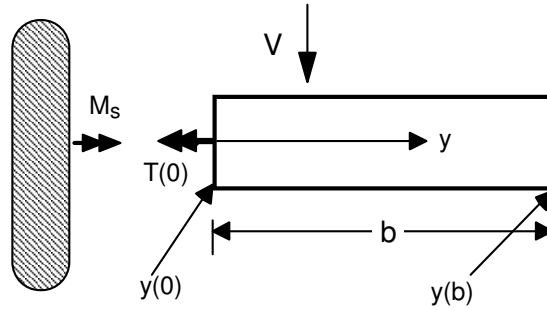
Figure 2.19.7 - Free body diagram of wing/fuselage junction

The internal torques present at the wing root are shown in Figure 2.19.7. The attachment spring torque, M_s, and the internal wing torque, T, at the wing root are defined as

$$M_S \equiv K_T \theta(0) \tag{2.19.32a}$$

and

$$T(0) \equiv GJ\theta'(0) \tag{2.19.32b}$$

Torque equilibrium at $y = 0$ is a boundary condition. As indicated in Figure 2.19.7, the torque from the torsion spring, M_s, and the torque at the wing root must be in equilibrium so that $T(0) - M_s = 0$, or

$$K_T \theta(0) = GJ\theta'(0) \tag{2.19.33}$$

or

$$\frac{K_T}{GJ}\theta(0) = \theta'(0) \tag{2.19.34}$$

At the wing tip, $y = b$, the torque is zero.

$$T(b) = GJ\theta'(b) = 0 \tag{2.19.35}$$

Since GJ is nonzero; we divide by GJ to write the second boundary condition as:

$$\theta'(b) = 0 \tag{2.19.36}$$

Equations. 2.19.18, 2.19.34 and 2.19.36 form an eigenvalue problem. The general solution to the differential equation is $\theta(y) = A\sin\lambda y + B\cos\lambda y$ so that the derivative of the twist along the wing is $\theta'(y) = A\lambda\cos\lambda y - B\lambda\sin\lambda y$. The boundary condition at the wing/fuselage junction (Eqn. 2.19.34) becomes:

$$\frac{K_T}{GJ}\theta(0) = B\frac{K_T}{GJ} = \theta'(0) = A\lambda$$
$$B\frac{K_T b}{GJ} = A\lambda b$$
$$B = A\beta\lambda b$$

Finally $\qquad\qquad\qquad A\beta\lambda b - B = 0 \;\; \text{with} \;\; \beta = \frac{GJ}{K_T b}$ $\qquad\qquad$ (2.19.37)

The torque free condition at the wing tip (Eqn. 2.19.36) is written as:

$$\theta'(b) = A\lambda\cos\lambda b - B\lambda\sin\lambda b = 0 \qquad\qquad (2.19.38)$$

Written in matrix form, Eqns. 2.19.37 and 2.19.38 become:

$$\begin{bmatrix} \beta\lambda b & -1 \\ \lambda\cos\lambda b & -\lambda\sin\lambda b \end{bmatrix}\begin{Bmatrix} A \\ B \end{Bmatrix} = \begin{Bmatrix} 0 \\ 0 \end{Bmatrix} \qquad\qquad (2.19.39)$$

The determinant of this matrix equation is the characteristic equation for the divergence problem.

$$\Delta = \lambda(-\beta\lambda b\sin\lambda b + \cos\lambda b) = 0 \qquad\qquad (2.19.40)$$

When the attachment is rigid, K_T is infinite, $\beta = 0$, and Eqn. 2.19.40 reduces to Eqn. 2.19.27. Since the airspeed is greater than zero, $\lambda \neq 0$, so we can divide Eqn. 2.19.40 by λ to find the characteristic equation for divergence of this wing model in terms of the eigenvalue λb.

$$\beta\lambda b\tan\lambda b = 1 \qquad\qquad (2.19.41)$$

or $\qquad\qquad\qquad\qquad \tan\lambda b = \frac{1}{\beta\lambda b}$ $\qquad\qquad$ (2.19.42)

The solution for λb is the intersection between the two functions, $\tan\lambda b$ and $\dfrac{1}{\beta\lambda b}$. When $\beta = 0$ (K_T is infinite) the root is rigid and the eigenvalue for Eqn. 2.19.42 is $\lambda b = \frac{\pi}{2}$. Figure 2.19.8 shows the solution to Eqn. 2.19.42 for three different values of β: $\beta = \frac{1}{8}$, $\beta = \frac{1}{4}$, and $\beta = \frac{3}{4}$. The abscissa in Figure 2.19.8 is $\dfrac{\lambda b}{\pi/2}$ where the clamped wing root reference value is $\dfrac{\pi}{2}$.
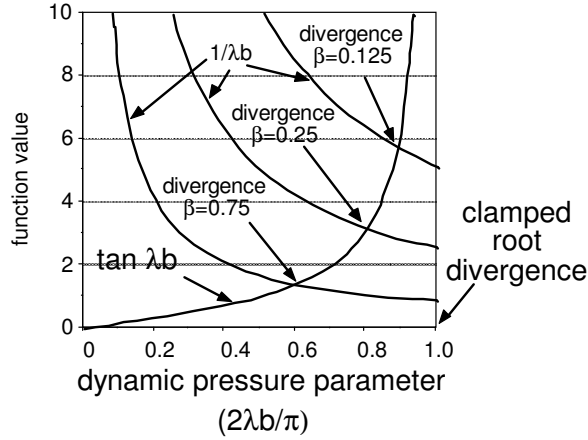
Figure 2.19.8 - Eigenvalue solutions for three different values of β

For example, with $\beta = 0.25$, Figure 2.19.8 shows that

$$\frac{\lambda b}{\pi/2} = 0.8051 \ or \ \lambda b = \sqrt{\frac{qcec_{l_\alpha}}{GJ}} b = 1.2646 \tag{2.19.43}$$

Stiffer (larger) values of the wing/fuselage attachment spring stiffness correspond to small values of β, so, as the fuselage attachment becomes stiffer, the eigenvalue associated with wing divergence is closer to that associated with a torsionally clamped wing root.

Using Eqn. 2.19.43 and the divergence dynamic pressure for $\beta = 0.25$ is:

$$\lambda^2 = \frac{q_D cec_{l_\alpha}}{GJ} = \left(\frac{1.2646}{b}\right)^2$$

or
$$q_D = \left(\frac{1.2646}{b}\right)^2 \frac{GL}{cec_{l_\alpha}} = 1.60 \frac{GL}{cb^2 ec_{l_\alpha}} = \left(0.805 \frac{\pi}{2}\right)^2 \frac{GL}{cb^2 ec_{l_\alpha}} \tag{2.19.44}$$

since the airspeed involves a square root of the answer in Eqn. 2.19.44 we conclude that with $\beta = 0.25$ the flexibility of the wing root attachment reduces the wing divergence airspeed by about 20% when compared to a rigid attachment.

Figure 2.19.9 shows a plot of the wing divergence speed relative to the clamped wing divergence speed, as a function of β.
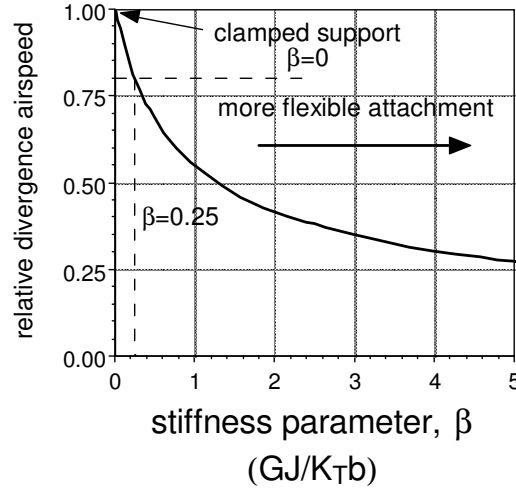
Figure 2.19.9 - The effect of the support stiffness conditions on divergence

From Eqn. 2.19.39 we find that $A\beta\lambda b = B$ so that the eigenfunction for divergence in this case is $\theta(y) = A\sin\lambda y + B\cos\lambda y = A(\sin\lambda y + \beta\lambda b\cos\lambda y)$. In this case we have both sine and cosine participation in the mode shape.

2.19.3 – Stiffness criteria – an energy approach

The importance of wing torsional stiffness was recognized in the early years of aviation, both for load and stress determination and flutter. Because high fidelity analysis was not available, much of the certification for safety was left to flight test. While this ensured a safe airplane, if a problem was discovered during flight testing, the modifications were likely to be costly. During the early development, instead of extensive analysis, designers were likely to use stiffness criteria, requiring that the wing torsional stiffness exceed a certain level.

Flax[19] developed one such criterion for divergence. His analysis began with the continuous model shown in Figure 2.19.1, although this model was not restricted to a uniform planform. Assume that we are operating at the divergence dynamic pressure and we give the system the usual perturbation, in this case a perturbation from static equilibrium. From Conservation of Energy we know that the wing structure strain energy and the work done by the external aerodynamic loads must be equal. This gives the following equation:

$$U = \frac{1}{2}\int_0^b GJ\left(\frac{d\theta}{dx}\right)^2 dx = W_{aero} = \frac{1}{2}\int_0^b \left(q_D cc_{l_\alpha}(x)\right)\left(e\theta(x)\right)dx \qquad (2.19.48)$$

The factor ½ appears in the aerodynamic work expression because the load is assumed to have been very slowly applied from a zero value. In Eqn. 2.19.48 the torsional stiffness is a function of the spanwise coordinate, x. Similarly, the lift distribution expression need not be so simple as it was in our previous analysis. We recognize that the solution for $\theta(x)$ involves considerable effort and a closed-form solution may not even exist.

The next step is to choose a reference torsional stiffness, GJ_o, at the wing root for instance, and similar reference values for the wing chord, c_o, and the elastic axis offset, e_o. This produces the following relationship.

$$GJ_o \int_0^b \left(\frac{GJ}{GJ_o} \right) \left(\frac{d\theta}{dx} \right)^2 dx = q_D c_o e_o \int_0^b \left(\frac{c}{c_0} c_l(x) \right) \left(\frac{e}{e_o} \theta(x) \right) dx \qquad (2.19.49)$$

Now define the torsional deflection and lift distribution as $\theta = \theta_o f(x)$ and $c_{l_\alpha} \theta = c_{l_\alpha} \theta_o f(x)$ then we have:

$$GJ_o \theta_o^2 \int_0^b \left(\frac{GJ}{GJ_o} \right) \left(\frac{df}{dx} \right)^2 dx = q_D c_o e_o \theta_o^2 \int_0^b \left(\frac{c}{c_0} c_{l_\alpha} \right) \left(\frac{e}{e_o} f^2 \right) dx \qquad (2.19.50)$$

and

$$GJ_o = \frac{q_D c_o e_o c_{l_\alpha} \int_0^b \left(\frac{c}{c_0} \right) \left(\frac{e}{e_o} f^2 \right) dy}{\int_0^b \left(\frac{GJ}{GJ_o} \right) \left(\frac{df}{dy} \right)^2 dy} \qquad (2.19.51)$$

Equation 2.19.51 is a stiffness criterion for divergence at the specified divergence dynamic pressure. Although we do not know the exact deflected shape at divergence (the eigenfunction) we can approximate the shape $f(x)$ and estimate the required torsional stiffness. If the wing has constant chord the expression reduces to

$$GJ_o = \frac{q_D c_o e_o c_{l_\alpha} \int_0^b \left(\frac{c}{c_0} \right) \left(\frac{e}{e_o} \right) (f^2) dx}{\int_0^b \left(\frac{GJ}{GJ_o} \right) \left(\frac{df}{dx} \right)^2 dx} = \frac{q_D c_o e_o c_{l_\alpha} \int_0^b (f^2) dx}{\int_0^b \left(\frac{df}{dx} \right)^2 dx} \qquad (2.19.52)$$

With an approximation for the torsional divergence deflected shape an approximation for the wing root torsional stiffness is generated. When the exact mode shape is known, Eqn. 2.19.52 provides the exact required value for torsional stiffness. (Use the mode shape $\sin \lambda x$ to find the required GJ and compare it to the exact value computed in Section 2.19.1.)

Summary

Aeroelastic models must include enough details to allow us to predict what happens to the lifting surface structure when we fly at different speeds and altitudes. It does not need to have exquisite detail like a stress analysis model. The models considered in this chapter were simple and assumed that both the structure and aerodynamic behavior is linear - output is proportional to the input. We introduced the typical section model with pitching (structural twisting) and "bending" (called plunging) displacement degrees of freedom. This model illustrated that aeroelasticity is a natural feedback process between structural deflections and aerodynamic forces and moments.

From a structural mechanics standpoint, aeroelastic problems are *statically indeterminate* problems; the structural deformation creates loads that enter into the equilibrium equations. This chapter has presented an overview of the matrix method structural analysis approach and introduced the *shear center* and *elastic axis* concepts as structural reference points. It also illustrated the relationship between the strain energy stored in a structure and the structural stiffness matrix. We reviewed fundamental low speed aerodynamics and introduced *aerodynamic* coefficients and aerodynamic reference points – the center of pressure and the aerodynamic center.

Aeroelastic and load amplification and static stability is a stiffness problem; aerodynamic loads create aerodynamic stiffness (or "de-stiffness") just as structural geometry creates elastic stiffness. The effect of aerodynamic stiffness is to reduce unswept wing torsional stiffness; this effect leads to aerodynamic load amplification and ultimately static instability known as divergence.

If the total wing lift is held constant (the wing angle of attack can change) twist deformation is small, even at the divergence speed. It is only when the angle of attack is fixed and the load is allowed to become large that twist deformation becomes unbounded at divergence and extremely large even at speeds considerably below the divergence speed. As a result, we place the wing in static equilibrium with a small (or even zero) angle of attack, perturb the wing and then observe what happens to the response.

With a linear analysis, at divergence we encounter a "bifurcation" situation in which there are multiple static equilibrium states in addition to the original equilibrium state. This is Euler's criteria for static stability; the boundary between stable and unstable states occurs at a transition point defined by the appearance of multiple static equilibrium states. We showed that a nonlinear model also predicts the appearance of multiple equilibrium states, but with finite, not infinite, deformations.

We also examined the effects of flow compressibility on divergence; flow compressibility introduces a compressibility correction factor, the Prandtl-Glauert transformation. As a result, the Mach number is introduced into the problem. We found a "match point" for which the Mach number at a given altitude matches the Mach number at divergence.

Divergence is a theoretical problem that requires that the wing support is securely fixed to an immovable aircraft. This "immovable aircraft" condition cannot occur in flight. Inertia effects such as weight distribution *cannot appear in the results of a static stability analysis since they cannot produce deflection dependent loads without acceleration*. Still, the theoretical wing divergence dynamic pressure allows us to understand when aeroelasticity is likely to be an important problem.

We also considered multi-degree of freedom problems and determined that the divergence problem is an eigenvalue problem involving the search for self-equilibrating conditions, combinations of dynamic pressures (eigenvalues) and mode shapes (eigenvectors or eigenfunctions). The multi-degree of freedom eigenvalue problem can be solved in simple cases by forming the determinant of the aeroelastic stiffness matrix and setting it to zero. This is the so-called characteristic equation, a polynomial involving the divergence dynamic pressure.

We also introduced the Virtual Work approach to developing the required homogeneous equilibrium equations for divergence analysis. In addition we developed a differential equation model, as well as presenting a torsional stiffness criteria, based on an energy approach, to define the minimum required torsional stiffness for specified divergence dynamic pressure.

In the next sections we will continue aeroelastic studies by examining the effects of static aeroelasticity on control effectiveness, particularly roll effectiveness, and then examine how we might link together control systems and the wing to change aeroelastic stability.

2.20 Control surface effectiveness

A wing with planform area S is shown in cross-sectional view in Figure 2.20.1. A control surface (an aileron in the case of a wing, a rudder in the case of a vertical tail or an elevator in the case of a horizontal tail) is connected to the wing section by a rigid hinge. The wing may be cambered (although the cross-section in Figure 2.20.1 is not); control surface rotation δ_o (positive clockwise) creates additional camber, lift and a pitching moment that twist the wing an amount θ. As we will show in this section, the twisting deflection creates negative lift, with the result that the amount of lift generated by a flexible wing is less than that for a rigid wing.
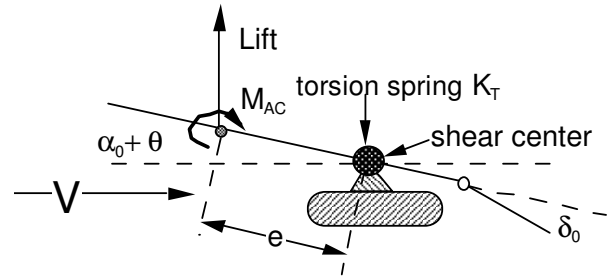

Figure 2.20.1 - Torsionally flexible wing segment with moveable trailing edge control surface.

Control effectiveness is defined as the ability of a control surface such as an elevator, aileron or rudder to produce lift or a moment to change the airplane pitching moment, rolling moment, or yawing moment, respectively. Horizontal tail, wing or vertical stabilizer torsional flexibility reduces control effectiveness of unswept lifting surfaces.

When the control surface is deflected, the flexible wing lift is

$$L = qSC_{L_\alpha}(\alpha_o + \theta) + qSC_{L_\delta}\delta_o \tag{2.20.1}$$

If there were no twisting, the lift due to the control deflection is $L_r = qSC_{L_\delta}\delta_o$. The twisting moment about the wing aerodynamic center is:

$$M_{AC} = qScC_{MAC} + qScC_{MAC_\delta}\delta_o \tag{2.20.2}$$

The terms C_{L_δ} and C_{MAC_δ} are defined as

$$C_{L_\delta} = \frac{\partial C_L}{\partial \delta} \text{ and } C_{MAC_\delta} = \frac{\partial C_{MAC_\delta}}{\partial \delta} \tag{2.30.3}$$

Since positive δ_o causes a negative C_{MAC_δ} value, this term results in nose-down wing twist that decreases the wing angle of attack. Summing moments (clockwise positive) about the shear center,

$$Le + M_{AC} = M_S = K_T\theta \tag{2.20.4}$$

Substituting Eqns. 2.20.1 and 2.20.2 into 2.20.4 and solving for θ,

$$\theta = \frac{qSeC_{L_\alpha}\left[\alpha_o + \left(\frac{c}{e}\right)\frac{C_{MAC}}{C_{L_\alpha}}\right] + qSe\left[C_{L_\delta} + \left(\frac{c}{e}\right)C_{MAC_\delta}\right]\delta_o}{K_T - qSeC_{L_\alpha}} \qquad (2.20.5)$$

The effects of α_o and δ_o on θ are additive. We confine our attention solely to the second term of Eqn. 2.20.5, written as

$$\frac{\theta}{\delta_o} = \left(\frac{qSeC_{L_\delta}}{K_T}\right)\frac{\left(1 + \left(\frac{c}{e}\right)\left(\frac{C_{MAC_\delta}}{C_{L_\delta}}\right)\right)}{1 - \frac{q}{q_D}} \qquad (2.20.6)$$

From Eqns. 2.20.1 and 2.20.5 the lift due to δ_o is

$$L = qS\left(C_{L_\delta} + C_{L_\alpha}\frac{\theta}{\delta_o}\right)\delta_o$$

or

$$L = qsC_{L_\delta}\delta_o\left[\frac{1 - q\frac{Sc}{K_T}\left(\frac{C_{L_\alpha}}{C_{L_\delta}}\right)(-C_{MAC_\delta})}{1 - \frac{q}{q_D}}\right] \qquad (2.20.7)$$

The second term in the numerator in Eqn. 2.20.7 contains a reference dynamic pressure, called the *reversal dynamic pressure, q_R*:

$$q_R = \frac{-K_T}{ScC_{MAC_\delta}}\left(\frac{C_{L_\delta}}{C_{L_\alpha}}\right) \qquad (2.20.8)$$

The term $-C_{MAC_\delta}$ is a positive number so that the reversal dynamic pressure is positive. The ratio $C_{L_\delta} / C_{L_\alpha}$ is

$$\frac{C_{L_\delta}}{C_{L_\alpha}} = \frac{\partial C_L}{\partial \delta} \times \frac{\partial \alpha}{\partial C_L} = \frac{\partial \alpha}{\partial \delta} \qquad (2.20.9)$$

a ratio that represents the change in wing angle of attack due to a unit control deflection, δ_o.

Two-dimensional airfoil control surface aerodynamic coefficients

In the late 1920's Herman Glauert developed a theory and the equations to predict coefficients c_{l_δ} and c_{mac_δ} for a two dimensional airfoil (as opposed to the wing model we have here) as functions of the ratio of a "flap-to-chord dimension," defined as $E = \dfrac{c_f}{c}$.[20] The flap is what we are calling the control surface and its chord dimension is c_f. These two relationships are

$$\frac{c_{l_\delta}}{c_{l_\alpha}} = \frac{1}{\pi}\left(\cos^{-1}(1-2E) + 2\sqrt{E(1-E)}\right) \tag{2.20.10}$$

$$\frac{c_{mac_\delta}}{c_{l_\alpha}} = -\frac{1}{\pi}(1-E)\sqrt{(1-E)E} \tag{2.20.11}$$

Note that, for the two-dimensional airfoil in incompressible flow, the lift curve slope is $c_{l_\alpha} = 2\pi$. Before continuing with the aeroelastic analysis, let's examine how the flap-to-chord ratio affects the location of the airfoil center of pressure location due to the control deflection on a two-dimensional airfoil.

Effect of control surface size on center of pressure location

The control surface deflection creates lift and a nose-down pitching moment. The additional lift increases twist while the nose-down pitching moment decreases twist. Which effect dominates? To answer this question, let's return to the three-dimensional wing model.

Figures 2.20.2 (a) and (b) show two different ways of representing the lift and pitching moment due to δ_o. Figure 2.20.2(a) shows the lift acting at the aerodynamic center, together with the pitching moment due to the aileron deflection. Figure 2.20.2(b) shows the lift due to the same aileron deflection acting at the center of pressure location so that there is no moment. The center of pressure is located a distance d downstream (aft) of the airfoil quarter chord.

(a) aerodynamic center coordinates
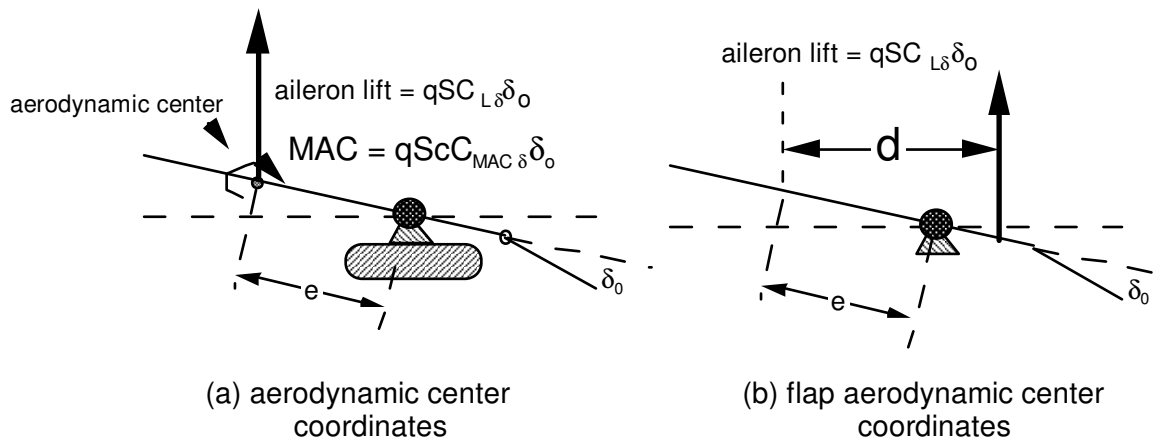
(b) flap aerodynamic center coordinates

Figure 2.20.2 (a,b) - Force and moment equivalence for aileron deflection showing center of pressure coordinate

The two representations must produce the same moment about the ¼ chord point. This is called moment equivalence and is written as

$$-Ld = qSdC_{L_\delta}\delta_o = M_{AC_\delta} = qScC_{MAC_\delta}\delta_o$$

$$-C_{L_\delta}d = cC_{MAC_\delta}$$

$$\frac{d}{c} = -\frac{C_{MAC_\delta}}{C_{L_\delta}} \tag{2.20.12}$$

For the two dimensional airfoil, this gives

$$\frac{d}{c} = -\frac{c_{mac_\delta}}{c_{l_\delta}} = \frac{(1-E)\sqrt{(1-E)E}}{\left(\cos^{-1}(1-2E)+2\sqrt{E(1-E)}\right)} \tag{2.20.13}$$

The airfoil ratio d/c in Eqn. 2.20.13 is plotted in Figure 2.20.3 as a function of aileron flap-to-chord ratio, E. This figure shows that when the aileron chord is extremely small, the center of pressure is near the midchord (d/c = 0.25) but then moves forward towards the ¼ chord as E increases.

This plot explains why wings with some control surfaces will reverse. The dashed red line represents a possible location of the shear center, in this case it is 35% of the chord aft of the leading edge. The roughly triangular area above the dashed line represents a design region where the aileron center of pressure is behind (aft) of the shear center and configurations that will twist the wing nose down, even as the control increases lift according to the relationship $L_r = qSC_{L_\delta}\delta_o$. As a result, the sum of the fundamental lift

Figure 2.20.3 - Aileron center of pressure location with respect to the airfoil ¼ chord vs. flap to chord ratio

$L_r = qSC_{L_\delta}\delta_o$ and the lift due to twist is smaller than the fundamental lift. Only when the control surface has a large chord will the center of pressure lie forward of the elastic axis. In this case the flap to chord ratio would have to be about 0.5, a very large control surface.
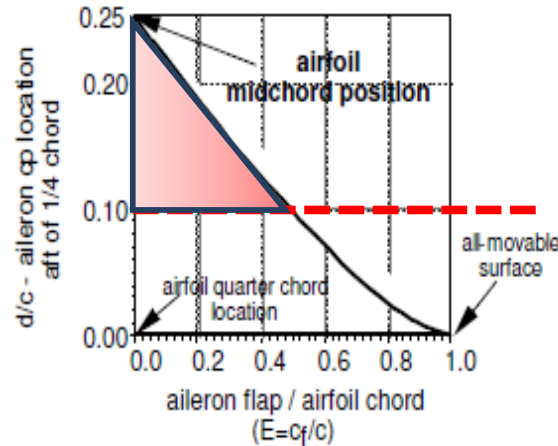
The reversal dynamic pressure and its relationship to divergence

We already know the expression for divergence dynamic pressure for this wing is $q_D = \dfrac{K_T}{SeC_{L_\alpha}}$.

Where is the reversal dynamic pressure in comparison to divergence? Substituting Eqn. 2.20.13 into Eqn. 2.20.8 the reversal dynamic pressure expression becomes

Chapter 2

$$q_R = \frac{-K_T}{ScC_{MAC_\delta}}\left(\frac{C_{L_\delta}}{C_{L_\alpha}}\right) = \frac{-K_T}{Sc}\left(-\frac{c/d}{C_{L_\alpha}}\right) = \frac{K_T}{SeC_{L_\alpha}}\left(\frac{e}{d}\right) = q_D\left(\frac{e}{d}\right) \qquad (2.20.14)$$

Equation 2.20.7 can be written as:

$$L = L_r\left[\frac{1-\dfrac{q}{q_R}}{1-\dfrac{q}{q_D}}\right] \qquad (2.20.15)$$

where $L_r = qSC_{L_\delta}\delta_o$ is the lift generated by control surface deflection δ_o, ignoring aeroelastic effects. ***Control effectiveness, when the primary purpose of the control deflection is to produce lift, is defined as:***

$$\frac{L}{L_r} = \left(\frac{1-\dfrac{q}{q_R}}{1-\dfrac{q}{q_D}}\right) \qquad (2.20.16)$$

Assuming that the wing dynamic pressure is less than the divergence dynamic pressure, then, as dynamic pressure increases and approaches q_R, the ratio L/L_r decreases and becomes zero when $q = q_R$. At this point no net lift is produced by the control deflection, although the wing segment will twist and thus cancel the effects of control deflection lift (see Eqn. 2.20.6).

Two different plots are necessary to examine lift effectiveness since q_R can be either greater than or less than q_D, depending on where the aileron center of pressure is (which in turn depends on how large the aileron is). The divergence dynamic pressure appears in Eqn. 2.20.16 so we define a parameter, R, as

or

$$R = \frac{q_D}{q_R} = \frac{K_T/SeC_{L_\alpha}}{-K_T/ScC_{MAC_\delta}\left(\dfrac{C_{L_\delta}}{C_{L_\alpha}}\right)} \qquad (2.20.17)$$

$$R = \frac{c}{e}\left(\frac{-C_{MAC_\delta}}{C_{L_\delta}}\right) = \frac{c}{e}\frac{d}{c} = \frac{d}{e}$$

With this definition of R, Eqn. 2.20.16 becomes

$$\frac{L}{L_r} = \left(\frac{d}{e}\right)\left[\frac{1-\dfrac{q}{q_R}}{\dfrac{d}{e}-\dfrac{q}{q_R}}\right] = \left[\frac{1-\dfrac{q}{q_R}}{1-\left(\dfrac{e}{d}\right)\left(\dfrac{q}{q_R}\right)}\right] \qquad (2.20.18)$$
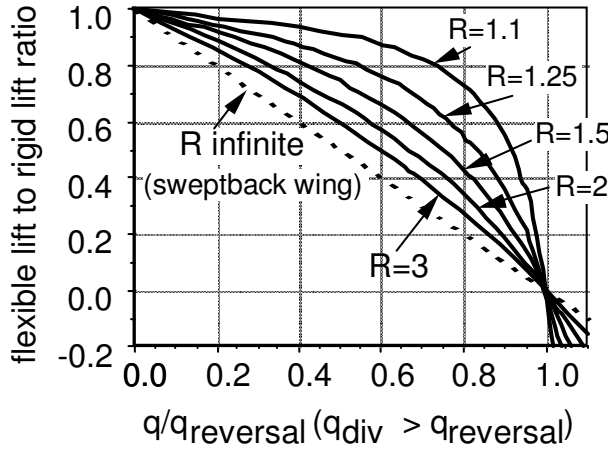
Figure 2.20.4 - Control effectiveness as a function of dynamic pressure ratio, q / q_R (R>1).

In Figure 2.20.4, the ratio L / L_r is plotted when $R > 1$. Note that there are two limiting conditions in Figure 2.20.4. When $q_R = q_D$, then $R = 1$ and rigid surface and flexible control effectiveness are identical. When $R = 1$ then $e/c = d/c = -C_{M_\delta} / C_{L_\delta}$. An additional limiting case in Figure 2.20.4 occurs when R is very large ($q_D >> q_R$) so that

$$\lim_{R \to \infty} \frac{L}{L_r} = 1 - \frac{q}{q_R} \qquad (2.20.19)$$

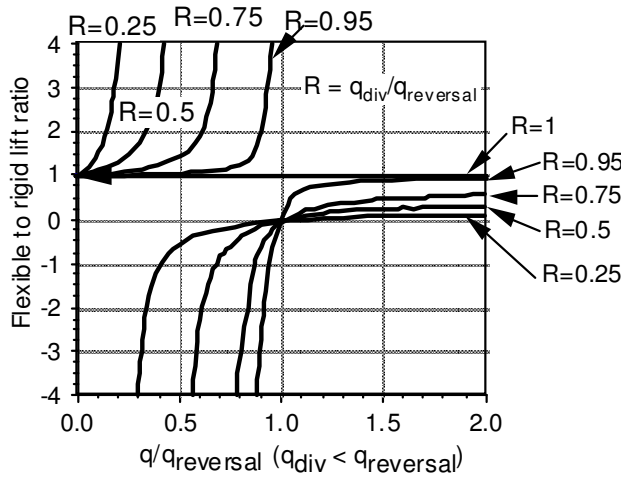Notice that Eqn. 2.20.19 plots as a straight line in Figure 2.20.4.

Figure 2.20.5 - Control (lift) effectiveness as a function of q / q_R (R<1).

Figure 2.20.5 plots control effectiveness vs. dynamic pressure when $R \leq 1$. In this case, control effectiveness always increases when dynamic pressure increases. For instance, when R=0.5 the aileron control effectiveness is always greater than 1 in the range of practical values of q / q_R.

The reversal dynamic pressure defined in Eqn. 2.20.8 contains Mach number dependent aerodynamic derivatives. We can rewrite Eqn. 2.20.8 as

$$q_R = \frac{-K_T}{ScC_{M\delta_o}} \left(\frac{C_{Lo_\delta}}{C_{Lo_\delta}} \right) \sqrt{1 - M^2} \qquad (2.20.20a)$$

or
$$q_R = q_{R_0} \sqrt{1 - M^2} \qquad (2.20.20b)$$

where q_{R_0} is the reversal dynamic pressure computed assuming incompressible flow. As in the case of divergence, we must match the reversal dynamic pressure including Mach number with the atmospheric flight value $q_R = \frac{1}{2} \rho a^2 M_R^2 = q_{R_0} \sqrt{1 - M_R^2}$.

2.20.1 Aileron effectiveness including rolling motion

In the last section the examination of control effectiveness was restricted to a wing/control surface combination fixed to a wind tunnel. In this case aileron effectiveness was measured as an ability to create lift which was in turn transmitted to a wind tunnel support so that the wing/control surface could not move.   This situation approximates what happens with a horizontal tail/elevator combination or the rudder/vertical tail where motion is small or nonexistent. It does not simulate wing/aileron rolling motion about an aircraft roll axis. The purpose of this section is to introduce another measure of control surface effectiveness - aileron effectiveness – in which motion occurs.
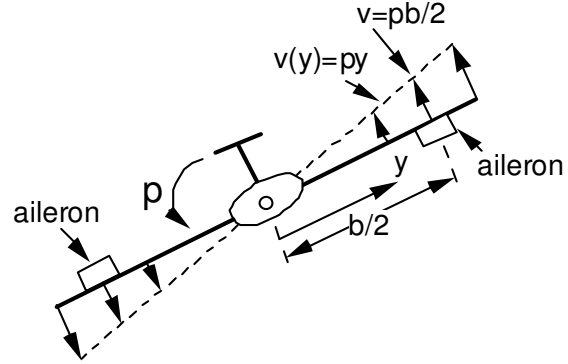

Figure 2.20.6 - Rolling airplane with ailerons deflected, as viewed from the rear.

The ability to create motion, in particular a large *terminal* or *steady-state roll rate* (defined as p in Figure 2.20.6), is the measure of wing/aileron effectiveness. Figure 2.20.6 shows a rear view of an airplane flying at an airspeed V. Downward aileron deflection on the right wing (and upward deflection on the left accelerates the wing upward to produce a roll rate *p(t)* (radians/sec.). Airplane roll produces a velocity component $v(y)$ along the wing, given by the relationship $v(y) = py$, as shown in Figure 2.20.6. If the aileron span is small the aileron rolling velocity $v(y)$ at the wing/aileron surface is approximately $v = p\,b/2$.

From the wing's perspective, air appears to be moving downward with velocity v and rearward with airspeed V so that there is an apparent negative angle of attack, $\alpha_v = -v/V$. This creates a lift term $qSC_{L_\alpha}\left(\dfrac{v}{V}\right) = qSC_{L_\alpha}\left(\dfrac{pb}{2V}\right)$ called the *aerodynamic damping force* that acts downward, opposing upward motion. This force produces a rolling moment that retards motion and is called "damping in roll." Eventually, as the roll rate increases and $v = \dfrac{pb}{2}$ increases, the damping in roll becomes so large that the roll rate will cease to increase and p and v will become constant. The unsteady aerodynamic effects during this event are complicated and will not be discussed here.

In figure 2.20.6 the lift on the left wing/aileron combination at the wing aerodynamic center has three input components:

$$L = qSC_{L_\alpha}\left(\theta - \frac{v}{V}\right) + qSC_{L_\delta}\delta \qquad (2.20.21a)$$

This lift creates a rolling moment $M_{roll}(t)$ that accelerates the wing upward so that (the factor of ½ on the right hand side is there because there is an aileron on the left wing doing the same thing).

$$M_r(t) = L\left(\frac{b}{2}\right) = qSC_{L_\alpha}\left(\frac{b}{2}\right)\left(\theta - \frac{v}{V}\right) + qSC_{L_\delta}\left(\frac{b}{2}\right)\delta = \frac{I_{roll}}{2}\frac{dp}{dt} \qquad (2.20.21b)$$

Since θ is unknown, the roll rate is an unknown. The steady-state condition in which $\frac{dp}{dt} = 0$ is seldom reached in flight, but it represents a limiting condition. To find a reversal speed we first find the (unknown) steady state rolling velocity, p, as a function of the aileron deflection angle δ_o by using a typical section idealization to simulate wing/aileron motion at a constant speed.

To capture this situation with an idealization we imagine a very tall wind tunnel with a wing on frictionless bearings shown in Figure 2.20.7 that permit upward or downward frictionless movement. The velocity generated by the aileron is $v = \frac{pb}{2}$.
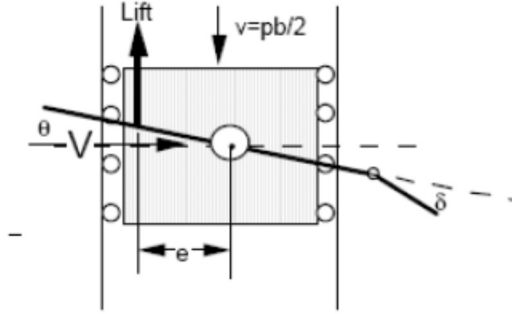

Figure 2.20.7 - Rolling effectiveness idealization showing wing/aileron combination free to move

Because of the opposing aerodynamic damping force, the wing will accelerate until v becomes so large that the acceleration is zero. In this case Eqn. 2.20.21b becomes

$$M_r(t) = L\left(\frac{b}{2}\right) = qSC_{L_\alpha}\left(\frac{b}{2}\right)\left(\theta - \frac{v}{V}\right) + qSC_{L_\delta}\left(\frac{b}{2}\right)\delta = 0$$

or $\qquad\qquad\qquad\qquad\qquad\qquad\qquad\qquad\qquad\qquad\qquad\qquad$ (2.20.22)

$$L = qSC_{L_\alpha}\left(\theta - \frac{v}{V}\right) + qSC_{L_\delta}\delta = 0$$

Equation 2.20.22 has two unknown, the terminal value of v and the wing twist θ. he problem resembles a statics problem. We use Eqn. 2.20.22 to solve for the terminal velocity.

$$\frac{v}{V} = \theta + \frac{C_{L_\delta}}{C_{L_\alpha}}\delta_o \qquad (2.20.23)$$

This analysis can be confusing because in the previous section we used the *L=0* condition to define control effectiveness. Now we use this condition to define the terminal velocity. Next we solve for the wing twist.
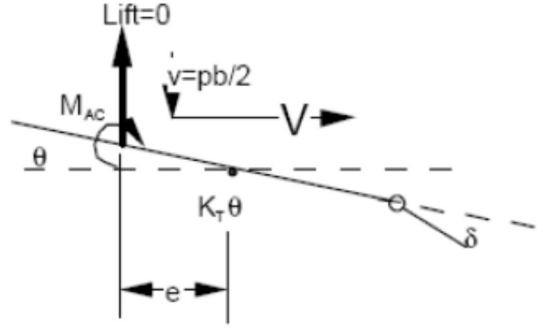
Chapter 2

Figure 2.20.8 – Free body diagram – wing/aileron combination free to move upward with constant speed, v.

To find the twist angle we need to consider the wing/aileron free-body diagram shown in Figure 2.20.8. A torsion spring with a spring constant K_T lb-in/radian restrains the wing twist, θ. Although the lift is zero when the terminal condition is reached, the wing pitching moment, $M_{AC} \neq 0$ and is resisted by the torque in the torsion spring. Moment equilibrium (with $L=0$) requires that:

$$K_T \theta = M_{AC} = qScC_{MAC_\delta}\delta_o \tag{2.20.24a}$$

or

$$\theta = qSc\frac{C_{M_\delta}}{K_T}\delta_o \tag{2.20.24b}$$

From Eqn. 2.20.23, the steady state or terminal velocity, $v = \dfrac{pb}{2}$, is:

$$\frac{v}{V} = \frac{pb}{2V} = \left[qSc\left(\frac{C_{MAC_\delta}}{K_T}\right) + \left(\frac{C_{L_\delta}}{C_{L_\alpha}}\right) \right]\delta_o \tag{2.20.25}$$

The pitching moment coefficient is negative so, if the dynamic pressure is large enough, a downward aileron rotation will produce a negative terminal velocity. The reversal condition occurs when Eqn. 2.20.25 is zero.

$$\frac{v}{V} = \frac{pb}{2V} = 0 = \left[q_R Sc\left(\frac{C_{MAC_\delta}}{K_T}\right) + \left(\frac{C_{L_\delta}}{C_{L_\alpha}}\right) \right]\delta_o$$

$$or \tag{2.20.26}$$

$$q_R = -\left(\frac{K_T}{ScC_{MAC_\delta}}\right)\left(\frac{C_{L_\delta}}{C_{L_\alpha}}\right)$$

The reversal dynamic pressure in Eqn. 2.20.26 is identical to that found in the previous section. We now write v/V as

$$\frac{v}{V} = \frac{p\,b}{2\,V} = \left(\frac{C_{L_\delta}}{C_{L_\alpha}} \right) \left[1 - \frac{q}{q_R} \right] \delta_o$$

$$o\,r$$

$$p = 2\,\frac{V}{b}\left(\frac{C_{L_\delta}}{C_{L_\alpha}} \right)\left[1 - \frac{q}{q_R} \right]\delta_o$$

(2.20.27a,b)

The term $\dfrac{pb}{2V}$ in Eqn. 2.20.27a is a helix angle traced out in space by the wing/aileron located at distance b/2 from the roll axis, rolling at a constant rate p and moving forward at airspeed V.

Figure 2.20.9 plots Eqn. 2.20.27b (divided by *b/2* and *δo*) for this wing/aileron model when $q_R = 150 \; psf$. As airspeed increases, steady-state roll rate reaches a maximum and then declines as airspeed increases, finally going to zero at the reversal airspeed. Compare Figure 2.20.9 with Figure 1.17 in Chapter 1.

Aileron reversal and aileron effectiveness were important topics for researchers in many countries during the 1920's and 1930's. Since torsional stiffness plays an important part in this phenomenon, the wing skin thickness becomes important since it determines a major part of torsional stiffness. The Japanese Zero, the Mitsubishi A6M2, was one of the finest fighters produced before World War II. However, the designer's objective of producing an ultra-light-weight maneuverable fighter led to a thin wing skin. At 160 mph (260 km/h), the Zero had a roll rate of 56° per second. Because of wing torsional flexibility, roll effectiveness dropped to zero at about 483 km/h (300 mph). This fault led U.S. pilots to guard against low speed encounters and try to get the Japanese pilots to engage at higher speeds where they were less maneuverable.
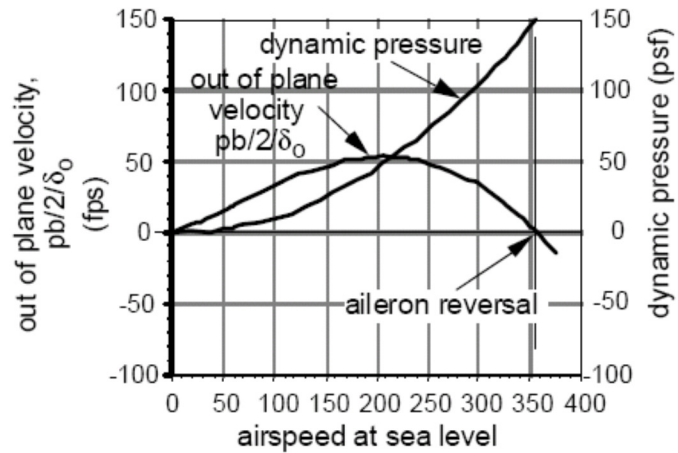

Figure 2.20.9 - Steady state terminal damping in roll airspeed vs. forward airspeed, V

2.21 Two degree of freedom wing aileron reversal

In the previous section we considered a one degree of freedom wing model and defined aileron effectiveness two different ways: 1) the ability of the aileron to increase lift on the wing, defined as $L_{flex}\big/L_{rigid}$ when $\alpha_o = 0$ and $\delta = \delta_o$; 2) the ability of the aileron to provide a rolling moment. The reversal airspeed was the same in both cases. In this section we will show that the aileron reversal airspeed depends on the definition of aileron effectiveness if the wing model has more than one degree of freedom.
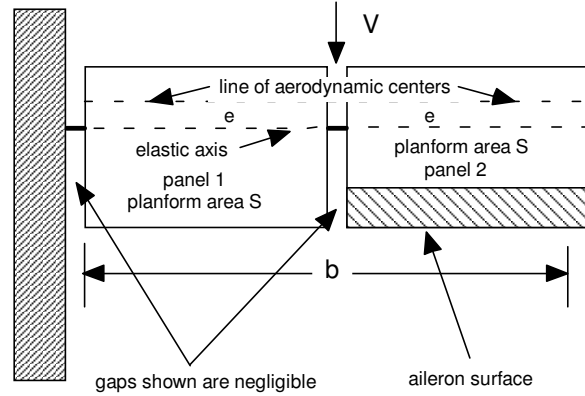

Figure 2.21.1 - Wing/aileron idealization

The configuration shown in Figure 2.21.1, previously considered in Section 2.14, is a wing idealization with two elastically connected surfaces, each with planform area S, with an aileron attached to the outer panel. For the present example the torsional spring constants have been changed so that they are both equal to K_T.

As indicated in Figure 2.14.1, shown previously, the section twist angles are measured from the initial angle of attack position. The difference between this model and the model in Section 2.14 is that an aileron has been added to the outboard panel.
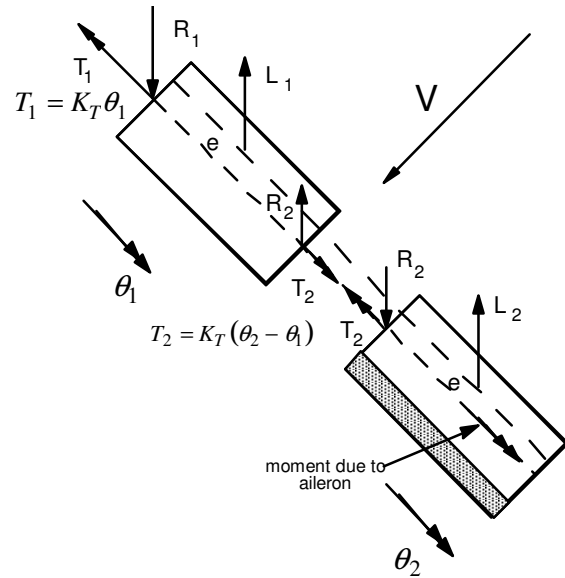
Figure 2.21.2 - Wing/aileron combination free body diagram

Figure 2.21.2, shows a free body diagram; the internal torques due to these torsional restraints are given as $T_1 = K_T\theta_1$ and $T_2 = K_T(\theta_2 - \theta_1)$ The aerodynamic forces acting on each panel are, with $\alpha_o = 0$,

$$L_1 = qSC_{L_\alpha}\theta_1 \tag{2.21.1}$$

$$L_2 = qSC_{L_\alpha}\theta_2 + qSC_{L_\delta}\delta_o \tag{2.21.2}$$

Summing forces on each panel gives two equations.

Section 2 (outer)

$$\Sigma F_2 = 0$$

$$L_2 - R_2 = 0 \tag{2.21.3}$$

$$R_2 = L_2 = qSC_{L_\alpha}\theta_2 + qSC_{L_\delta}\delta_o \tag{2.21.4}$$

and ***(Section 1, inner)***

$$\Sigma F_1 = 0$$

$$L_1 + R_2 - R_1 = 0 \tag{2.21.5}$$

$$R_1 = L_1 + L_2$$

Equations 2.21.4 and 2.21.5 are not useful, except to compute the internal shear forces. On the other hand, summing moments about the elastic axis (positive nose-up) in Figure 2.21.1 gives two additional, useful, equations

$$\Sigma M_1 = 0 = L_1 e + K_T(\theta_2 - \theta_1) - K_T\theta_1 \tag{2.21.6}$$

and

$$\sum M_2 = 0 = L_2 e - K_T(\theta_2 - \theta_1) + qScC_{M\delta}\delta_o \tag{2.21.7}$$

Substituting the expressions for L_1 and L_2 into Eqns. 2.21.6 and 2.21.7 and writing these two equations in matrix form gives

$$\begin{bmatrix} 2K_T - qSeC_{L_\alpha} & -K_T \\ -K_T & K_T - qSeC_{L_\alpha} \end{bmatrix} \begin{bmatrix} \theta_1 \\ \theta_2 \end{bmatrix} = qSeC_{L_\alpha}\left(\frac{C_{M\delta}}{C_{L_\alpha}}\left(\frac{c}{e}\right) + \frac{C_{L_\delta}}{C_{L_\alpha}} \right)\begin{Bmatrix} 0 \\ \delta_o \end{Bmatrix} \tag{2.21.8}$$

Let's use the following data to illustrate some features of aileron reversal for this type of model.

$$C_{M\delta} = -0.18\pi \qquad C_{L_\alpha} = 2\pi \qquad \frac{c}{e} = 10 \qquad \frac{C_{L_\delta}}{C_{L_\alpha}} = \frac{\partial\alpha}{\partial\delta} = 0.4 \tag{2.21.9}$$

With the nondimensional aeroelastic parameter $\bar{q} = \dfrac{qSeC_{L_\alpha}}{K_T}$ Eqn. 2.21.8 becomes

$$\begin{bmatrix} 2 - \bar{q} & -1 \\ -1 & 1 - \bar{q} \end{bmatrix}\begin{Bmatrix} \theta_1 \\ \theta_2 \end{Bmatrix} = \bar{q}\begin{Bmatrix} 0 \\ -0.5 \end{Bmatrix}\delta_o \tag{2.21.10}$$

The wing segment twist angles are

$$\begin{Bmatrix} \theta_1 \\ \theta_2 \end{Bmatrix} = \frac{\bar{q}}{\Delta}\begin{bmatrix} 1 - \bar{q} & 1 \\ 1 & 2 - \bar{q} \end{bmatrix}\begin{Bmatrix} 0 \\ -0.5 \end{Bmatrix}\delta_o \tag{2.21.11}$$

where the determinant of the aeroelastic stiffness matrix is

$$\Delta = \bar{q}^2 - 3\bar{q} + 1 \qquad (2.21.12)$$

The characteristic equation for q_D is

$$\bar{q}_D^2 - 3\bar{q}_D^2 + 1 = 0 \qquad (2.21.13)$$

From this polynomial we find two eigenvalues

$$\bar{q}_D = 0.3820 \ and \ \bar{q}_D = 2.618$$

The smaller of these two eigenvalues is the nondimensional divergence dynamic pressure. It is not a function of aileron parameters.

The total lift created by aileron input δ_o, (with $\alpha_o = 0$) is

$$L_{flex} = L_1 + L_2 = qSC_{L_\alpha}(\theta_1 + \theta_2) + qSC_{L_\delta}\delta_o \qquad (2.21.14)$$

From Eqn. 2.21.11, the section twist angles are

$$\theta_1 = \frac{-0.5}{\Delta}\bar{q}\delta_o \qquad (2.21.15)$$

and

$$\theta_2 = \frac{-0.5\bar{q}(2-\bar{q})}{\Delta}\delta_o = \frac{-\bar{q}+0.5\bar{q}^2}{\Delta}\delta_o \qquad (2.21.16)$$

Substituting these expressions for θ_1 and θ_2 into Eqn. 2.21.14, we find the lift on the flexible wing.

$$L_{flex} = qSC_{L_\alpha}\left[\frac{-0.5}{\Delta}\bar{q}\delta_o - \frac{\bar{q}-0.5\bar{q}^2}{\Delta}\delta_o\right] + qSC_{L_\delta}\delta_o \qquad (2.21.17)$$

or

$$L_{flex} = \frac{qSC_{L_\alpha}}{\Delta}\left[-0.5\bar{q} - \bar{q} + 0.5\bar{q}^2 + \frac{C_{L_\delta}}{C_{L_\alpha}}\Delta\right]\delta_o \qquad (2.21.18)$$

Simplify Eqn. 2.21.18 to obtain

$$L_{flex} = \frac{qSC_{L_\alpha}}{\Delta}\left[-0.5\bar{q} - \bar{q} + 0.5\bar{q}^2 + \frac{C_{L_\delta}}{C_{L_\alpha}}(\bar{q}^2 - 3\bar{q} + 1)\right]\delta_o \qquad (2.21.19)$$

or

$$L_{flex} = \frac{qSC_{L_\alpha}}{\Delta}\left[0.9\bar{q}^2 - 2.7\bar{q} + \frac{C_{L_\delta}}{C_{L_\alpha}}\right]\delta_o \qquad (2.21.20)$$

Copyright Terrence A. Weisshaar

The total lift due to aileron displacement when the wing is rigid is:

$$L_{rigid} = qSC_{L_\delta}\delta_o \qquad (2.21.21)$$

Since $\dfrac{C_{L_\delta}}{C_{L_\alpha}} = 0.4$, the ratio $\dfrac{L_{flex}}{L_{rigid}}$ is written as

$$\frac{L_{flex}}{L_{rigid}} = \frac{\dfrac{qSC_{L_\alpha}}{\Delta}\delta_o}{qSC_{L_\delta}\delta_o}\left\{0.9\overline{q}^2 - 2.7\overline{q} + 0.4\right\} \qquad (2.21.22)$$

This simplifies to

$$\frac{L_{flex}}{L_{rigid}} = \frac{9\overline{q}^2 - 27\overline{q} + 4}{4(\overline{q}^2 - 3\overline{q} + 1)} \qquad (2.21.23)$$

A plot of $L_{flex}\Big/L_{rigid}$ versus $\overline{q}$ is presented in Figure 2.21.3, *together with the plots of the numerator and denominator of Eqn. 2.21.23*.

If the purpose of the aileron is to generate lift, at reversal the lift is zero, or

$$L_{flex} = 0 \qquad (2.21.24)$$

At reversal, the numerator of Eqn. 2.21.23 is zero. This condition is written as

Figure 2.21.3 - $\dfrac{L_{flex}}{L_{rigid}}$ *vs.* $\overline{q}$ *showing reversal and divergence* $\overline{q}$ *values.*

$$9\overline{q}_R^2 - 27\overline{q}_R + 4 = 0 \qquad (2.21.25)$$

This equation is quadratic in $\overline{q}_R$ so there are two values of $\overline{q}_R$.

$$\overline{q}_{R_1} = 0.1563 \qquad (2.21.26)$$

$$\overline{q}_{R_2} = 2.8437 \qquad (2.21.27)$$

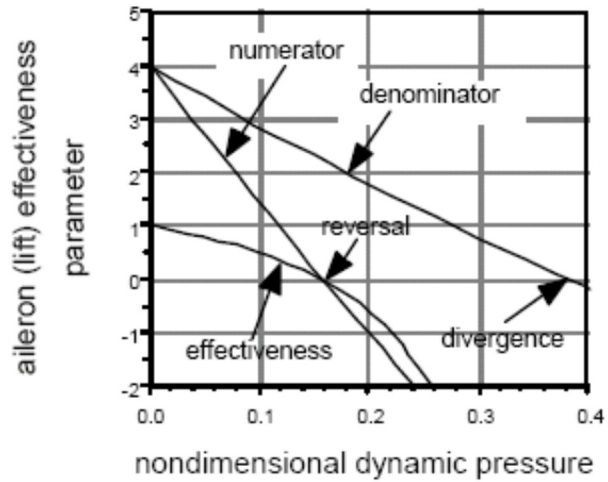Reversal occurs at the lower of these two values.

Divergence occurs when the denominator in Eqn. 2.21.23 becomes zero. Note that aileron effectiveness, defined as when $L_{flex}\big/L_{rigid}$ becomes zero, occurs before the divergence q is reached.

The traditional measure of aileron effectiveness - generating airplane rolling moment

The function of an aircraft aileron is to create a rolling moment, not just lift. The rolling moment for our two-segment idealization is computed by assuming that the lift on each wing panel is centered at the respective panel mid-span. This results in the expression for flexible wing rolling moment created by the aileron input.

$$M_{flex} = (L_1 \frac{b}{4}) + (L_2 \frac{3b}{4}) \tag{2.21.28}$$

where the wing semi-span dimension is b. We begin with Eqns. 2.21.1 and 2.21.2 and substitute the previously derived expressions for the twist of each panel to get the panel lift due to aileron rotation. Equation 2.21.28 is then written as

$$M_{flex} = \left[\frac{b}{2}(qSC_{L_\alpha})\left(\frac{1}{2}\theta_1 + \frac{3}{2}\theta_2 \right) + \frac{3}{4}b(qSC_{L_\delta})\delta_o \right] \tag{2.21.29}$$

Substituting expressions for θ_1 and θ_2 from Eqns. 2.21.15 and 2.21.16 (with $C_{L_\delta}\big/C_{L_\alpha} = 0.4$) we have

$$M_{flex} = \frac{qSC_{L_\alpha}}{\Delta}\left(\frac{b}{4} \right)\left(2.7\bar{q}^2 - 7.1\bar{q} + 1.2 \right)\delta_o \tag{2.21.30}$$

or

$$M_{flex} = \frac{qSC_{L_\alpha}b}{4}\left[\frac{2.7\bar{q}^2 - 7.1\bar{q} + 1.2}{\bar{q}^2 - 3\bar{q} + 1} \right]\delta_o \tag{2.21.31}$$

The rolling moment created by the aileron on the rigid wing is

$$M_{rigid} = \frac{3b}{4}qSC_{L_\delta}\delta_o \tag{2.21.32}$$

The ratio $M_{flex}\big/M_{rigid}$ is

$$\frac{M_{flex}}{M_{rigid}} = \frac{2.5(2.7\bar{q}^2 - 7.1\bar{q} + 1.2)}{3(\bar{q}^2 - 3\bar{q} + 1)} \tag{2.21.33}$$

In this case, control reversal is defined as $M_{flex} = 0$; we find the reversal point by setting the numerator of Eqn. 2.21.33 to zero.

$$2.7\bar{q}_R^2 - 7.1\bar{q}_R + 1.2 = 0 \tag{2.21.34}$$

Equation 2.21.34 yields two values:

$$\bar{q}_{R1} = 0.1815 \tag{2.21.35a}$$

and

$$\bar{q}_{R2} = 2.448 \tag{2.21.35b}$$

Aileron reversal occurs at the lower of these two values.

$$\bar{q}_{R1} = 0.1815 \tag{2.21.36}$$

Because the definition of effectiveness is different in this case, this reversal dynamic pressure is different than that given in Eqn. 2.21.27. Although we have not included the rolling motion in our analysis, this result is the same as we would find from that analysis. Aileron rolling moment effectiveness, defined as the ability to create a rolling moment (Eqn. 2.21.33), is plotted in Figure 2.21.4.
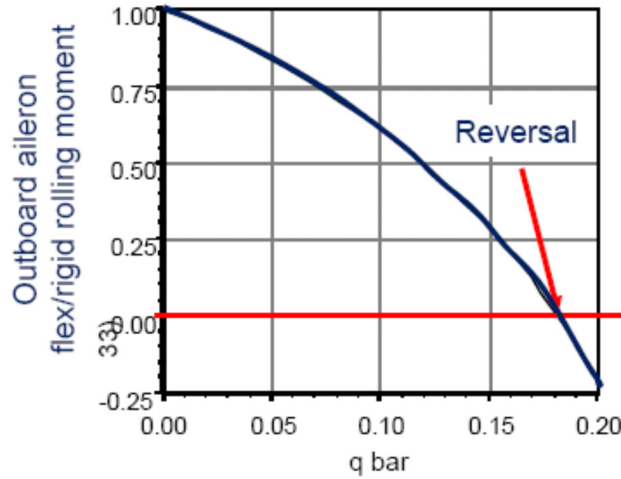

Figure 2.21.4 - Rolling moment effectiveness M_{flex} / M_{rigid} *vs.* $\bar{q}$

The effect of moving the outboard aileron to the inboard panel

When we move the aileron inboard the free body diagram for the configuration becomes as shown in Figure 2.21.5. The lift on each panel is

$$L_1 = qSC_{L_\alpha}\theta_1 + qSC_{L_\delta}\delta_o \tag{2.21.37}$$

$$L_2 = qSC_{L_\alpha}\theta_2 \tag{2.21.38}$$

Summing the twisting moments on each panel, we have

$$\Sigma M_1 = 0 = L_1 e + K_T(\theta_2 - \theta_1) - K_T\theta_1 + qScC_{M_\delta}\delta_o \tag{2.21.39}$$

and $$\Sigma M_2 = 0 = L_2 e - K_T(\theta_2 - \theta_1) \qquad (2.21.40)$$
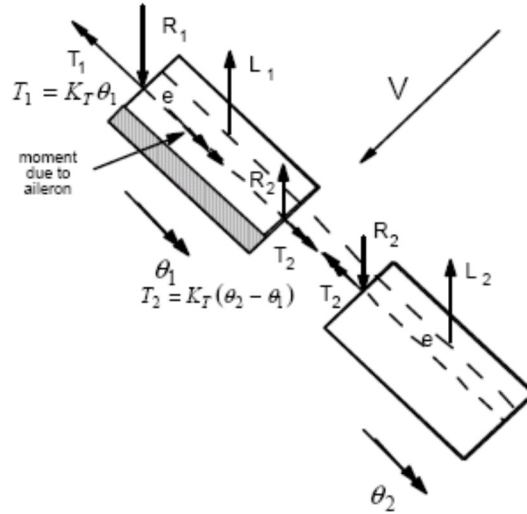

Figure 2.21.5 - Free-body diagram for inboard aileron/panel

These equations in matrix form are

$$\begin{bmatrix} 2K_T - qSeC_{L_\alpha} & -K_T \\ -K_T & K_T - qSeC_{L_\alpha} \end{bmatrix} \begin{Bmatrix} \theta_1 \\ \theta_2 \end{Bmatrix} = qSeC_{L_\alpha} \begin{bmatrix} \dfrac{C_{M_\delta}}{C_{L_\alpha}}\left(\dfrac{c}{e}\right) + \dfrac{C_{L_\delta}}{C_{L_\alpha}} \end{bmatrix} \begin{Bmatrix} \delta_o \\ 0 \end{Bmatrix} \qquad (2.21.41)$$

With the parameter values defined previously, we get:

$$\begin{bmatrix} 2 - \bar{q} & -1 \\ -1 & 1 - \bar{q} \end{bmatrix} \begin{Bmatrix} \theta_1 \\ \theta_2 \end{Bmatrix} = \bar{q} \begin{Bmatrix} -0.5 \\ 0 \end{Bmatrix} \delta_o \qquad (2.21.42)$$

The left hand side of Eqn. 2.21.42 is identical to Eqn. 2.21.10, but the aileron input has been moved from the lower element to the upper element in the vector on the right hand side of Eqn. 2.21.42. The divergence dynamic pressure is unchanged.

To find the lift reversal dynamic pressure for this configuration, the lift on the flexible wing is computed. The panel twist angles $\{\theta_i\}$ are:

$$\begin{Bmatrix} \theta_1 \\ \theta_2 \end{Bmatrix} = \frac{\bar{q}}{\Delta} \begin{bmatrix} 1 - \bar{q} & 1 \\ 1 & 2 - \bar{q} \end{bmatrix} \begin{Bmatrix} -0.5 \\ 0 \end{Bmatrix} \delta_o \qquad (2.21.43)$$

so that

$$\theta_1 = \frac{-0.5\bar{q}(1-\bar{q})}{\Delta}\delta_o = \frac{-0.5\bar{q}+0.5\bar{q}^2}{\Delta}\delta_o$$

$$\theta_2 = \frac{-0.5\bar{q}}{\Delta}\delta_o$$

(2.21.44)

The lift created by deflecting the inboard control surface is:

$$L_{flex} = qSC_{L_\alpha}(\theta_1 + \theta_2) + qSC_{L_\delta}\delta_o$$

(2.21.45)

Substituting the expressions in Eqn. 2.21.44 into Eqn. 2.21.45, we have

$$L_{flex} = qSC_{L_\alpha}\left[\frac{0.5\bar{q}^2 - 0.5\bar{q} - 0.5\bar{q}}{\Delta}\right]\delta_o + qSC_{L_\delta}\delta_o$$

(2.21.46)

Re-writing Eqn. 2.21.46 we have:

$$L_{flex} = \frac{qSC_{L_\alpha}}{\Delta}\left[0.9\bar{q}^2 - 2.2\bar{q} + 0.4\right]\delta_o$$

(2.21.47)

With aileron reversal defined as the *inability to create lift* ($L_{flex} = 0$) we have the following equation for reversal.

$$0.9\bar{q}_R^2 - 2.2\bar{q}_R + 0.4 = 0$$

(2.21.48)

The two solutions for $\bar{q}_R$ are:

$$\bar{q}_{R_1} = 0.1978$$

(2.21.49)

$$\bar{q}_{R_2} = 2.2466$$

(2.21.50)

Reversal occurs at the lowest value of $\bar{q}_R$.

$$\bar{q}_R = 0.1978$$

(2.21.51)

Comparing the value of $\bar{q}_R$ in Eqn. 2.21.51 to that in Eqn. 2.21.27 we see that the value of the reversal parameter $\bar{q}$ in Eqn. 2.21.51 is 1.27 times that presented in Eqn. 2.21.27. The wing with the inboard aileron has a higher reversal speed. However, it is not necessarily more effective in generating lift at some airspeeds.

Rolling moment with the inboard aileron
To compute the rolling moment due to the inboard aileron, we begin with the expression for rolling moment.

$$M_{flex} = \left(\frac{b}{4}\right)L_1 + \left(\frac{3b}{4}\right)L_2 + qSC_{L_\delta}\delta_o\left(\frac{b}{4}\right) \qquad (2.21.52)$$

or

$$M_{flex} = \frac{qSC_{L_\alpha}}{\Delta}\left(\frac{b}{4}\right)\left[\frac{1}{2}\bar{q}^2 - 2\bar{q} + \frac{2}{5}\right] \qquad (2.21.53)$$

Since rolling moment generation is the objective, then, from Eqn. 2.21.53, aileron reversal requires that the numerator in that expression be zero. This means that

$$\frac{1}{2}\bar{q}_R^2 - 2\bar{q}_R + \frac{2}{5} = 0 \qquad (2.21.54)$$

The solution to Eqn. 2.21.54 yields two values.

$$\bar{q}_{R_1} = 0.2112 \qquad (2.21.55a)$$

$$\bar{q}_{R_2} = 3.789 \qquad (2.21.55b)$$

Reversal occurs when

$$\bar{q}_R = 0.2112 \qquad (2.21.56)$$

Comparing Eqn. 2.21.56 with Eqn. 2.21.36, we see that the roll moment reversal dynamic pressure with the inboard aileron is 1.163 times that of the outboard aileron so moving the aileron inboard increases the reversal speed. On the other hand, before it reverses, the rolling moment due to the outboard aileron is larger than that for the inboard aileron because it has a larger moment arm.

With real operational aircraft, different surfaces, located at different positions on the wing, are used to generate roll moments at high airspeeds that at low speeds. The low speed ailerons are located farther outboard than the low speed ailerons, but are "locked out" after a high speed is reached so they are prevented from operating. To understand why this is so, let's look at the relative effectiveness of each of the two surfaces in this problem.

First, compute the ratio of M_{flex} for the outboard aileron to M_{flex} for the inboard aileron, to get the following expression

$$M_{ratio} = \frac{M_{flex/outboard}}{M_{flex/inboard}} = \frac{2.7\bar{q}^2 - 7.1\bar{q} + 1.2}{0.5\bar{q}^2 - 2\bar{q} + 0.4} \qquad (2.21.57)$$

or

$$M_{ratio} = \frac{5.4\bar{q}^2 - 14.2\bar{q} + 2.4}{\bar{q}^2 - 4\bar{q} + 0.8} \qquad (2.21.58)$$

If, at a chosen dynamic pressure, M_{ratio} is greater than unity, then it is better to use the outboard aileron for roll control. Figure 2.21.6 plots the ratio in Eqn. 2.21.58.
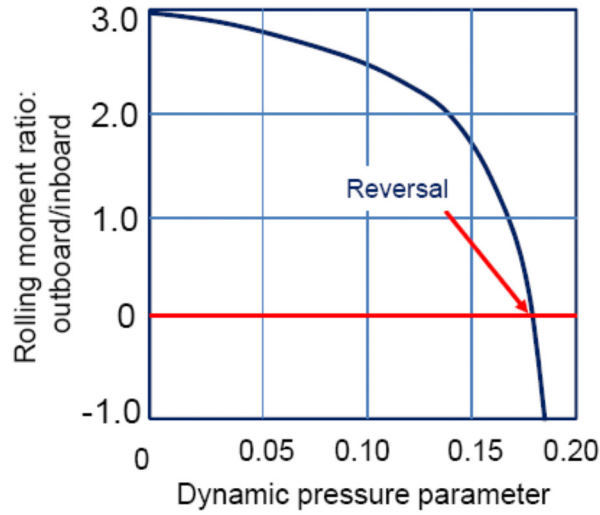
---

*Figure 2.21.6 - Relative effectiveness of ailerons
to create a rolling moment (Eqn. 2.21.58) showing relative effectiveness of the two ailerons*

The "cross-over" dynamic pressure at which the inboard aileron becomes more effective occurs when M_{ratio} is equal to 1. The cross-over point is found by setting the numerator in Eqn. 2.21.58 equal the denominator of Eqn. 2.21.58 so that, at the cross-over point

$$5.4\bar{q}^2 - 14.2\bar{q} + 2.4 = \bar{q}^2 - 4\bar{q} + 0.8 \tag{2.21.59}$$

or

$$4.4\bar{q}^2 - 10.2\bar{q} + 1.6 = 0 \tag{2.21.60}$$

The solutions to Eqn. 2.21.60 are

$$\bar{q}_1 = 0.1692 \tag{2.21.61a}$$

and

$$\bar{q}_2 = 2.149 \tag{2.21.61b}$$

From Eqn. 2.21.61a and Figure 2.21.6 we see that the outboard aileron is more effective for moment generation as long as $\bar{q} < 0.1692$. The outboard aileron configuration reverses at $\bar{q}_R = 0.1815$, as indicated in Figure 2.21.6. At larger values of dynamic pressure the inboard surface is more effective but will reverse at dynamic pressures above $\bar{q} = 0.2112$.

2.22 Artificial stabilization - wing divergence feedback control

Since aerodynamic forces and moments are naturally fed back to create displacement dependent airloads that may create instabilities, we can use an "unnatural" feedback process to control loads and create an artificial situation to change the divergence speed.

2.22.1 – A two dimensional example

The purpose of this section is to show how the natural aeroelastic feedback process is changed by an actively controlled aileron. For our example we will use the configuration previously considered in

Section 2.14, Figure 2.14.1. The addition of an aileron to the outboard panel, labeled as panel 2, is indicated in Figure 2.22.1. *Both angle of attack and control deflection are inputs.*
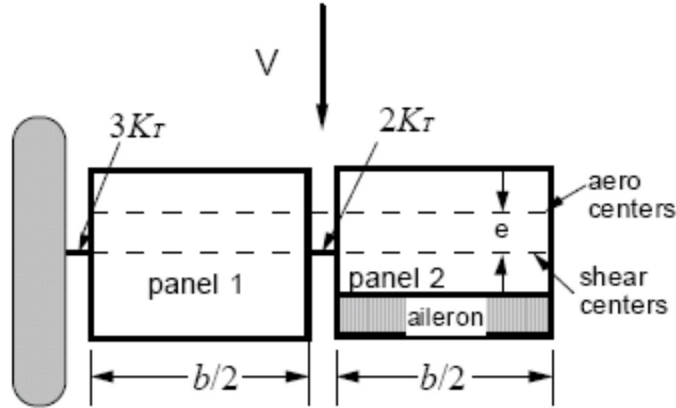

Figure 2.22.1 - Two degree of freedom wing idealization with aileron.

When the aileron is deflected an amount δ_o the lift on panel 2 is:

$$L_2 = qSC_{L_\alpha}(\alpha_o + \theta_2) + qSC_{L_\delta}\delta_o \tag{2.22.1}$$

Control surface deflection also causes a pitching moment about the panel 2 axis of rotation, written as:

$$M_2 = L_2 e + qScC_{M_\delta}\delta_o \tag{2.22.2}$$

Expanding Eqn. 2.22.2, we have:

$$M_2 = qSeC_{L_\alpha}(\alpha_o + \theta_2) + qSeC_{L_\alpha}\left(\frac{C_{L_\delta}}{C_{L_\alpha}} + \left(\frac{c}{e}\right)\frac{C_{M_\delta}}{C_{L_\alpha}}\right)\delta_o \tag{2.22.3}$$

We include this modified equation in our original model in Section 2.14 to find the matrix equation for static equilibrium.

$$\left[\begin{bmatrix} 5 & -2 \\ -2 & 2 \end{bmatrix} + \bar{q}\begin{bmatrix} -1 & 0 \\ 0 & -1 \end{bmatrix}\right]\begin{Bmatrix} \theta_1 \\ \theta_2 \end{Bmatrix} = \bar{q}\alpha_o\begin{Bmatrix} 1 \\ 1 \end{Bmatrix} + \bar{q}\left(\frac{C_{L_\delta}}{C_{L_\alpha}} + \frac{c}{e}\frac{C_{M_\delta}}{C_{L_\alpha}}\right)\begin{Bmatrix} 0 \\ 1 \end{Bmatrix}\delta_o \tag{2.22.4}$$

Equation 2.22.4 shows that the aeroelastic divergence problem in Section 2.14 is unchanged; α_o and δ_o are inputs, independent of θ_1 and θ_2. Let us suppose that we include a feedback control system so that the aileron deflection, δ_o, responds to a sensor that measures the twist deformation, θ_1. The sensor, perhaps a strain gage, senses and sends signals to an aileron actuator to rotate the control surface an amount δ_o given by the relationship

$$\delta_o = \lfloor G \quad 0 \rfloor\begin{Bmatrix} \theta_1 \\ \theta_2 \end{Bmatrix} \tag{2.22.5}$$

The row matrix $\lfloor G \quad 0 \rfloor$ is called the *control gain matrix*. The constant G is a *"gain"* and can be chosen by the control system designer arbitrarily; it can be either a positive or negative number.

The second term on the right hand side of Eqn. 2.22.4 is now written as

$$\overline{q}\left(\frac{C_{L_\delta}}{C_{L_\alpha}} + \left(\frac{c}{e}\right)\frac{C_{M_\delta}}{C_{L_\alpha}}\right)\begin{Bmatrix} 0 \\ 1 \end{Bmatrix}\lfloor G \quad 0 \rfloor\begin{Bmatrix} \theta_1 \\ \theta_2 \end{Bmatrix} \tag{2.22.6}$$

or

$$\overline{q}\left(\frac{C_{L_\delta}}{C_{L_\alpha}} + \left(\frac{c}{e}\right)\frac{C_{M_\delta}}{C_{L_\alpha}}\right)\begin{bmatrix} 0 & 0 \\ G & 0 \end{bmatrix}\begin{Bmatrix} \theta_1 \\ \theta_2 \end{Bmatrix} = \overline{q}\begin{bmatrix} 0 & 0 \\ k & 0 \end{bmatrix}\begin{Bmatrix} \theta_1 \\ \theta_2 \end{Bmatrix} \tag{2.22.7}$$

with

$$k = G\left(\frac{C_{L_\delta}}{C_{L_\alpha}} + \left(\frac{c}{e}\right)\frac{C_{M_\delta}}{C_{L_\alpha}}\right) \tag{2.22.8}$$

Eqn. 2.22.7 is a function of θ_1 and θ_2; it belongs on left hand side of Eqn. 2.22.4. The divergence eigenvalue problem for the wing system with this feedback control loop is:

$$\begin{bmatrix} (5-\overline{q}) & (-2) \\ (-2-\overline{q}k) & (2-\overline{q}) \end{bmatrix}\begin{Bmatrix} \theta_1 \\ \theta_2 \end{Bmatrix} = \begin{Bmatrix} 0 \\ 0 \end{Bmatrix} \tag{2.22.9}$$

The characteristic equation for static stability is again found by taking the determinant of the aeroelastic stiffness matrix in Eqn. 2.22.9 and setting it to zero.

$$\Delta = \overline{q}^2 - 7\overline{q} + 6 - 2\overline{q}k = 0 \tag{2.22.10}$$

Figure 2.22.2 plots Eqn. 2.22.10 for five different values of k, including the *open loop* case, *k=0* (labeled "baseline.").

When *k>0* the divergence dynamic pressure decreases as the eigenvalue (the crossing points) move away from each other. This is because when $\theta_1 > 0$ the aileron will rotate downward and increase lift on the outboard panel; as a result, the two segment system is destabilized. However, if $k < 0$ when $\theta_1 > 0$) the aileron will rotate upward to "dump" lift from the outboard panel. On The two-panel system is stabilized. Notice that, as k becomes more negative, the value of the lowest eigenvalue (crossing points) increases while the second eigenvalue
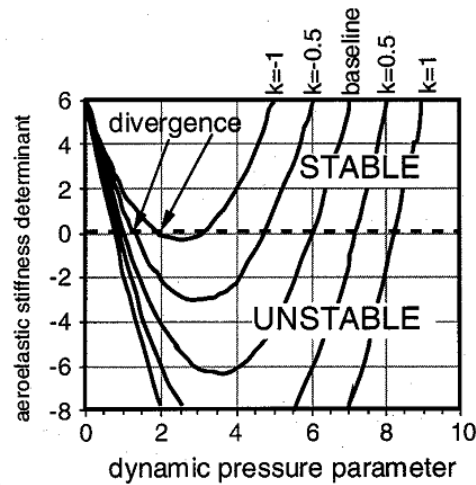

Figure 2.22.2 - Stability determinant vs. $\overline{q}$ for 5 different values of control constant, k

Chapter 2

(originally at $\overline{q} = 6$) declines so that they approach each other. At some value k <-1 there are no real solutions since the determinant will not cross the horizontal axis. The solutions to the characteristic equation are complex numbers.

To take a look at this from a different perspective, we separate the terms in Eqn. 2.22.10 by defining the term Δ_o as:

$$\Delta_o = \overline{q}^2 - 7\overline{q} + 6 \qquad (2.22.11)$$

The term Δ_O is the characteristic equation for the "open-loop" system. The divergence condition in Eqn. 2.22.10 is written in terms of Δ_O as

$$\Delta = \Delta_o - 2\overline{q}k = 0 \quad or \quad \Delta_o = 2\overline{q}k \qquad (2.22.12)$$

Equation 2.22.10 is again plotted, but this time the range of dynamic pressure values is smaller than in Figure 2.22.2. Five lines corresponding to k = 1, 0.5, 0, -0.5 and -1are shown together with the function $f(\overline{q}) = 2\overline{q}k$ plotted as a dashed line for the values k=1, k= -1 and k= -1.05.

Intersection points (circled in Figure 2.22.3) between the Δ_o curve (labeled k=0) and the dashed lines correspond to eigenvalue solutions to the closed-loop problem and are indicated for the three values shown. These circled values give the same values for the crossing points of the full characteristic equation with the controller included.

When $k = -1.05$, the $2\overline{q}k$ line is tangent to the Δ_o curve at $\overline{q}_D = 2.45$. As a result there is a single intersection point at this dynamic pressure where the two eigenvalues merge. If k < -

Figure 2.22.3 - Effect of control gain k on divergence stability determinant crossing points

1.05 then the line $2\overline{q}k$ never intersects the baseline determinant and divergence is impossible.

2.22.2 Example - Active control of typical section divergence speed

This section examines the typical section wing shown in Figure 2.22.4 with an actively controlled aileron used to increase the divergence speed. The controller operates all the time so it not only changes the divergence airspeed but it will also change the wing torsional equilibrium position. We want to: 1) find the control constant k (defined below) necessary to double the divergence dynamic pressure compared to the uncontrolled case; 2) find the value of k for which divergence is totally eliminated; and, 3) find how much the aileron must rotate in normal flight.
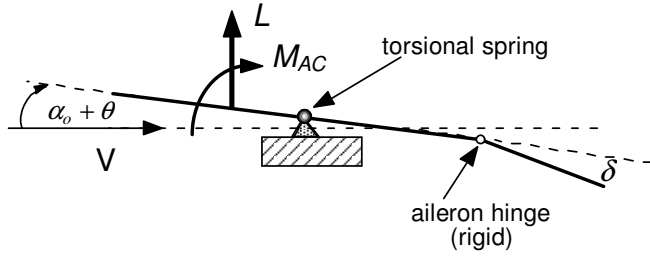
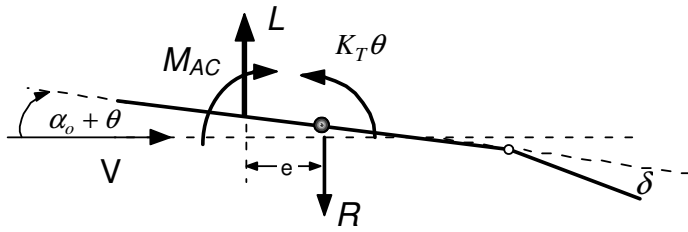**Figure 2.22.4 - Typical section with control surface and free body diagram**

Figure 2.22.5 - Free body diagram showing forces and moments

As indicated in Figure 2.22.4 the lift acting at the aerodynamic center is a function of α_o, θ and δ (the initial angle of attack, elastic twist, and aileron angle, respectively). A restoring moment $K_T\theta$ is furnished by the spring.

The aileron angle δ is related to the elastic twist θ by the linear relationship $\delta = k\theta$ where k is a control constant that may be positive, negative, or zero. The effect of the control relationship $\delta = k\theta$ is to torsionally stiffen (or de-stiffen) the wing to increase (or decrease) the divergence dynamic pressure.

Figure 2.22.5 shows the free body diagram. The moment equilibrium relation is found by summing moments in the clockwise direction:

$$+ \Sigma M_{pin} = Le + M_{AC} - K_T\theta \tag{2.22.12}$$

For divergence calculations, α_o is zero and the twist θ is a perturbation. The lift and pitching moment about the aerodynamic center are

$$L = qSC_{L_\alpha}\left(\theta + \frac{C_{L_\delta}}{C_{L_\alpha}}\delta\right) \tag{2.22.13}$$

$$M_{AC} = qScC_{MAC_\delta}\delta \tag{2.22.14}$$

Substituting the relations for lift and pitching moment into Eqn. 2.22.12 with $\delta = k\theta$ gives the condition for neutral stability.

$$\left(K_T - qSeC_{L_\alpha} - qSeC_{L_\alpha}\left(\frac{C_{L_\delta}}{C_{L_\alpha}}\right)k - qScC_{MAC_\delta}k\right)\theta = 0 \tag{2.22.15}$$

The term contained in the outer brackets of Eqn. 2.22.15 is the aeroelastic torsional stiffness. The divergence dynamic pressure is found by setting this stiffness to zero.

$$q_D = \cfrac{K_T / SeC_{L_\alpha}}{1 + k\left(\cfrac{C_{L_\delta}}{C_{L_\alpha}}\right)\left(1 + \left(\cfrac{c}{e}\right)\left(\cfrac{C_{MAC_\delta}}{C_{L_\delta}}\right)\right)} \qquad (2.22.16)$$

If $k = 0$, Eqn. 2.22.16 reduces to the "open-loop" (control off) divergence dynamic pressure found in previous sections.

Define the parameter $q_o = K_T / SeC_{L_\alpha}$ (the value of q_D with $k = 0$). We want to increase the open loop divergence dynamic pressure by a factor, n, then $\dfrac{q_D}{q_o} = n$

$$\frac{q_D}{q_o} = n = \cfrac{1}{1 + k\left(\cfrac{C_{L_\delta}}{C_{L_\alpha}}\right)\left(1 + \left(\cfrac{c}{e}\right)\left(\cfrac{C_{MAC_\delta}}{C_{L_\delta}}\right)\right)}$$

$$k = \cfrac{1/n - 1}{\left(\cfrac{C_{L_\delta}}{C_{L_\alpha}}\right)\left(1 + \left(\cfrac{c}{e}\right)\left(\cfrac{C_{MAC_\delta}}{C_{L_\delta}}\right)\right)} \qquad (2.22.17 \text{ a,b})$$

When n=2
$$k = \cfrac{-1}{2\left(\left(\cfrac{C_{L_\delta}}{C_{L_\alpha}}\right)\left(1 + \left(\cfrac{c}{e}\right)\left(\cfrac{C_{MAC_\delta}}{C_{L_\delta}}\right)\right)\right)} \qquad (2.22.18)$$

If the denominator in Eqn. 2.22.16 is less than or equal to zero, then $q_D < 0$ and divergence won't occur.

$$1 + k\left(\left(\cfrac{C_{L_\delta}}{C_{L_\alpha}}\right)\left(1 + \left(\cfrac{c}{e}\right)\left(\cfrac{C_{MAC_\delta}}{C_{L_\delta}}\right)\right)\right) \leq 0 \qquad (2.22.19)$$

or

$$k \leq k_{cr} = \cfrac{-1}{\left(\cfrac{C_{L_\delta}}{C_{L_\alpha}}\right)\left(1 + \left(\cfrac{c}{e}\right)\left(\cfrac{C_{MAC_\delta}}{C_{L_\delta}}\right)\right)} \qquad (2.22.20)$$

This is identical to the result we get when we let $n \to \infty$ in Eqn. 2.22.17b.

When $\alpha_o \neq 0$ the wing lift is $L = qSC_{L_\alpha}\left(\alpha_o + \theta + \dfrac{C_{L_\delta}}{C_{L_\alpha}}\delta_o\right)$.

The **equilibrium** twist angle θ is:

$$\theta = \frac{\bar{q}\alpha_o}{1 - \bar{q} - \bar{q}k\left(\left(\dfrac{C_{L_\delta}}{C_{L_\alpha}}\right)\left(1 + \left(\dfrac{c}{e}\right)\left(\dfrac{C_{MAC_\delta}}{C_{L_\delta}}\right)\right)\right)} \qquad (2.22.21a)$$

When $\dfrac{q_D}{q_o} = n$ this equation becomes, after substitution of Eqn. 2.22.17b,

$$\theta = \frac{\bar{q}\alpha_o}{1 - \dfrac{\bar{q}}{n}} \qquad (2.22.21b)$$

where $\bar{q} = \dfrac{qSeC_{L_\alpha}}{K_T}$. The aileron deflection is:

$$\delta = k\theta = \bar{q}\alpha_o \frac{\left(\dfrac{1}{n} - 1\right)}{\left(\dfrac{C_{L_\delta}}{C_{L_\alpha}}\right)\left(1 + \left(\dfrac{c}{e}\right)\left(\dfrac{C_{MAC_\delta}}{C_{L_\delta}}\right)\right)} \frac{1}{\left(1 - \dfrac{\bar{q}}{n}\right)} \qquad (2.22.22a)$$

When $n \to \infty$ we have

$$\delta_{div-free} = k_{cr}\theta = k_{cr}\bar{q}\alpha_o = \bar{q}\alpha_o \frac{-1}{\left(\dfrac{C_{L_\delta}}{C_{L_\alpha}}\right)\left(1 + \left(\dfrac{c}{e}\right)\left(\dfrac{C_{MAC_\delta}}{C_{L_\delta}}\right)\right)} \qquad (2.22.22b)$$

The wing lift is $L = qSC_{L_\alpha}(\alpha_o + \theta) + qSC_{L_\delta}\delta$ so that

$$\frac{L}{qSC_{L_\alpha}\alpha_o} = \frac{1}{1 - \dfrac{\bar{q}}{n}} + \frac{\bar{q}\left(1 - \dfrac{1}{n}\right)}{\left(1 + \left(\dfrac{e}{c}\right)\left(\dfrac{C_{L_\delta}}{C_{MAC_\delta}}\right)\right)\left(1 - \dfrac{\bar{q}}{n}\right)} \qquad (2.22.23a)$$

At the divergence free condition $n \to \infty$

$$\frac{L}{qSC_{L_\alpha}\alpha_o} = 1 + \frac{\bar{q}}{\left(1 + \left(\dfrac{e}{c}\right)\left(\dfrac{C_{L_\delta}}{C_{MAC_\delta}}\right)\right)} \qquad (2.22.23b)$$

Chapter 2

Combining the two terms in Eqn. 2.22.23 over a common denominator,

$$L = qSC_{L_\alpha}\alpha_o \left(\frac{1 + \left(\dfrac{e}{c}\right)\left(\dfrac{C_{L_\delta}}{C_{MAC_\delta}}\right) + \bar{q}}{\left(1 + \left(\dfrac{e}{c}\right)\left(\dfrac{C_{L_\delta}}{C_{MAC_\delta}}\right)\right)} \right) \qquad (2.22.24)$$

If the aircraft weighs W pounds and this wing supports half of this weight, then the angle of attack is

$$\alpha_o = \frac{W}{2qSC_{L_\alpha}} \left(\frac{1 + \left(\dfrac{e}{c}\right)\left(\dfrac{C_{L_\delta}}{C_{MAC_\delta}}\right)}{1 + \left(\dfrac{e}{c}\right)\left(\dfrac{C_{L_\delta}}{C_{MAC_\delta}}\right) + \bar{q}} \right) \qquad (2.22.25)$$

or

$$\alpha_o = \frac{We}{2\bar{q}K_T} \left(\frac{1 + \left(\dfrac{e}{c}\right)\left(\dfrac{C_{L_\delta}}{C_{MAC_\delta}}\right)}{1 + \left(\dfrac{e}{c}\right)\left(\dfrac{C_{L_\delta}}{C_{MAC_\delta}}\right) + \bar{q}} \right) \qquad (2.22.26)$$

We can now solve for the aileron deflection. Since $\delta_{div-free} = k_{cr}\bar{q}\alpha_o$ we find the expression for the aileron deflection required for the actively controlled divergence free wing.

$$\delta_{div-free} = -\frac{We}{2K_T} \left(\frac{\left(\dfrac{e}{c}\right)\left(\dfrac{C_{L_\alpha}}{C_{MAC_\delta}}\right)}{1 + \left(\dfrac{e}{c}\right)\left(\dfrac{C_{L_\alpha}}{C_{MAC_\delta}}\right)\left(\dfrac{C_{L_\delta}}{C_{L_\alpha}}\right) + \bar{q}} \right) \qquad (2.22.27a)$$

or

$$\delta_{div-free} = \frac{1}{2}\frac{W/S}{q_R C_{MAC_\delta}} \left(\frac{\left(\dfrac{e}{c}\right)^2 \dfrac{C_{L_\delta}}{C_{MAC_\delta}}}{1 + \left(\dfrac{e}{c}\right)\left(\dfrac{C_{L_\delta}}{C_{MAC_\delta}}\right) + \bar{q}} \right) \qquad (2,22,27b)$$

Changing the divergence speed requires a steady, non-zero, value of δ at all times, not just when the wing is perturbed. Equation 2.22.27a is plotted in Figure 2.22.6 as a function of $\bar{q}$. From this plot we can see that the aileron will be required to deflect to large angle unless its chord is a substantial fraction of the chord of the wing or unless the elastic axis offset e is small.

Figure 2.22.7 plots the results from Eqn. 21.21.27 at three different values of dynamic pressure and shows that the best size flap-to-chord ratio will depend upon the dynamic pressure parameter $\bar{q}$ at which the wing operates.
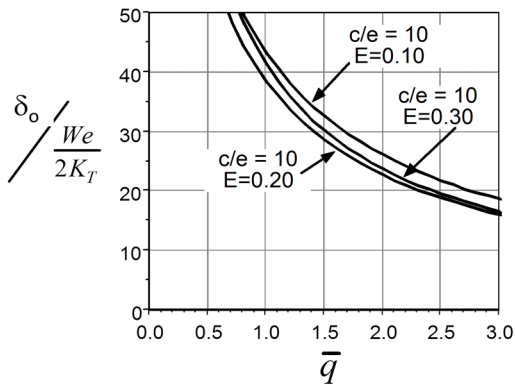

Figure 2.22.6 - Aileron deflection requirements for divergence suppression
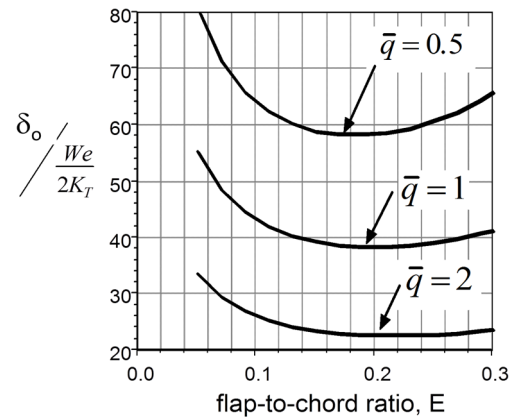

Figure 2.22.7 – The effect of flap-to-chord ratio on divergence suppression requirements.

Control effectiveness - summary

Unlike divergence, control reversal is not an aeroelastic instability. With divergence a small input, α_o, produces a large output, θ. For reversal a large input δ_o produces no output. Above the reversal speed, a control input δ_o produces lift or moment opposite to that intended (hence the term *reversal*). At pressures larger than the divergence speed, the wing is statically unstable and will diverge or twist off.

Two examples of control reversal were considered. In the first, control effectiveness was defined as the ability of a wing/control surface (an elevator or rudder) to create lift which then produced a moment about an unspecified flight mechanics axis. In the second example, a wing/aileron combination produced rolling motion which was allowed to attain a terminal, steady-state condition. The procedure to find the terminal roll rate was illustrated. For this second example, the dynamic pressure at the reversal condition was found to be identical to the first case, even though the boundary conditions were different.

In the final example, an aileron was used to increase the divergence dynamic pressure by creating a control law relating aileron displacement to wing twist. While not an effective method to produce divergence changes, this example does illustrate how feedback control changes aeroelastic eigenvalues. In our final section we will illustrate the relationship between static instabilities and dynamic response.

2.23 The relationship between divergence and dynamic instability-typical section torsional vibration with quasi-steady airloads

In Chapter 4 we will consider flutter, a dynamic instability. To complete the discussion of divergence we consider what might happen if a system that diverges is perturbed dynamically instead of statically so that it vibrates in the airstream. For this illustration we woll use the simplest model, a wing model, shown in side-view in Figure 2.23.1 mounted on a pin is identical to that used in Section 2.10 and shown in Figure 2.10.1.

This wing has span, l, chord, c, and total mass *M=ml*. The plunge degree of freedom of this typical section is zero $(h = 0)$; twist θ is measured as a perturbation away from the static equilibrium position. The twist angle θ is created by an initial disturbance with initial conditions (twist displacement and twist velocity). We assume that the aerodynamic loads on the vibrating system are time dependent but identical in form to the static system. This is an approximation and not strictly not unless the oscillations occur very slowly. In Chapter 4 we will improve on this formulation.
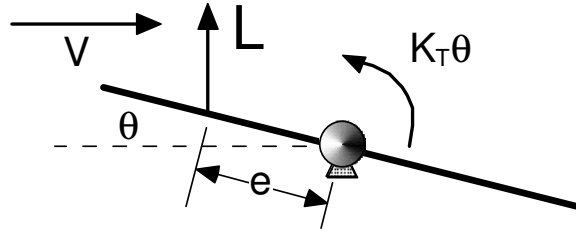

Figure 2.23.1 - Typical section model for vibration analysis

Summing moments about the pin (positive clockwise) and equating them to $I_\theta \ddot{\theta}$ where I_θ is the mass moment of inertia computed *about the fixed pin*, the equation of motion is

$$I_\theta \ddot{\theta} = -K_T \theta + qSeC_{L_\alpha} \theta \ \ or \ \ I_\theta \ddot{\theta} + K_T \theta - qSeC_{L_\alpha} \theta = 0 \qquad (2.23.1)$$

With $\overline{K}_T = K_T - qSeC_{L_\alpha}$ Eqn. 2.23.1 is written as

$$I_\theta \ddot{\theta} + \overline{K}_T \theta = 0 \qquad (2.23.2)$$

To solve Eqn. 2.23.2 assume that

$$\theta(t) = \theta_0 e^{st} \qquad (2.23.3)$$

where s is an unknown, t represents the time parameter and θ_o is the vibration amplitude. Equation 2.23.4 becomes

$$s^2 I_\theta \theta_0 e^{st} + \overline{K}_T \theta_0 e^{st} = \left(s^2 I_\theta + \overline{K}_T \right)\theta_0 e^{st} = 0 \qquad (2.23.4)$$

Since the vibration amplitude is not zero and e^{st} is not zero, Eqn. 2.23.4 requires that $\left(s^2 I_\theta + \overline{K}_T \right) = 0$. This means that the solution for the parameter s is

$$s^2 = -\frac{\overline{K}_T}{I_\theta} \quad or \quad s = \sqrt{-\frac{\overline{K}_T}{I_\theta}} \tag{2.23.5}$$

Since the term $\overline{K}_T$ can be positive, negative or zero, there are three different solutions to Eqn. 2.23.5: (1) if $\overline{K}_T > 0$, implying operation at a dynamic pressure below the divergence q, then

$$s = \sqrt{-\frac{\overline{K}_T}{I_\theta}} = \sqrt{-1}\sqrt{\frac{\overline{K}_T}{I_\theta}} = \pm i\omega;$$ (2) if we are operating above the divergence dynamic pressure

then $K_T < 0$ and we have $s = \pm\sqrt{\left|\frac{\overline{K}_T}{I_\theta}\right|}$; and, 3) when we are operating right at the divergence

dynamic pressure, $K_T = 0$, s=0. Let's examine all three cases.

Case (1) Below the divergence dynamic pressure, we have $\omega > 0$ and the solution

$$\theta(t) = \theta_1 \sin \omega t + \theta_2 \cos \omega t \quad (\omega = \sqrt{\frac{\overline{K}_T}{I_\theta}} > 0) \tag{2.23.6}$$

The constants θ_1 *and* θ_2 are amplitude constants determined by initial conditions. The wing, when perturbed, vibrates forever, but its amplitude does not change. The natural frequency is determined by the aeroelastic stiffness.

Case (2) The aeroelastic stiffness is less than zero.

$$\theta(t) = \theta_1 e^{pt} + \theta_2 e^{-pt} \quad (s = p = \sqrt{\frac{-\overline{K}_T}{I_\theta}} > 0) \tag{2.23.7}$$

Static analysis says that the displacement is infinite, but dynamic analysis says that the motion has two parts. For one part the motion decays but for the other it is exponentially increasing or *divergent.*

Case (3) $K_T = 0$. When $\overline{K}_T$ is exactly equal to zero, Eqn. 2.23.2 becomes $I_\theta \ddot{\theta} = 0$ so the solution is $\theta = \theta_1 + \theta_2 t$ The motion is neither oscillatory nor divergent. If the system has a small displacement it stays there. If it is given an impulse it travels away from equilibrium at constant velocity. It is neutrally stable.

Figure 2.23.2 shows a plot of nondimensional natural frequency (actual frequency divided by the reference frequency $\omega_\theta = \sqrt{\dfrac{K_T}{I_\theta}}$ vs. airspeed this example. At zero airspeed the natural frequency is identical to the so-called *in vacuo* natural frequency, our reference frequency $\omega_\theta = \sqrt{\dfrac{K_T}{I_\theta}}$.
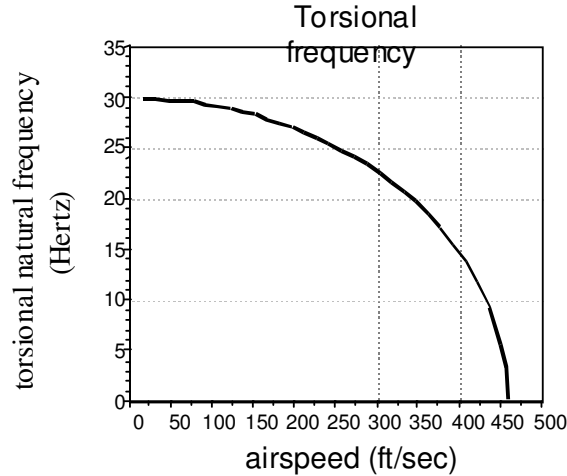

Torsional frequency

Figure 2,23.2 - Nondimensional natural frequency vs. airspeed

Divergence is a special case of dynamic instability. At the so-called statically unstable point, perturbed dynamic motion changes from simple harmonic oscillation to exponentially divergent motion. At this transition point the natural frequency is zero. Divergence has been called *flutter at zero frequency*. However, this term is not really correct since flutter, as we will show in Chapter 4, has a different instability mechanism.

2.24 Summary - lift effectiveness, divergence and aileron effectiveness

After over 100 pages of text and examples (with pages and pages of detailed algebra and equations), what should we take away from this chapter? First of all, if we had this material in 1920, when aviation was in its infancy, we would have been very popular with airplane designers. Our simple models could be used to explain the source of observed problems that had begun to be important and suggested ways to fix them. Despite the tremendous progress made in theoretical modeling over the last half century, this ability to use fundamental models to understand, avoid, diagnose and outline fixes to aeroelastic problems remains.

The aeroelastic problems we considered in this chapter have been exhaustingly discussed by others. Several interesting articles cover the early years of structural development and aeroelastic problems and are both informative and entertaining.[21, 22, 23, 24] Two references, one by Fung (Reference 25), the other by Bisplinghoff, Ashley and Halfman (Reference 26) stand out, both for their clear discussions and the wealth of back-up references.

Torsional stiffness is fundamental to all aeroelastic problems

The fundamental importance of wing torsional stiffness to the sources and solutions to aeroelastic problems was confirmed in all sections of Chapter 2. The interactions between wing torsional

stiffness and the aerodynamic loads produce an aerodynamic wing de-stiffening effect that works its way into phenomena such as load amplification, ultimately culminating in divergence, and control effectiveness, leading to aileron reversal.

We also introduced and defined terminology with definitions that included terms such as elastic axis, shear center, aerodynamic center, stiffness matrix and aerodynamic stiffness matrix. These terms helped us to characterize the important features of configurations that allow us to make preliminary assessments of problem areas.

Boundary conditions are important

In the area of analysis we also showed the importance of boundary conditions, restrictions and assumptions. For instance, when the wing angle of attack is held fixed, as it would be in a wind tunnel experiment, twist deformation increases without bound as airspeed increases. This unbounded distortion is caused by the approach of a static instability, divergence. However, when the angle is adjusted to keep the lift constant, as it would be in flight, this unboundedness is not present.

These analytical features led us to consider what happens when we introduce small perturbations into the static equilibrium analysis. In this case we developed an eigenvalue problem from which we could solve for the divergence speed. We also found that the eigenvalue problem was simply the static equilibrium problem, but with all inputs set to zero and with the interpretation that deflections were perturbations rather than real deformations. We also introduced a simple vibration problem and showed that there is a relationship between the more realistic dynamic analysis and the static analysis. At divergence, one of the system natural frequencies goes to zero and the dynamic response is exponentially divergent in time.

Divergence and control effectiveness are different but have the same origin

Wing divergence happens when a small input, α_o, produces a large output, θ. Control reversal is a performance problem related to wing torsional stiffness. With aileron reversal a large control input δ_o produces no output. Two control reversal situations were examined. In the first case, control effectiveness was defined as the ability of a wing/control surface (an elevator or rudder) to create lift which then produced a moment about an unspecified flight mechanics axis. In the second example, a wing/aileron combination produced rolling motion which was allowed to attain a terminal, steady-state condition. The value of the terminal roll rate was found. Reversal was defined as the inability to create a roll rate, not a roll moment. In both cases the reversal condition was found to be identical, even though the goal was different.

As indicated in Figure 2.24.1 the offset between the wing section aerodynamic center and the shear center (or elastic axis) is a critical parameter for divergence. The shear center (elastic axis) depends on structural geometry, primarily the placement and size of major elements like wing spars. For aileron effectiveness the shear center is not important. Instead, aileron size defines the aileron center of pressure. The difference between the center of pressure and the aero center, shown as the dimension *d*, defines reversal. In both cases the torsional stiffness is important.
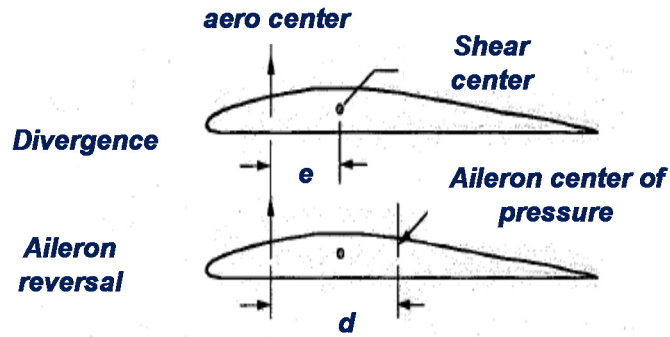
Figure 2.24.1 – Two different geometric parameter define divergence and lift effectiveness.

In Chapter 3 we will complete our study of the fundamentals of static aeroelasticity by considering aeroelastic effects on swept wings. For swept wings, aeroelastic interaction is more complicated because bending introduces additional loads.

2.25   Homework problems

2.1 An uncambered wing is mounted in a wind tunnel on a shaft that is free to rotate. The mount is restrained by the usual torsion spring K_T. In addition, a pendulum is attached to the wing mounting shaft outside the wind tunnel. If the wing c.g. is located at the pivot point, solve for the divergence dynamic pressure.
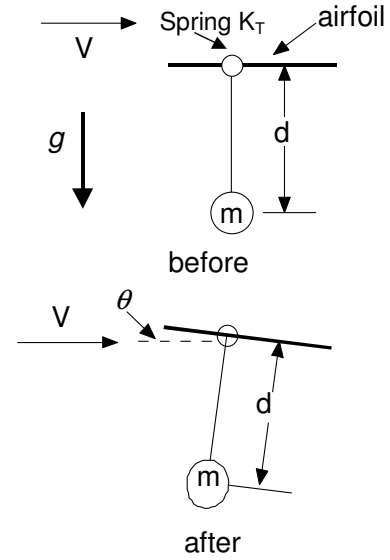
2.2 An all-movable, uncambered wing segment with planform area S and lift curve slope C_{L_α} is used to control an air vehicle. The idealized model of this system is shown. It consists of a rigid rod that can rotate about a forward pivot, but is restrained by a torsion spring, K_1. This rotation is measured as the small angle α shown. No aerodynamic forces act on this rod.

At the right end of the rod is an wing segment that is "all-movable" (as a result, $C_{L_\delta} = C_{L_\alpha}$ and $C_{MAC_\delta} = 0$) about a pivot located a distance b from the left end of the rigid rod. This wing is mounted on the rod with another torsion spring K_2 that resists wing torsion, θ. The torsion spring K_1 is unstretched when $\alpha = 0$ and the torsion spring K_2 is unstretched when $\theta = 0$. The wing segment is given a rotation input angle δ_o. The total angle of attack of the wing is then $-\alpha + \theta + \delta_o$.
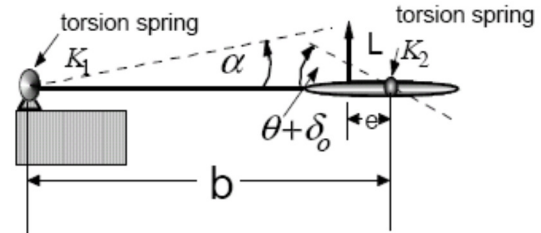
Problem 2.1

2.2 Problem statement
 (a) Break the deformed system into two pieces. Draw the two free body diagrams of the deformed system.   Derive the coupled static equilibrium equations and write them in matrix form as

Problem 2.2

$$\begin{bmatrix} \overline{K}_{11} & \overline{K}_{12} \\ \overline{K}_{21} & \overline{K}_{22} \end{bmatrix} \begin{Bmatrix} \theta \\ \alpha \end{Bmatrix} = \overline{q}\,\delta_o \begin{Bmatrix} Q_1 \\ Q_2 \end{Bmatrix} \quad \text{where} \quad \overline{q} = \frac{qSeC_{L_\alpha}}{K_2}$$

(b) Solve for the divergence dynamic pressure at which this system is neutrally stable. Input the ratio $\dfrac{b}{e} = 11$ into this expression and find the value of $\dfrac{K_1}{K_2}$ for which this configuration will not diverge.
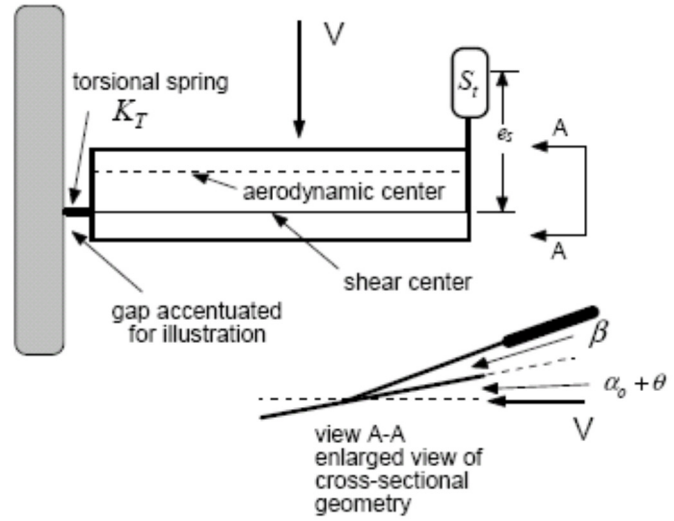
2.3 A rigid wing is attached to a wind-tunnel wall by a linear torsion spring. This wing also has a small wing attached to its tip. The idealized tip surface produces lift L_S according to the assumed simple relationship

$$L_S = qS_{tip}C_{L_{\alpha S}}\alpha_S$$

where α_S is the streamwise angle of attack of this small surface; $C_{L_{\alpha S}}$ is the tip surface lift curve slope, while S_{tip} is the tip surface area.

The tip device is connected to the wing tip by a torsion spring with stiffness k in-lb/radian. When the tip device rotates an angle β with respect to the wing tip a restoring torque $k\beta$ is generated to oppose this rotation.

Problem 2.3 - Wing with flexible tip

The idealized wing lift is $L = qSC_{L_\alpha}\alpha$ with $\alpha = \alpha_o + \theta$.

2.3 Problem statement
a) Write the equations of torsional equilibrium for this system when the entire system is given an initial angle of attack. Express these equations in terms of the following non-dimensional parameters; $\bar{q} = \dfrac{qSeC_{L_\alpha}}{K_T}$; $S_R = \dfrac{S_{tip}C_{L_{\alpha\delta}}e_s}{SC_{L_\alpha}e}$; $k_R = \dfrac{k}{K_T}$. Derive the characteristic equation for aeroelastic divergence $\bar{q}_D$ in terms of these parameters.

b) Plot the divergence dynamic pressure parameter $\bar{q}_D$ as a function of S_R when $k_R = 10$ and $k_R = 1$

Problem 2.4
Two identical uncambered wing segments are connected to each other by a torsional spring and to the wind tunnel walls by two other torsion springs, as indicated in the figure. The three torsion springs have the same spring constant K_T. The two segments are mounted on bearings on a spindle attached
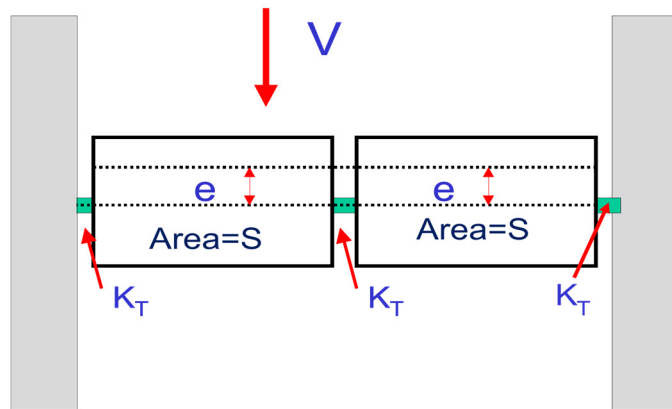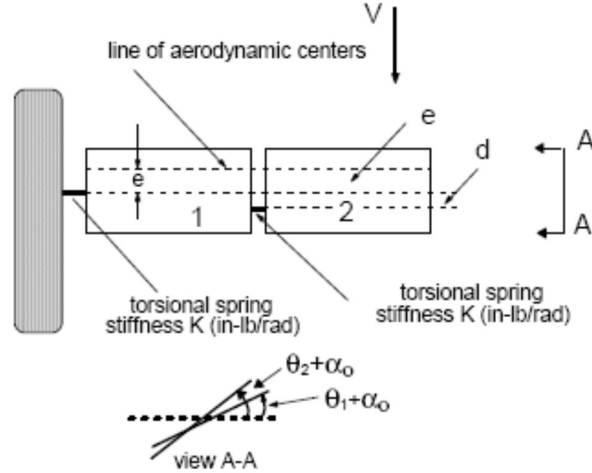
Problem 2.4

to the tunnel walls. Solve for the divergence dynamic pressure. Find the mode shape at divergence. Describe this mode shape (how do the surfaces move relative to each other?).

Problem 2.5

Two wing sections are mounted on shafts and attached to each other and to a wind tunnel wall, as indicated. Note that the torsion spring stiffnesses are equal, but are offset an amount d. This configuration is similar to, but not identical to, the example in Section 2.18. When the airfoils are placed at an angle of attack α_o, the springs deform. Lift on the two, identical, uncambered wing sections is
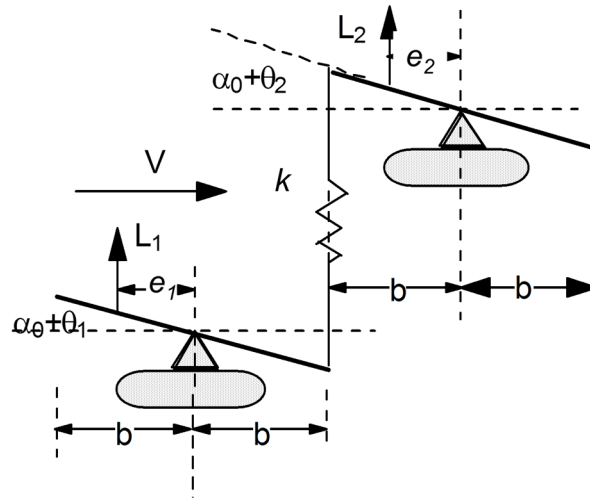

Problem 2.5

$$L_1 = qSC_{L\alpha}(\alpha_o + \theta_1)$$

$$L_2 = qSC_{L\alpha}(\alpha_o + \theta_2)$$

(a) Derive the matrix equations of torsional static equilibrium for this model when it is placed at an angle of attack α_o. Express these equations in the form $\left[\overline{K}_{ij}\right]\begin{Bmatrix}\theta_1 \\ \theta_2\end{Bmatrix} = \begin{Bmatrix}Q_1 \\ Q_2\end{Bmatrix}$. Do not solve for the deflections, but *identify* the structural stiffness matrix and the aerodynamic stiffness matrix in these equations ("Identify" means put some words together and attach an arrow.)

(b) Solve for the divergence dynamic pressure; solve for the value of d that eliminates divergence. The shaft attaching the two segments can be re-positioned, but the outer wing segment always remains in-line with the inner segment.

(c) Place an aileron on the outer (right-hand) section. Develop the static equilibrium equations for the system when there is no initial angle of attack, but the control surface is deflected downward an amount δ_o.

(d) Solve for the rolling moment generated by the aileron. Solve the reversal speed in terms of general parameters such as C_{L_δ} and C_{MAC_δ}.

Problem 2.6

A side view of two idealized wings is shown in the figure. This example is similar to that discussed in Section 2.15, but has one spring removed. These wings are connected by a single spring, with spring constant k *lb/inch*; each wing has planform area S. The spring is pinned to each wing and develops an internal force in response to relative deflection between its ends. This configuration differs from that discussed in Section 2.15 because it can rotate without stretching or compressing the spring. This is called *rigid body freedom*.

Problem 2.7 - Tandem wing geometry with single spring

The lift on each wing is given by

$$L_1 = qSC_{L\alpha}(\theta_1 + \alpha_o)$$
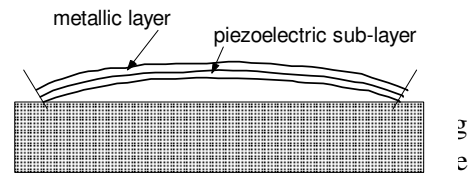$$L_2 = qSC_{L\alpha}(\theta_2 + \alpha_o)$$

where α_o is an initial angle of attack common to both wings and θ_1 and θ_2 are the two twist angles.

a) Solve for the characteristic equation Δ for static stability
b) If $e_1 = e_2 = e$, identify a dynamic pressure parameter $\bar{q}$ and plot the characteristic equation as a function of this parameter.
c) Find the value(s) of the pressure parameter at which $\Delta = 0$. Solve for the mode shape(s). Will the system diverge? Why or why not?
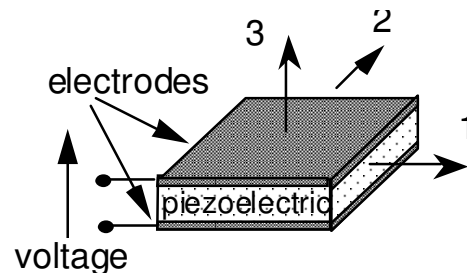
Problem 2.7

A wing test article consists of a low density, symmetrical ae[...] stiffness, wrapped around the two layer piezoelectric plate [...] creates an electric field E shown in Figure (b) that causes e[...] surface is formed.

Problem 2.7(a) - Piezoelectric layered actuator

The wing idealization is shown in Figure (c); for analysis purposes we have only drawn the chord line. This model has two lift components; the first is due to an initial angle of attack and the wing twist. The second is due to the applied voltage that creates camber.

Problem 2.7(b) - Piezoelectric actuator

We will represent the added lift and pitching moment combination created by camber as a single force L_2 acting on the wing at a distance e_2 aft of the shear center (this is the center of pressure). This location of the center of pressure for the additional force and we assume that it does not move with applied voltage.

$$L_1 = qSC_{L_\alpha}(\alpha_o + \theta)$$

$$L_2 = qSC_{L_V}V$$

torsion spring K_T
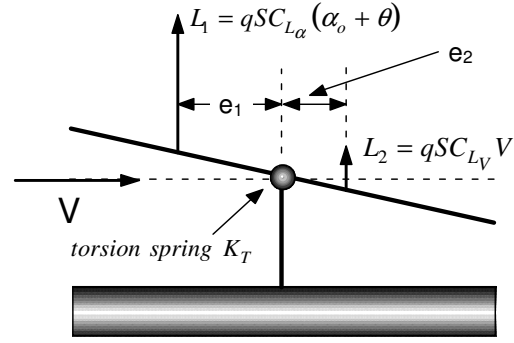
Problem 2.7(c) - Active airfoil with applied loads

The relationship between lift L_2 and the applied voltage V is:

$$L_2 = (qSC_{L_V})V$$

V is voltage, not airspeed. Since the change in camber produces lift and pitching moment, the aerodynamic coefficient $C_{L_V} = \dfrac{\partial C_L}{\partial\, camber}\dfrac{\partial\, camber}{\partial V}$ tells us how much lift we get per volt across the active material per unit wing area per unit dynamic pressure.

Problem statement
(a)   When the airfoil initial angle of attack is zero ($\alpha_o = 0$) solve for the lift on the wing as a function of the applied voltage V.

(b)   Find the wing divergence dynamic pressure q_D as a function of the aerodynamic and structural parameters. (Voltage should not appear).

(c)   Let's create a feedback system where we measure the twist θ and feed this back a to the voltage, so that $V = k\theta$ (k is an arbitrary number that we can choose). In this case, the voltage term should move to the left side of your equation. If the wing is placed at an initial angle of attack α_o, solve for the wing twist and solve for the divergence dynamic pressure.

Solution hints
The total airfoil lift is written as

$$L = L_1 + L_2 = qSC_{L_\alpha}\alpha + qSC_{L_V}V$$

where
$$\alpha = \alpha_o + \theta$$

In this problem $\alpha_o = 0$. When $V = k\theta$, the equation of torsional static equilibrium is

$$qSe_1C_{L_\alpha}(\alpha_o + \theta) - qSe_2C_{L_V}k\theta - K_T\theta = 0$$

Problem 2.8

The 1 dof wing shown in Figure (a) has leading edge and trailing edge control surfaces. There is no initial angle of attack when the two control surfaces are undeflected. Three lift components act on the idealized wing. Each force has its own location with respect to the shear center pin shown in the figure. Twisting is resisted by the torsional spring with torsional stiffness K_T.
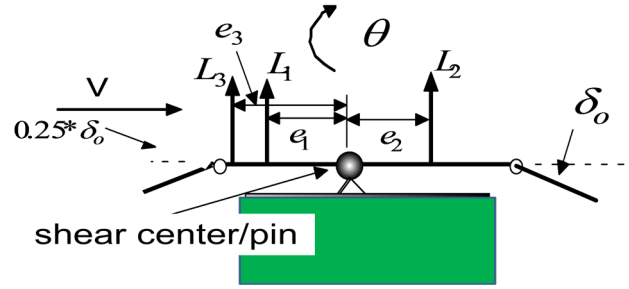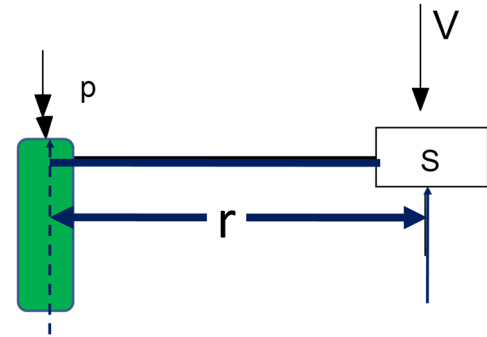

Problem 2.8(a)

The entire assembly is mounted at the end of a long bar a distance r from the center of rotation. This assembly will move upward at a terminal speed ***v = pr*** when the surfaces are deflected. The leading edge surface and the trailing edge flap are geared together so that the three lift components are as follows:

$$L_1 = qSC_{L\alpha}\theta + qSC_{L\alpha}\left(-\frac{v}{V}\right) \text{ (where } v = pr\text{)}$$

$$L_2 = qSC_{L\delta}\delta_0$$

$$L_3 = 0.25qSC_{L\delta}\delta_0$$

The rolling moment is $M_{roll} = Lr = (L_1 + L_2 + L_3)r$.

Problem 2.8(b) – Top view of wing assembly showing rotational rate, p.

Problem statement
   a) Solve for the twist θ.
   b) Find the expression for the steady state roll rate p.
   c) Find the reversal dynamic pressure

Problem 2.9
An uncambered wing with span, b, is attached to both walls of a wind tunnel and placed at an angle of attack α_0. The wing is idealized as a torsionally flexible, uniform property element like that discussed in Section 2.19. Use Figure 2.19.1 as your reference, but with span b instead of L and with an additional support on the right.

The differential equation of torsional equilibrium used to model wing twist deformation is:

$$\frac{d^2\theta}{dx^2} + \frac{qcea_o}{GJ}\theta = \frac{qcea_o\alpha_o}{GJ}$$

   (a) Find the divergence dynamic pressure of this wing.
   (b) Torsion springs with stiffness, k in-lb./radian is placed at the left and right ends of the test article (at x=0). Solve for the expression characteristic equation for

divergence in terms of a parameter β = kb/GJ. Plot the divergence dynamic pressure as a function of β to generate a figure similar to Figure 2.19.9.

Problem 2.10

Classical wing divergence ignores the fact that the wing is attached to the fuselage with pitch and plunge freedom. Consider the idealized, uncambered wing attached to a torsion spring which is, in turn, attached to an idealized fuselage, as shown in Figure 1. The torsional spring resists torsion by developing a restoring moment M_s equal to $K_T\theta$, where θ is the relative rotation of the wing with respect to the fuselage.

The fuselage is a freely flying article, but for our model it is attached to a frictionless pin to simulate the ability of the aircraft to rotate about its own center of gravity (cg). The wing has two degrees of rotational freedom α and θ, that generate lift.

An all-movable tail on the fuselage provides a pitching moment about the aircraft c.g. by generating lift, L_{tail}, given by the expression

$$L_{tail} = qS_{tail}C_{L_{\alpha_{tail}}}(\alpha + \beta) \tag{1}$$

In Eqn. 1, β is the tail rotation with respect to the fuselage while α represents the rotation of the fuselage about the airplane cg or model pin.
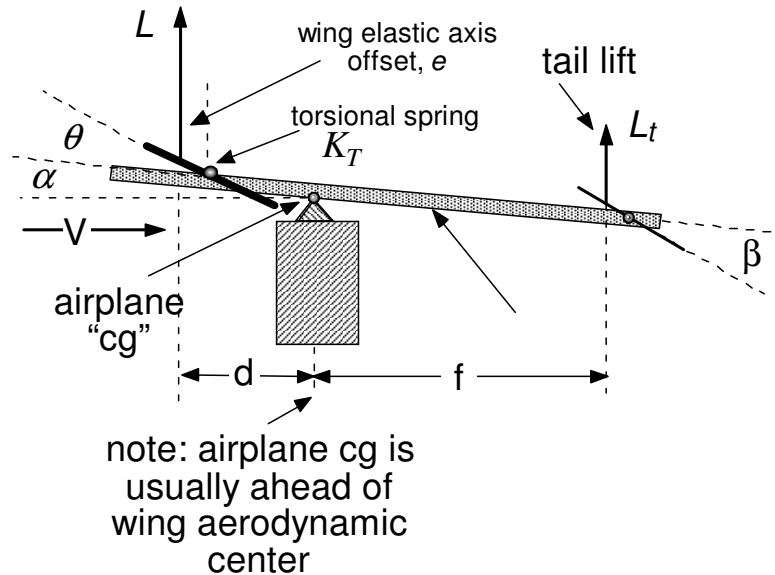

Figure 2.10.1 - Wing fuselage configuration geometry

Problem statement

(a)   Solve for expressions for α and θ in response to the tail angle, β using the following definitions

$$\bar{q} = \frac{qSeC_{L_\alpha}}{K_T} \qquad (2)$$

$$R = \left(\frac{f}{d}\right)\left(\frac{S_{tail}}{S}\right)\left(\frac{C_{L_{\alpha tail}}}{C_{L_\alpha}}\right) > 1$$

As noted on Figure 2.10.1, the pin representing the c.g. is usually ahead of the wing aerodynamic center. If this is so, then the dimension d will be negative. When the parameter R defined in Eqn. 2 is multiplied by -1 the result is similar to the definition of the *tail volume* used in stability and control studies. If $R > 1$ (or $-R < -1$) then the configuration is stable in pitch in forward flight.

(b) The purpose of the tail control surface is to create a change in pitch angle. Define control reversal as the condition that occurs when we deflect the tail surface, but there is no change in aircraft attitude angle. Set up an analysis to determine whether or not tail control reversal q occurs. Solve for the tail control reversal dynamic pressure.

(c) Solve for divergence dynamic pressure parameter $\bar{q} = \dfrac{qSeC_{L_\alpha}}{K_T}$ as a function of R. Plot

this divergence pressure parameter as a function of R. What value of R is required to make the divergence pressure parameter equal to 1?

Helpful hints – The FBDs are set up in Figure 2.10.2. They must be useful. My equilibrium equations are also shown below. So, too, is the characteristic equation.
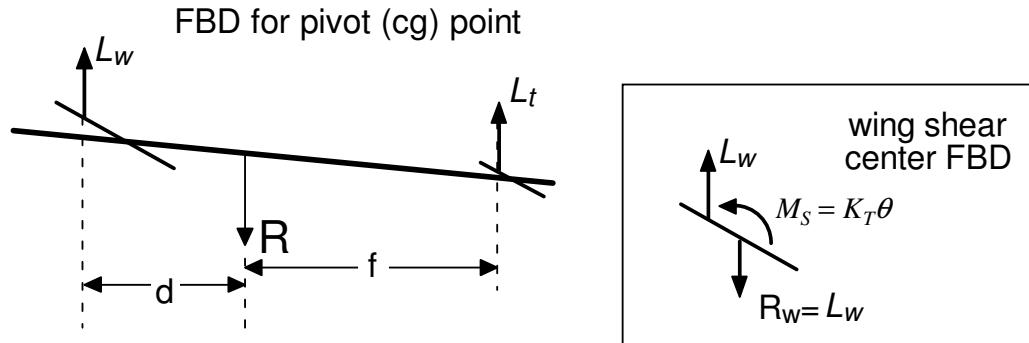

FBD for pivot (cg) point

Figure 2.10.2 - Wing/fuselage free body diagram

$$\bar{q}\left[1 - \left(\frac{f}{d}\right)\left(\frac{S_{tail}}{S}\right)\left(\frac{C_{L_{\alpha tail}}}{C_{L_\alpha}}\right)\right]\alpha + \bar{q}\theta = \bar{q}\left(\frac{f}{d}\right)\left(\frac{S_{tail}}{S}\right)\left(\frac{C_{L_{\alpha tail}}}{C_{L_\alpha}}\right)\beta$$

and $\bar{q}\alpha - [1 - \bar{q}]\theta = 0$ so that $\Delta = -\bar{q}[(1-R)(1-\bar{q}) + \bar{q}] = -\bar{q}(1 - R + R\bar{q})$

2.26 Chapter 2 References

1. B.A. Rommel and A.J. Dodd, "Practical considerations in aeroelastic design," *Proceedings of a Symposium on Recent Experiences in Multi-disciplinary Analysis and Optimization*, NASA CP-2327, April 24-26, 1984.

2. D.B. Thurston, *The World's Most Significant and Magnificent Aircraft Evolution of the Modern Airplane*, Society of Automotive Engineers (SAE), Warrendale, Pennsylvania, 2000.

3. D. Stinton, *The Anatomy of the Airplane (2nd Edition)*, AIAA, Reston, Virginia, 1998.

4. J. Cutler, *Understanding Aircraft Structures,* BSP Professional Books, 1981.

5. R. Miller and D. Sawyers, *TheTechnical Development of Modern Aviation,* Praeger Publishers, New York, 1968.

6. C. H. Gibbs-Smith, *Aviation: An historical survey from its origins to the end of World War II,* Her Majesty's Stationery Office, London, 1970.

7. G. Pahl and H. Betz, *Engineering Design: A Systematic Approach*, Second Edition, Springer-Verlag, New York, 1995.

8. C.L. Dym, *Principles of Mathematical Modeling (Second Edition),* Elsevier, 2004.

9. M.J. Turner, R. Clough, C. Martin and L. Topp, "Stiffness and deflection analysis of complex structures," *Journal of the Aeronautical Sciences* Vol. 23, No. 9, 1956, pp. 805-823.

10. H.C. Kermode, *Mechanics of Flight,* 10th Edition, revised by R.H. Barnard and D.R. Philpot; Prentice-Hall/Pearson Education, 1996).

11. J.D. Anderson, Jr., *A History of Aerodynamics*, Cambridge University Press, 1997

12. *Britannica Concise Encyclopedia.* Copyright © 1994-2008 Encyclopedia Britannica, Inc.

13. McGraw-Hill Concise Encyclopedia of Physics. © 2002 by The McGraw-Hill Companies, Inc.

14. I.E. Garrick and W.H. Reed, "Historical Development of Aircraft Flutter," *Journal of Aircraft,* Vol. 18, No. 11, November 1981. (This reference, despite its title, covers both static and dynamic aeroelasticity. It also debunks as incorrect the oft-made assertion that Langley's Aerodrome failed due to divergence).

15. T.A. Weisshaar, Morphing Aircraft Systems-Historical Perspectives and Future Challenges, Journal of Aircraft, 2013.

16. G.R. Anderson, D.L. Cowan, D.J. Piatek, "Aeroelastic Modeling, Analysis and Testing of a Morphing Wing Structure," AIAA Paper 2007-1734, 48th AIAA/ASME/ASCE/AHS/ASC Structures, Structural Dynamics and Materials Conference, 23-26 April 2007, Honolulu, Hawaii.

17. M.H. Love, P.S. Zink, R.L. Stroud, D.R. Bye, S. Rizk, D. White. "Demonstration of Morphing Technology through Ground and Wind Tunnel Tests," 48th AIAA/ASME/ASCE/AHS/ASC Structures, Structural Dynamics and Materials Conference, AIAA Paper 2007-1729, Honolulu, Hawaii, 23-26 April 2007.

18. D.O. Dommasch, S.S. Sherby and T.F. Connolly, *Airplane Aerodynamics*, Pitman Publishing Company, New York, 1967, pp. 115.

19. A.H. Flax, "The influence of structural deformation on airplane characteristics," *Journal of the Aeronautical Sciences,* Vol.12, 1945, pp. 94-102.

20. H. Glauert, *The Elements of Wing Segment and Airscrew Theory*, Cambridge University Press, 1959. (This book was first published in 1926 and has gone through several editions).

21. N.J. Hoff, "Innovation in Aircraft Structures," AIAA Paper 84-0840,

22. I.E. Garrick and W.H. Reed, "Historical Development of Aircraft Flutter," *Journal of Aircraft,* Vol. 18, No. 11, November 1981. (This reference, despite its title, covers both static and dynamic aeroelasticity. It also debunks as incorrect the oft-made assertion that Langley's Aerodrome failed due to divergence).

23. A.R. Collar, "The First Fifty Years of Aeroelasticity," *Aerospace*, Vol. 5, Feb. 1978, pp. 12-20.

24. D. Paul, L. Kelly, V. Venkayya and T. Hess, "Evolution of U.S. Military Aircraft Structures Technology," *Journal of Aircraft,* Vol. 39, No. 1, January-February 2002, pp. 18-29. (This paper has numerous references to explain the development of both military and civilian aircraft structures.)

25. Y.C. Fung, *An Introduction to the Theory of Aeroelasticity,* Dover Publications, New York, 1965.

26   R.L. Bisplinghoff, H. Ashley, R.L. Halfman, *Aeroelasticity,* Addison-Wesley, Reading, Mass., 1955. This book has also been re-published as a Dover edition.